UNIVERSIDADE da MADEIRA
CCM-Centro de Ciências Matemáticas

The fraction of the Universe going into Primordial Black Holes

Report of Progress of PhD Work
(First year full time)

Laurindo Sobrinho, Pedro Augusto
Universidade da Madeira
Departamento de Matemática e Engenharias
9000-390 Funchal, Madeira
Portugal

CCM Nr. 126/07

CCM – Centro de **C**iências **M**atemáticas
Universidade da Madeira, P-9000 Funchal, Madeira
Tel. + 351 291 705181, Fax: +351-91-705189
e-mail: ccm@uma.pt
http://www.uma.pt/ccm

The fraction of the Universe going into Primordial Black Holes

Report of Progress of PhD Work
(First year full time)

Laurindo Sobrinho, Pedro Augusto[1]
Departamento de Matemática e Engenharias, Universidade da Madeira

March 2007

Abstract

The Universe is a well developed structure on the scale of galaxies and smaller formations. This requires that at the beginning of the expansion of the Universe there should have existed fluctuations which leaded to the formation of such structures. Inflation, a successful cosmological paradigm, allows us to consider the quantum origin of the fluctuations. Within this paradigm, we can explain not only all the inhomogeneities we see today but also the formation of Primordial Black Holes (PBHs). We conducted a review of the production of PBHs in a radiation dominated Universe from where we calculated the fraction of the Universe going into PBHs at a given epoch β. We have considered four known different models for the spectrum of the primordial fluctuations: i) scale–free power law spectrum; ii) scale–free power law spectrum, with a pure step; iii) broken scale invariance spectrum; iv) a running–tilt power law spectrum. Our results gives $\beta \approx 0$ to $\beta \sim 10^{-7}$, and imply a non–negligible fraction of PBHs (at leat within some models).

[1] PhD Supervisor

Contents

Preface

Black Holes are objects predicted by the laws of Physics. So far, black holes (or black hole candidates) have been detected only by indirect means. On this PhD thesis we plan to investigate the possibility of direct detection of a black hole. We have started with primordial black holes (i.e., black holes formed in the early universe) because, as far as we know, those are the only ones that could have formed with substellar masses which makes them potential candidates for the *nearest detectable black hole*. In this report we present the PhD work done during the first year (full time).

Sections 1 to 4 are devoted to literature revision although they have also some original work. In Section 1 we make a brief review of the primordial Universe and in Section 2 we explore the conditions and mechanisms of Primordial Black Hole formation from primordial density fluctuations in a radiation dominated Universe. In Section 3 we introduce the main formulae needed to determine the fraction of the Universe going into Primordial Black Holes (β) and in Section 4 we introduce different alternative models for the primordial fluctuations spectrum: i) scale–free power law spectrum; ii) scale–free power law spectrum with a pure step; iii) broken scale invariance spectrum; iv) running–tilt power law spectrum.

In Section 5 we present our results. So far, we have determined β for all of the primordial fluctuations spectra considered in Section 4. The basic observational input needed in the calculations comes from the cosmic microwave background radiation. Model i) above gives $\beta \approx 0$. For the remaining models we have to give values to two additional parameters. We have explored the set of values leading to higher values for β (up to $\sim 10^{-7}$).

In Section 6 we present our future work plan. In the near future we want to improve the calculus of β (e.g., including the Initial Mass Function). In the not so near future we want to determine the Primordial Black Hole distribution function in the universe and, consequently, determine the mean distance to the nearest black hole and the probability of its detection.

José Laurindo de Góis Nóbrega Sobrinho
Universidade da Madeira
March 2007

1 Introduction

The Universe is a well developed structure on the scale of galaxies and smaller formations. This requires that at the beginning of the expansion of the Universe there should have existed fluctuations which leaded to the formation of such structures. It is natural to assume that the amplitude of fluctuations was even larger at smaller scales (e.g. Novikov et al., 1979). Some regions might have got so compressed that they underwent gravitational collapse to produce primordial black holes (PBHs). The first person to realize that was Hawking (1971). Zeldovich & Novikov (1967) also discussed the inhnomogenities in the early Universe but they were considering "retarded cores" rather than BHs (e.g. Carr, 2003).

There must have been many such volumes for which the gravitational energy considerably exceeded the kinectic energy of expansion. These regions would not have continued to expand with the rest of the Universe but would have collapsed again (Hawking, 1971). One would expect therefore at least a few regions to become sufficiently compressed for gravitational attraction to overcome pressure forces and the velocity of expansion and cause collapse to a PBH (Carr & Hawking, 1974). This is the only way to produce BHs with mass smaller than about $3M_{\odot}$, except possibly by the production of BHs in accelerators such as the *Large Hadron Collider* (LHC) in the speculative framework of branes (e.g. Cavaglia et al., 2003) or even when cosmic–rays collide with the upper layers of the atmosphere (e.g. Anchordoqui et al., 2002).

Hawking (1974) has shown that, when quantum effects are taken into account, BHs radiate like a blackbody. This process pratically does not affect stellar mass BHs, but it could be very significative in the case of smaller mass PBHs. In fact PBHs with initial masses bellow 10^{15}g should have been completely evaporated by now and PBHs with initial masses of order 10^{15}g are supposed to be exploding by the present time contributing to the γ–ray background (e.g. Page & Hawking, 1976). The Hawking radiation emitted by a BH on the final stage of evaporation could be detected at X-rays or γ–rays from $\sim 10^{8}$m (Earth–Moon distance) up to $\sim$ 20pc depending on the stage of the evaporation process (Sobrinho, 2003).

PBHs are interesting for several reasons: PBHs are the only BHs small enough for quantum emission effects to be important (e.g. MacGibbon & Carr, 1991) and thus they would play a key role in studying quantum gravitational effects, PBHs with any mass could be an excellent indicator of the conditions in the early universe, PBHs could (in principle) contribute with a major part to dark matter, PBHs are unique since they alone could be expected to survive the dissipative effects which erase all other imprints of conditions in the first second of the Universe (Carr, 1975), and PBHs probe scales which are many orders of magnitude smaller than the scales probed by *Large Scale Structure* (LSS) surveys and *Cosmic Microwave Background* (CMB) angular anisotropy observations giving the possibility to probe a very distinct part of the inflaton potential (Polarski, 2001).

It has been proposed that PBHs can explain certain observational anom-

alies such as: the unexpectedly high fraction of antiprotons in cosmic ray, the positron background spectrum and the annihilation line radiation coming from the galactic center (e.g. MacGibbon & Carr, 1991).

A definite observation of γ–rays from a PBH would be a tremendous vindication of general relativity and quantum theory and would give us important information about the early universe and strong interactions at high energies. On the other hand, negative observations which placed a strong upper limit on the density of PBHs would also give us valuable information because they would indicate that the early Universe was probably nearly homogeneous and isotropic with a hard equation of state (Page & Hawking, 1976). Even if PBHs never formed, their nonexistence provides useful cosmological information (MacGibbon & Carr, 1991).

1.1 The primordial universe

According to observation we live in a flat, homegeneous and isotropic expanding universe (e.g. Jones & Lambourne, 2004). Such a universe can be described by the *Friedmann–Robertson–Walker* (FRW) metric (e.g. d'Inverno, 1993)

$$ds^2 = dt^2 - R^2(t)\left[\frac{dr^2}{1-\kappa r^2} + r^2\left(d\theta^2 + sin^2\theta d\phi^2\right)\right] \tag{1}$$

where $R(t)$ is a *scale function* which describes the time dependence of the geometry and κ is a constant which fixes the sign of the spatial curvature ($\kappa = 0$ for Euclidean space, $\kappa = +1$ for a closed elliptical space of finite volume and $\kappa = -1$ for an open hyperbolic space). Besides the metric (1) we need an equation of state to describe the universe. In general we may write (e.g. Carr, 2003)

$$p = \theta\rho \tag{2}$$

where p is the pressure, ρ the density and θ the adiabatic index ($0 < \theta < 1$). The primordial universe was radiation dominated (i.e., it was opaque to light), described by the equation of state (e.g. Carr, 2003)

$$p = \frac{\rho}{3} \tag{3}$$

The radiation and matter densities in the universe decrease as the expansion dilutes the numbers of atoms and photons. Radiation is also diminished due to the cosmological redshift, so its density falls faster than that of matter. When the age of the universe was $\sim 10^6$ years it becomed matter dominated ($\theta = 0$). During the radiation dominated era θ will usually be $1/3$ (equation 3). However if the universe experiences a dust–like phase, during a phase transition, one may have $\theta = 0$ (Carr et. al., 1994).

In order to explain problems such as the flatness problem and the horizon problem, the present paradigm makes use of an inflationary stage of expansion in the very early Universe. During inflation the scale factor $R(t)$ has grown up exponentially from an intial value R_i, corresponding to the instant $t_i \sim 10^{-35}$s

when the electroweak and strong forces separate (e.g. Narlikar & Padmanabhan, 1991, cf. Table 1) to a value R_e according to (e.g. d'Inverno, 1993)

$$\frac{R_e}{R_i} = e^{N(t_e)} \tag{4}$$

where

$$N(t_e) = Ht_e \tag{5}$$

gives the number of *e–folds* that elapsed during inflation. For example, the value $N = 70$ means that during inflation the scale factor have grown up by a factor of e^{70} ($\approx 10^{30}$). Although the exact value of $N(t_e)$ is unknown, suggested values are in the range $50 < N(t_e) < 70$ (e.g. Narlikar & Padmanabhan, 1991).

Inflation gives a possible solution to the crucial problem of where the primordial fluctuations leading to the observed LSS come from. In fact, they have their origin in the ubiquitous vacuum fluctuations. The seed of the LSS has been observed in the form of tiny fluctuations imprinted on the CMB at the time of decoupling. Each inflationary model makes precise predictions about the spectrum of its primordial fluctuations and this is how these models can be constrained by observations (e.g. Bringmann et al., 2002).

Solving the field equations of General Relativity we find that $R(t) \sim t^{1/2}$ in a radiation dominated universe and that $R(t) \sim t^{2/3}$ in a matter dominated universe (e.g. d'Inverno, 1993). It is convenient to set the present value of the scale factor equal to unity

$$R_0 = R(t_0) = 1 \tag{6}$$

so that at any time the scale factor is related to the redshift z simply by (e.g. Liddle & Lyth, 1993)

$$R = \frac{1}{1+z} \tag{7}$$

We may write for the matter dominated stage

$$R(t) = \left(\frac{t}{t_0}\right)^{2/3}, \quad t_{eq} \leq t \leq t_0 \tag{8}$$

and for the radiation dominated stage

$$R(t) = \left(\frac{t_{eq}}{t_0}\right)^{2/3} \left(\frac{t}{t_{eq}}\right)^{1/2}, \quad t_e \leq t \leq t_{eq} \tag{9}$$

where t_0 is the present time (i.e. the age of the universe), t_{eq} is the age of the universe at the last scattering surface (corresponding to the instant when photons decoupled from matter) and t_e is the age of the universe at the end of inflation. The Hubble parameter H is defined as (e.g. d'Inverno, 1993)

$$H(t) = \frac{\dot{R}(t)}{R(t)} \tag{10}$$

Thus, with the help of equations (8) and (9) it turns out that

$$H(t) = \tfrac{2}{3t}, \quad t_{eq} \leq t \leq t_0 \tag{11}$$

and

$$H(t) = \tfrac{1}{2t}, \quad t_e \leq t \leq t_{eq} \tag{12}$$

The present value of the Hubble parameter H_0 (also known as the *Hubble constant*) is, according to the most recent WMAP observations (Spergel et al., 2006)

$$H_0 = 73.4\,\mathrm{kms}^{-1}\,\mathrm{Mpc}^{-1} \tag{13}$$

The value of t_0 can be determined inserting H_0 into equation (11). It turns out that

$$t_0 \approx 2.8 \times 10^{17}\mathrm{s} \tag{14}$$

The value of t_{eq} can be obtained with the help of equations (7) and (8) considering that $z \approx 1100$ for the last scatering surface (e.g. Padmanabhan, 2001)

$$t_{eq} \approx 7.7 \times 10^{12}\mathrm{s} \tag{15}$$

During inflation the Hubble parameter H remained constant (e.g. Narlikar & Padmanabhan, 1991). Considering $t_i = 10^{-35}$s in equation (12) we find out the constant value of the Hubble parameter during inflation, and then inserting it into equation (5) we obtain

$$t_e \sim 10^{-33}\mathrm{s} \tag{16}$$

valid for both $N(t_e) = 50$ and $N(t_e) = 70$.

The horizon mass, M_H, at a given epoch, defined as the mass inside one Hubble radius at that epoch, is given approximately by the expression (e.g. Carr, 2005)

$$M_H(t) \approx \frac{c^3 t}{G} \approx 10^{15} \left(\frac{t}{10^{-23}\mathrm{s}} \right) \mathrm{g} \tag{17}$$

where c is the speed of light in vacuum and G is the Gravitational constant. It is natural to assume that the mass of a PBH when it forms is of the order of M_H at that epoch (e.g. Carr, 2005). The horizon mass at matter–radiation equality is of order $10^{18} M_\odot$. If there where BHs with such large masses we should fall down into the gravitational field of the nearest one, see the anisotropy in the CMB radiation and the distortion in the local velocity field of galaxies (e.g. Eardley & Press, 1973; Novikov et al., 1979). In conclusion we may say that it is secure to assume that PBH formation occurs well within the radiation dominated era.

In Table 1 we present a timeline of the universe according to the inflationary big bang model.

Table 1: The universe timeline according to the inflationary Big Bang model (data was taken from Unsöld & Baschek (2002) and Jones & Lambourne (2004)).

Era	$t(s)$	$T(K)$	$T(GeV)$	Comments
Planck	–	–	–	Quantum Gravity rules
GUT	10^{-43}	10^{32}	10^{19}	Gravity separates
Quark	10^{-35}	10^{27}	10^{14}	Strong–electroweak phase transition Inflation begins
	$\sim 10^{-33}$	10^{27}	10^{14}	Inflation ends
	3×10^{-11}		180	Top quark threshold
	10^{-10}	10^{15}	100	Electroweak phase transition
	10^{-8}		4.25	Bottom quark threshold
	10^{-7}		1.78	Lepton τ threshold
			1.5	Charm quark threshold
			$1.6 - 1$	Hyperons threshold
Hadron	10^{-6}	10^{13}	1	Formation of neutrons and protons
	4×10^{-6}		0.50	Kaons threshold
	5×10^{-5}		0.14	Pions threshold
	10^{-4}		0.106	Muons threshold
Lepton	10^{-4}	0.05	0.06	Strange quark threshold and last pions decay
	0.02		0.01	Down quark threshold
	0.06		0.005	Up quark threshold
	1			Decoupling of ν_e
	2			Neutron production stops
Photon	3	5×10^9	5×10^{-4}	Electron threshold
	180	10^9		Nucleosynthesis of ^2H stable
	10^3			Nucleosynthesis stops
Matter	10^{13}			Decoupling of photons
	10^{15}			Reionization
	10^{17}	2.725		Present

2 Primordial Black hole formation

2.1 Fluctuations

It was realized already some time ago that a spectrum of primordial fluctuations can lead to the formation of PBHs (e.g. Carr & Hawking, 1974; Carr, 1975; Novikov et al., 1979). What was considered initially was a spectrum of classical fluctuations instead of a spectrum of quantum fluctuations. Now we have in cosmology a successful paradigm based on the existence of an inflationary stage which allow us to consider the quantum origin of the fluctuations. During inflation fluctuations of quantum origin of the *inflaton* (i.e. the scalar field driving inflation) are produced. These fluctuations are then stretched to scales much larger than the Hubble radius at the time when they were produced. As the expansion of the universe goes on each fluctuation will reenter at some stage inside the Hubble radius, depending on its wavelength. With this mechanism we can explain all the inhomogeneities we see today even on the largest cosmological scales as well as the production of PBHs (Polarski, 2001).

However the inhomogeneities that we observe today do not display any property typical of their quantum origin. On the large cosmological scales probed by the observations the fluctuations appear to us as random classical quantities. This means that there was at some time in the past a *quantum–to–classical* transition (Polarski, 2001).

Each field mode can be splited into two linearly independent solutions: the *growing mode* and the *decaying mode*. At reentrance inside the Hubble radius, during the radiation dominated or the matter dominated stage, the decaying mode is usually vanishingly small, and can therefore be safely neglected. As a result the field mode behaves like a stochastic classical quantity (for more details see Polarski (2001) and Polarski & Starobinsky (1996)).

The classical behaviour of the inflationary fluctuations is very accurate for the discription of the CMB temperature anisotropy and LSS formation. In the context of PBH formation this is not always the case. The smallest PBHs can be produced as soon as the fluctuations reenter the Hubble radius right after inflation. However at this stage the decaying mode still had no time to disappear completely and, as a consequence, one cannot speak about classical fluctuations (Polarski, 2001).

The degree to which the effective quantum–to–classical transition will occur is given by the ratio (Polarski, 2001)

$$D_k = \frac{\phi_{k,gr}}{\phi_{k,dec}} \tag{18}$$

of the growing mode (gr) to the decaying mode (dec) of the peculiar gravitational potential $\phi(k)$. Very large values of D_k will correspond to an effective quantum–to–classical transition. Equation (18) can be written as a function of the PBH mass (Polarski, 2001)

$$D(M) = 4AGH_k^2 \frac{M}{M_p^2} \tag{19}$$

where A is the growth factor of $\phi(k)$ between the inflationary stage and the radiation dominated stage, H_k is the Hubble parameter at Hubble radius crossing during the inflationary stage and M_p is the Planck mass. The ratio $D(M)$ will grow with increasing PBH masses M, due essentially to the last term in expression (19). Clearly there is a range of scales where D will not be large and the quantum nature of the fluctuations is important (Polarski, 2001).

PBHs with masses less than $M_* \approx 10^{15}$ g will have either completely evaporated or, in any case, be in the latest stage of their evaporation. Expression (19) evaluated at this natural cut–off for PBH masses gives $D(M_*) \simeq 10^{28}$ which means that one can safely use the effective classicality of the fluctuations for PBHs with initial masses $M \geq M_*$, i.e., all the non–evaporated PBHs. Hence, for all PBHs produced after approximately 10^{-23} s (cf. equation 17), the quantum–to–classical transition is already extremely effective. This means that quantum interference for these PBHs is essentially suppressed and one can really work to tremendously high accuracy with classical probability distributions (Polarski, 2001).

During the rest of the text we will consider only classical fluctuations. The simplest way of describing a classical fluctuation is in terms of an overdensity or density contrast (e.g. Carr, 1975)

$$\delta(m) = \frac{\Delta m}{m} \tag{20}$$

where m is the average mass of the perturbed region and Δm is the excess of mass associated with the perturbation. If we want to treat the evolution of the spectrum of fluctuations we must consider instead $\delta(\vec{r})$ which can be defined as (e.g. Musco et al., 2005)

$$\delta(\vec{r}) = \frac{\epsilon(\vec{r}, t) - \epsilon_b}{\epsilon_b} \tag{21}$$

where $\epsilon(\vec{r}, t)$ represents the density evolution inside a region of radius r and ϵ_b represents the background density. Each perturbation $\delta(\vec{r})$ can be written as a Fourier series defined in a comoving box much bigger than the observable universe (e.g. Liddle & Lyth, 1993)

$$\delta(\vec{r}) = \sum_k \delta_k e^{i\vec{k}.\vec{r}} \tag{22}$$

where k represents the wavenumber. Each physical scale $\lambda(t)$ is defined by some wavenumber k and evolves with time according to (Blais et al., 2003; Bringmann et al., 2002)

$$\lambda(t) = 2\pi \frac{R(t)}{k} \tag{23}$$

where $R(t)$ is the scale factor. The term scale is appropriate because features with size r are dominated by wavenumbers of order $k \sim r^{-1}$ (e.g. Liddle & Lyth,

1993). For a given physical scale the horizon crossing time t_k is conventionally defined by (e.g. Blais et al., 2003; Bringmann et al., 2002)

$$ck = R(t_k)H(t_k) \tag{24}$$

where H is the *Hubble parameter*. This corresponds to the time when that scale reenters the Hubble radius which will inevitably happen after inflation for scales that are larger than the Hubble radius at the end of inflation. It is at that time t_k that a PBH might form (e.g. Blais et al., 2003; Bringmann et al., 2002).

For a perturbation of a fixed size, it cannot begin to collapse until it passes within the cosmological horizon. The size of a PBH when it forms, therefore, is related to the horizon size, or equivalently to the horizon mass M_H (equation 17) when the collapsing perturbation enters the horizon.

In Table 2 we have for several epochs of interest the values of the wavenumber k (equation 24) corresponding to the fluctuations crossing the horizon at that times as well as the corresponding horizon mass M_H (equation 17). The selected epochs are: $t_e \sim 10^{-33}$s (end of inflation), $t_* \approx 10^{-23}$s (corresponding to the production of PBHs that are exploding by the present time, (e.g. Green & Liddle, 1997), $t = 10^{-10}$s (electroweak phase transition, (e.g. Unsöld & Baschek, 2002)), $t = 10^{-6}$s (quark–hadron phase transition, (e.g. Unsöld & Baschek, 2002)), $t = 6 \times 10^{-5}$s (corresponding to the minimum mass at which a stellar BH could form, (e.g. Padmanabhan, 2001)), $t = 20$s (corresponding to the maximum mass allowed for PBH in the *Cosmic Dark Matter* (CDM) context, (Afshordi et al., 2003)), $t = 2 \times 10^5$s (corresponding to the mass of the biggest *Supermassive Black hole* (SMBH) known candidates, (e.g. Kormendy, 2004), $t_{eq} = 7.7 \times 10^{12}$s (matter–radiation equality) and $t_0 = 2.8 \times 10^{17}$s (present time).

2.2 The condition for PBH formation

The collapse of an overdense region, forming a BH, is possible only if the *roat mean square* of the primordial fluctuations, averaged over a Hubble volume, is larger than a threshold δ_{min}. There is also an upper bound δ_{max} corresponding to the case for which a separate universe will form. Thus a PBH will form when the density contrast δ averaged over a volume of the linear size of the Hubble radius satisfies (Carr, 1975)

$$\delta_{min} \leq \delta \leq \delta_{max} \tag{25}$$

The lower and upper bounds of δ can be determined following analytic arguments. Consider for simplicity a spherically–symmetric region with radius R and density $\rho = \rho_c + \delta\rho$ embedded in a flat Universe with the critical density ρ_c. For spherical symmetry the inner region is not affected by matter in the surrounding part of the Universe. The expansion of this region will come to an halt at some stage, followed by a collapse. In order to reach a complete collapse, the potential energy, V, at the time of maximal expansion (e.g. Kiefer, 2003)

$$V \sim \frac{GM^2}{R} \sim G\rho^2 R^5 \tag{26}$$

Table 2: The wavenumber k (equation 24) of the fluctuation crossing the horizon at different epochs t_k and the corresponding horizon mass M_H (equation 17).

	t_k(s)	k(m^{-1})	M_H(g)	$M_H(M_\odot)$
t_e	10^{-33}	1.7×10^{-2}	10^{5}	5.0×10^{-29}
t_*	10^{-23}	1.7×10^{-7}	10^{15}	5.0×10^{-19}
	10^{-10}	5.5×10^{-14}	10^{28}	5.0×10^{-6}
	10^{-6}	5.5×10^{-16}	10^{32}	5.0×10^{-2}
	6×10^{-5}	7.1×10^{-17}	6.0×10^{33}	3
	20	1.2×10^{-19}	2×10^{39}	10^{6}
	2×10^{5}	1.2×10^{-21}	2×10^{43}	10^{10}
t_{eq}	7.7×10^{12}	2.6×10^{-25}	7.7×10^{50}	3.9×10^{17}
t_0	2.8×10^{17}	7.9×10^{-27}	2.8×10^{55}	1.4×10^{22}

has to exceed the inner energy, U, given by the pressure (e.g. Kiefer, 2003)

$$U \sim pR^3 \tag{27}$$

In the radiation dominated era (which is the era of interest for PBH formation) the equation of state is given by (3) yelding (e.g. Kiefer, 2003)

$$R \geq \sqrt{\frac{1}{3G\rho}} \tag{28}$$

In order to prevent the formation of a separate universe we must ensure that the radius of the collapsing region, R, is smaller than the curvature radius of the overdense region at the moment of collapse (e.g. Kiefer, 2003)

$$R < \frac{1}{\sqrt{G\rho}} \tag{29}$$

One then has the condition

$$1 > R \geq \sqrt{\frac{1}{3}} \tag{30}$$

evaluated at the time of collapse, for the formation of the PBH. In particular, when the fluctuation enters the horizon in a radiation dominated Universe one gets (e.g. Carr, 1975; Kiefer, 2003)

$$\delta_{min} \equiv \frac{1}{3} \leq \delta < 1 \equiv \delta_{max} \tag{31}$$

where the lower bound comes from condition (28) and the upper bound comes from condition (29). The extreme δ_{max} corresponds to the situation for which a separate Universe forms and δ_{min} corresponds to the threshold of PBH formation. If $\delta < \delta_{min}$ the fluctuation dissipates and there is no PBH formation (Section 2.4.3).

The correct value of δ_{min} has been (and continues to be) a matter of discussion (see Table 3). We have already seen that analytic arguments suggest the value $\delta_{min} = 1/3$. However, numerical simulations considering critical phenomena in the PBH formation (Section 2.4.1) reveale an higher value of $\delta_{min} \approx 0.7$ which is almost twice the old value. Another study using *peaks theory* (Green et al., 2004) lead to $\delta_{min} \approx 0.3 - 0.5$ which is in good agreement with the analytic approach $\delta_{min} = 1/3$. Taking into account that the threshold δ_{min} arises from critical behaviour we will refer to δ_{min} in the rest of the text as δ_c.

2.3 The Initial Mass Function for PBHs

It was belived for a long time that the PBH mass, at the time of formation, was aproximately equal to the mass of the collapsing region and thus to the horizon mass M_H (equation 17) at the epoch of formation (Niemeyer & Jedamzik, 1998).

A particularly interesting development has been the application of *critical phenomena* to PBH formation. Studies of the collapse of various types of spherically symmetric matter fields have shown that there is always a critical solution

which separates those configurations which form a BH from those which disperse to an asymptotically flat state. The configurations are described by some index δ and, as the critical index δ_c is approached, the BH mass is found to scale as $(\delta - \delta_c)^\gamma$ for some exponent γ. This effect was first dicovered for scalar fields (Choptuik, 1993). The index δ_c defines the threshold for PBH formation. It was demonstrated that scaling and self–similarity occurs in the gravitational collapse of a massless scalar field near the threshold of PBH formation.

Scale–invariant, or self–similar, solutions arise in fluid dynamics problems (without gravity) when there are two very different scales in the initial problem (for example an explosion with high initial density into a thin surrounding fluid), and that such solutions play the role of an intermediate asymptotic in the intermediate density regime (Gundlach, 1998). Roughly speaking, the kinetic energy of the massless field wants to disperse the field to infinity, whereas the gravitational potential energy, if suficiently dominant during the collapse, will result in the trapping of some amount of the mass–energy of the system in a BH. The key point is that the dynamical competition can be controlled by tuning the parameter δ in the initial conditions. It is possible to set up families of initial data such that if $\delta < \delta_c$ the scalar field completely disperses, while if $\delta > \delta_c$ a BH forms (Choptuik, 1993).

Choptuik (1993) demonstrated that on the case of a massless scalar field the BH masses are well–fit by a scaling law with an exponent $\gamma \approx 0.37$ which is family independent. Similar results were subsequently demonstrated for radiation (Evans & Coleman, 1994) and then more general fluids (Koike et al., 1999; Maison, 1996). Evans & Coleman (1994) studied the spherically symmetric collapse of a perfect fluid with the equation of state (3) obtaining a self–similar solution. They argued that the phase transition in the case of radiation fluid collapse should be characterized by continuous self–similarity. Once more, convincing evidence for mass-scaling in the super-critical regime, with $\gamma \approx 0.36$, was found. Koike et al. (1995) obtained for a collapsing radiation fluid $\gamma = 0.3558019$.

In all of these studies (e.g. Choptuik, 1993; Evans & Coleman, 1994; Koike et al., 1999) spacetime was assumed to be asymptotically flat. However, Niemeyer & Jedamzik (1998) have applied the same idea to study BH formation under the context of an expanding universe (asymptotically Friedmann model) and have found similar results. Based on the scaling relation it was possible to derive a universal two parameter *initial mass function* (IMF) applicable to PBH formation during one particular epoch. It was then possible to show that when the perturbation overdensity is sufficiently close to the critical overdensity for PBH formation, δ_c, the final mass of the resulting PBH may be an arbitrarily small fraction of the horizon mass given as function of the distance from the threshold, $\delta - \delta_c$ (Niemeyer & Jedamzik, 1998)

$$M_{BH} = K M_H \left(\delta - \delta_c\right)^\gamma \tag{32}$$

where K and γ are demensionless quantities to be determined according to the perturbation characteristics and M_H is the cosmological horizon mass at the horizon–crossing time (equation 17).

Entering the scaling regime requires a degree of fine–tuning of the initial data which was believed to be unnatural for any astrophysical application. However, it was noted that this fine–tuning occurs naturally in the case of PBHs forming from a steeply declining distribution of primordial density fluctuations (Niemeyer & Jedamzik, 1998).

Since $M \to 0$ as $\delta \to \delta c$, this suggests that PBHs may be much smaller than the particle horizon at the epoch of formation (Green & Liddle, 1999; Kribs et al., 1999; Yokoyama, 1998). The cosmological constraints, based on evaporating PBHs are slightly modified as a consequence of the production of not only horizon–size PBHs, as previously assumed, but also smaller, sub–horizon mass PBHs at each epoch (Niemeyer & Jedamzik, 1999a).

An important problem is to determine if whether the scaling law for PBH masses, given by equation (32) is likely to continue down to vanishingly small massses (Type II critical collapse) or if it stops at some finite value (Type I critical collapse) (Choptuik, 1998). This is a very challenging problem from the numerical calculation point of view because when $\delta \to \delta_c$ we have the appearance of strong shocks and deep voids outside the region where the PBH is forming (Musco et al., 2005). Hawke & Stewart (2002) addressed this problem using a purpose–built code. They claim that the formation of shocks prevents BHs forming on scales below $10^{-4}M_H$ but this has been disputed (see Miller, 2005). In their work Hawke & Stewart (2002) had considered centred and non–centred Gaussian pressure perturbations (see Section 2.4.1).

For supercritical evolutions leading to moderately large BHs ($M/M_H \geq 10^{-3}$), there is evidence for the scaling law with $\gamma \approx 0.35$ for the centred Gaussian profile and $\gamma \approx 0.36$ for the offset Gaussian pressure profile (see the right-hand graphs in Figures 1 and 2). This is consistent with the results reported by Niemeyer & Jedamzik (1999a). However, for lower BH masses the scaling law appears not to hold (see the left-hand graphs in Figures 1 and 2). There is evidence of a minimum BH mass $M/M_H \approx 10^{-4}$ (Hawke & Stewart, 2002).

In Figure 3 we have represented the allowed masses for PBHs as a functuion of time assuming that $10^{-4}M_H \leq M_{PBH} \leq M_H$. PBHs with intial masses of $\sim 10^{15}$g are supposed to be exploding by now. Ligther PBHs should have already completely evaporated.

In Table 3 it is shown the values for γ, K, and δ_c according to various authors. Notice that the value of γ does not depend very significantly of the type of perturbation considered. The some does not apply to K. Notice that the critical value δ_c is not consensual.

2.4 The mechanism of PBH formation

The dynamics of collapsing density perturbations in the early Universe are fully described by the general relativistic hydrodynamical equations of a perfect fluid, the field equations, the first law of Thermodynamics, and a suitable equation of state (e.g. Niemeyer & Jedamzik, 1999a). We shall restrict our attention to spherical collapse because the assumption of spherical symmetry is well justified

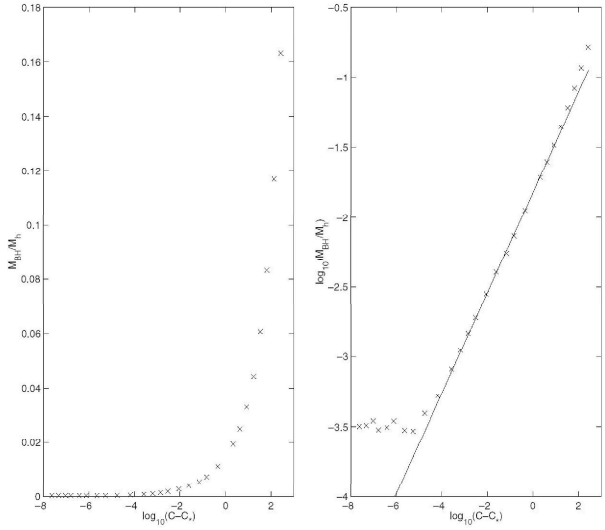

Figure 1: The BH mass as a function of the parameter C (which governs the strength of the density perturbation) for supercritical evolutions of initially centred Gaussian pressure profiles. The left figure shows the raw data. The right figure shows the line of best fit for that subset of the data which is consistent with the scaling law (equation 32) (Hawke & Stewart, 2002).

for large fluctuations in a Gaussian distribution (Bardeen et al., 1986) and besides that it simplifies considerably the calculations (e.g. Musco et al., 2005) because it reduces the problem to one spatial dimension.

For calculations in spherical symmetry it is convenient to divide the collapsing matter into a system of concentric shells and to label each shell with a comoving radial coordinate r (e.g. Musco et al., 2005). This approach is due to Misner & Sharp (1964) and the corresponding set of equations is called the Misner–Sharp equations. In the Misner–Sharp approach the metric is usually written in the form (e.g. Musco et al., 2005)

$$ds^2 = -a^2 dt^2 + b^2 dr^2 + R_s^2 \left(d\theta^2 + \sin^2(\theta) d\phi^2 \right) \tag{33}$$

where R_s (the Schwarzschild circumference radius), a and b are functions of r and the time coordinate t. Here the time coordinate plays the role of a cosmic time. In the absence of perturbations t reduces to the FRW time coordinate and R_s to what is commonly referred to as proper distance in Cosmology (Niemeyer & Jedamzik, 1999a).

For a classical fluid, composed of particles with nonzero rest–mass, it is convenient to use the rest–mass μ (or baryon number) contained interior to the surface shell as its co–moving coordinate r. For the case of a radiation fluid the rest–mass and baryon number are not available as conserved quantities (Musco et al., 2005). The energy density of the early Universe is dominated by photons

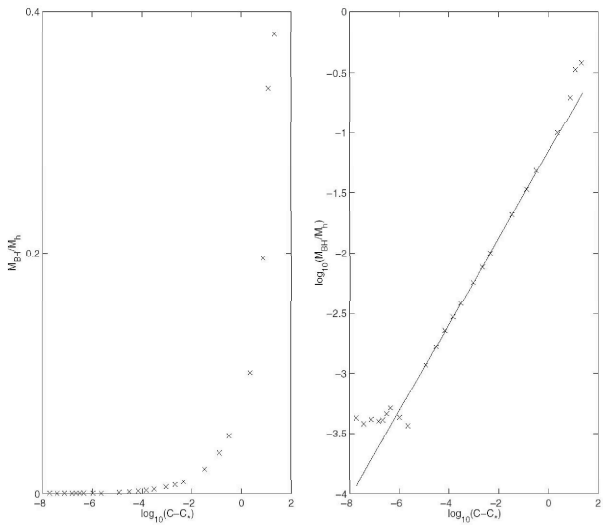

Figure 2: The BH mass as a function of the parameter C (which governs the strength of the density perturbation) for supercritical evolutions of initially centred offset Gaussian pressure profiles. The left figure shows the raw data. The right figure shows the line of best fit for that subset of the data which is consistent with the scaling law (equation 32) (Hawke & Stewart, 2002).

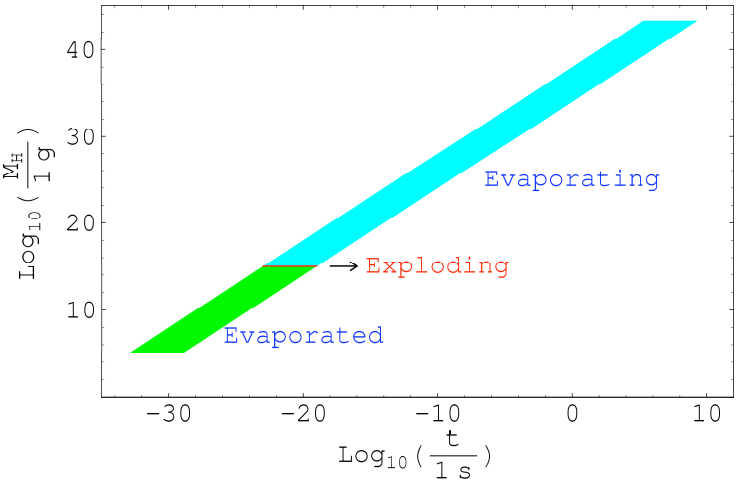

Figure 3: According to the numerical simulations PBHs may form with masses ranging from $10^{-4}M_H$ up to M_H. PBHs with intial masses smaller than 10^{15}g are supposed to be completely evaporated by now, PBHs with $\approx 10^{15}$g should be exploding by the present time and those with initial masses greater than 10^{15}g are still evaporating or accreting matter.

and relativistic particles such as electrons, muons, neutrinos and their respective antiparticles (e.g. Bicknell & Henriksen, 1979) and for this case we may use a *relative compression factor* ρ defined as (Musco et al., 2005)

$$d\mu = 4\pi\rho R_s^2 b dr \tag{34}$$

Identifying μ and r this gives

$$b = \frac{1}{4\pi\rho R_s^2} \tag{35}$$

It is usual to introduce the operators (e.g. Musco et al., 2005)

$$D_t = \frac{1}{a}\left(\frac{\partial}{\partial t}\right) \tag{36}$$

$$D_r = \frac{1}{b}\left(\frac{\partial}{\partial \mu}\right) \tag{37}$$

and the definitions (e.g. Musco et al., 2005)

$$U = D_t R_s \tag{38}$$

$$\Gamma = D_r R_s \tag{39}$$

where U is the radial component of the four–velocity and Γ is a generalisation of the Lorentz factor. We are interested in processes occurring in the radiation era of the Universe for which the equation of state can be given by (3). In this case the system of Einstein and hydrodynamic equations can be written as (Musco et al., 2005)

$$D_t U = -\left(\frac{\Gamma}{e+p} D_r p + \frac{M}{R_s^2} + 4\pi R_s p\right) \tag{40}$$

$$D_t \rho = -\frac{\rho}{\Gamma R_s^2} D_r\left(R_s^2 U\right) \tag{41}$$

$$D_t e = \frac{e+p}{\rho} D_t \rho \tag{42}$$

$$D_r a = -\frac{a}{e+p} D_r p \tag{43}$$

$$D_r M = 4\pi\Gamma e R_s^2 \tag{44}$$

where M is a measure of the mass–energy contained inside radius μ and Γ can be calculated either from (39) or from the constraint equation

$$\Gamma^2 = 1 + U^2 - \frac{2M}{R_s} \tag{45}$$

However,the Misner–Sharp equations are not suitable for the study of BH formation. That is because singularities are tipically formed rather early in calculations and it is not then possible to follow the subsequent evolution (e.g. Musco et al., 2005).

In early works this difficulty was overcomed by stopping the evolution in the region where the singularity would appear (e.g. Novikov et al., 1979). PBHs with mass of the order M_H formed. Bicknell & Henriksen (1979) used a method of integration which avoids the appearance of singularities. Their computation also shows the formation of PBHs with mass of the order of M_H or greater ($\sim 30M_H$) in cases where the overdensity in the initial perturbation was not compensated by a surrounding under–dense region.

In order to avoid such kind of problems Hernandez & Misner (1966) introduced the concept of *observer time*, using as the time coordinate the time which an outgoing radial light ray emanating from an event reaches a distant observer. For our purposes it is enough that the observer is located sufficiently far from the perturbed region to be unaffected by the perturbation. Taking into account that along an outgoing radial null geodesic the metric (33) reduces to

$$0 = adt - bdr \tag{46}$$

Hernandez & Misner (1966) defined the observer time, u, by

$$fdu = adt - bdr \tag{47}$$

where f is an integrating parameter (sometimes called the *lapse function*) to be determined. Inserting (47) into the metric (33) we obtain

$$ds^2 = -f^2du^2 - 2fbdrdu + R_s^2\left(d\theta^2 + \sin^2(\theta)d\phi^2\right) \tag{48}$$

The operators equivalent to (36) and (37) are now

$$D_t = \frac{1}{f}\left(\frac{\partial}{\partial u}\right) \tag{49}$$

$$D_k = \frac{1}{b}\left(\frac{\partial}{\partial r}\right) = 4\pi\rho R_s^2\left(\frac{\partial}{\partial \mu}\right) \tag{50}$$

and the system of Einstein and hydrodynamic equations can be written as (Musco et al., 2005)

$$D_tU = -\frac{1}{1-c_s^2}\left[\frac{\Gamma}{e+p}D_kp + \frac{M}{R_s^2} + 4\pi R_s\rho + c_s^2\left(D_kU + \frac{2U\Gamma}{R_s}\right)\right] \tag{51}$$

$$D_t\rho = \frac{\rho}{\Gamma}\left[D_tU - D_kU - \frac{2U\Gamma}{R_s}\right] \tag{52}$$

$$D_te = \frac{e+p}{\rho}D_t\rho \tag{53}$$

$$D_k f = \frac{f}{\Gamma}\left(D_k U + \frac{M}{R_s^2} + 4\pi R_s \rho\right) \tag{54}$$

$$D_k M = 4\pi R_s^2 \left(e\Gamma - pU\right) \tag{55}$$

where c_s is the sound speed, which is equal to $1/\sqrt{3}$ in the present case, and Γ can be calculated from the constraint equation (45) of from the relation (Musco et al., 2005)

$$\Gamma = D_k R_s - U \tag{56}$$

In order to numerically solve equations (51) to (55) we may start converting them to a set of finite difference equations (see Baumgarte et al., 1995). The description of the calculation method lies beyond the scope of this work (see e.g. Musco et al., 2005; Niemeyer & Jedamzik, 1999a, for more details). Here we will just point out that $f = \Gamma + U$ works as a boundary condition at the surface of the collapsing object and that the synchronization ($D_k R_s \to 0$, $f \to 0$) must be achieved in order to avoid unphysical results (Musco et al., 2005).

The idea is to introduce into the equations, as an initial condition, a density perturbation $\epsilon(R_s)$ superimposed on a uniform background with constant density ϵ_0 and then see the subsequent evolution of that perturbation.

Niemeyer & Jedamzik (1999a) considered three families of curvature perturbations expressed in the form of perturbations on the energy density. The first family of perturbations is described by a Gaussian–shaped overdensity that asimptotically approaches the FRW solution

$$\epsilon(R_s) = \epsilon_0 \left[1 + A \exp\left(-\frac{R_s^2}{2(R_h/2)^2}\right)\right] \tag{57}$$

The second is described by a mexican–hat function

$$\epsilon(R_s) = \epsilon_0 \left[1 + A\left(1 - \frac{R_s^2}{R_h^2}\right)\exp\left(-\frac{3R_s^2}{2R_h^2}\right)\right] \tag{58}$$

and the third by a sixth order polinomial

$$\epsilon(R_s) = \begin{cases} \epsilon_0 \left[1 + \frac{A}{9}\left(1 - \frac{R_s^2}{R_h^2}\right)\left(3 - \frac{R_s^2}{R_h^2}\right)^2\right] & , R_s < \sqrt{3} R_h \\ \epsilon_0 & , R_s \geq \sqrt{3} R_h \end{cases} \tag{59}$$

Here R_h represents the horizon length at the initial time (the instant when the perturbation begins). The amplitude A which appears in all the three families of perturbations, is a free parameter used to tune the initial conditions to sub or super criticality with respect to BH formation. The critical amplitude, A_c, is strongly shape dependent, varying between $A_c = 3.04$ for mexican–hat perturbations and $A_c = 2.05$ for the Gaussian curve (Niemeyer, 1998). The shape of all the three perturbations for the critical case are ilustrated in Figure 4. For the mexican–hat and polynomial perturbations, the excess energy in the overdense region is exactly balanced by the deficit in the outer underdense region,

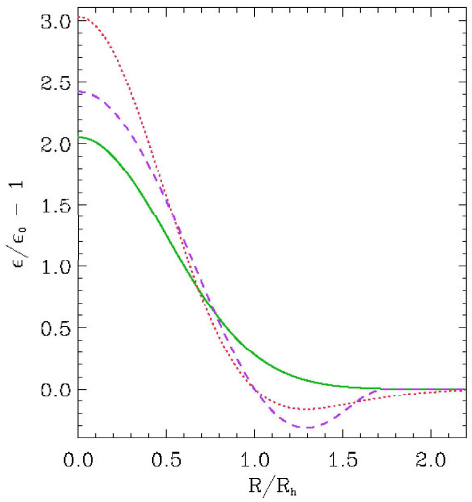

Figure 4: Shapes of the critical perturbations: Gaussian (solid line, equation 57), mexican–hat (dotted line, equation 58), and polynomial (dashed line, equation 59) (Niemeyer & Jedamzik, 1999a).

whereas the Gaussian ones have only an excess, decreasing assimptotically to the background value ϵ_0 (Musco et al., 2005).

Niemeyer & Jedamzik (1999a) finded similar values of δ_c for all the three families of perturbations considered – $\delta_c = 0.67$ (mexican–hat), $\delta_c = 0.70$ (Gaussian), and $\delta_c = 0.71$ (polynomial) – suggesting a universal value of $\delta_c \approx 0.7$. The results were confirmed by Musco et al. (2005) when considering perturbations on length–scales much larger than the horizon scale and well within the linear regime. However when considering growing–mode perturbations (which is more plausible if the fluctuations derive from inflation, Carr (2005)), within the linear regime and with length–scales larger than R_h Musco et al. (2005) encountred very similar curves and almost identical values of γ but substantially different values for the critical threshold ($\delta_c \simeq 0.43$ for mexican–hat perturbations and $\delta_c \simeq 0.47$ for polynomial perturbations).

We will mention also the early study of PBH formation due to Nadezhin et al. (1978) and Novikov et al. (1979) in which they considered metric perturbations rather than density or pressure perturbations. They considered spherically symmetric perturbed regions which communicate with the rest of the Universe via a transition region (see Figure 5).

The perturbation amplitude can be described by R_1 (the value of R_s on the boundary of the perturbed region). The transition region extends over the range $\Delta = R_2 - R_1$ with $R_2 > R_1$. Across Δ the solution gradually matches the external non–perturbed region. The formation of BHs strongly depends on the width of the transition region. If Δ is small enough then steep pressure gradients and hydrodynamic phenomena develop but if Δ is large then pressure

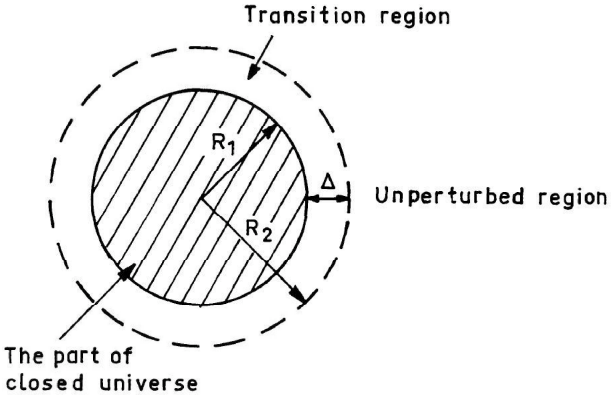

Figure 5: The spherical perturbation and the transition region (Novikov et al., 1979).

gradients are small. The narrower Δ, the greater is the role of pressure gradients that hinder PBH formation. It turns out that PBHs can form only for very large deviations from the Friedmann model which corresponds to $R_1 \approx 0.85-0.9R_{max}$ where $R_{max} = \pi/2$ (Novikov et al., 1979).

In Figure 6 we have the criterion for PBH formation. The moment of time at which a BH arises corresponds to the curve which is tangent to the line $\log(m/r) = 0$ (Novikov et al., 1979). In regions where the expansion is occuring, r increases, but m decreases because of the work of pressure forces. Hence the ratio m/r diminishes during expansion. When the expansion is replaced by contraction the m/r ratio will clearly increase. If the pressure gradient is unable to halt the contraction before m/r reaches 1 (dashed line) a BH will inevitably develop (Nadezhin et al., 1978).

In Figure 7 we have the dependence of the PBH formation on the amplitude of the perturbations and the transition region.

2.4.1 Evolution of super critical perturbations

As an example, we will consider (Musco et al., 2005) the formation of a $0.4415M_H$ PBH from a growing–mode mexican–hat perturbation with $R_0 = 5R_h$ (R_0 is the radius of the overdensity) and $\delta - \delta_c = 2.37 \times 10^{-3}$ at horizon crossing. In Figure 8 we have the evolution of the lapse function f. As $f \to 0$ the redshift of outgoing signals increases and the evolution as seen by a distant observer becomes frozen, corresponding to PBH formation (which occurs only assimptotically).

In Figure 9 we see the behaviour of the fluid worldlines where it is possible to devise the separation between the matter which goes to form the PBH and the matter which continues to expand with the rest of the Universe, as well as the semi–evacuated region being formed between them. Notice that some of the outer material first decelerates but then accelerates again before crossing this

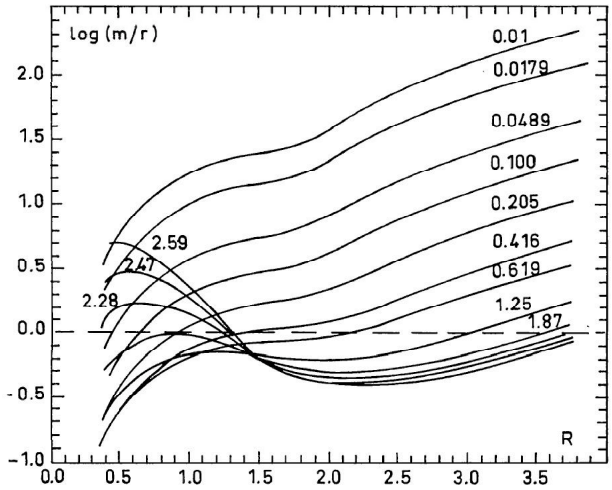

Figure 6: The criterion of BH formation. Different curves correspond to different moments of time. The moment ot time, when the BH arises, corresponds to the curve which is tangent to the line $\log(m/r) = 0$ (Novikov et al., 1979).

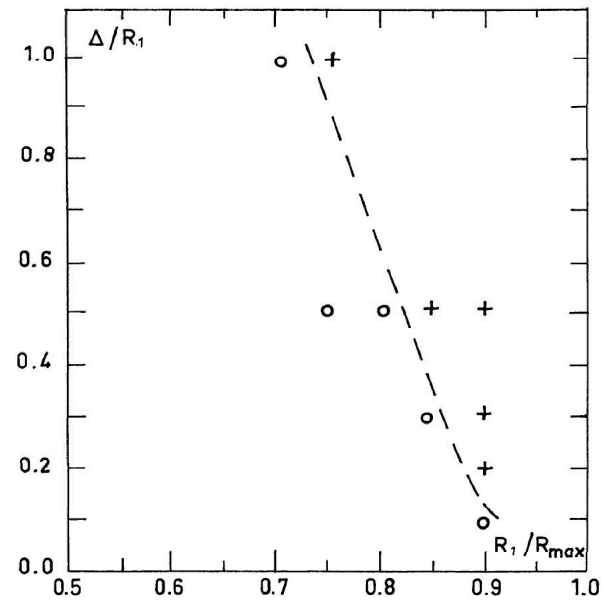

Figure 7: The dependence of the PBH formation on the amplitude R_1 of the perturbation and the transition region. The crosses correspond to the formation of PBHs, the circles correspond to the transmutation of the perturbation into the acoustic wave (Novikov et al., 1979).

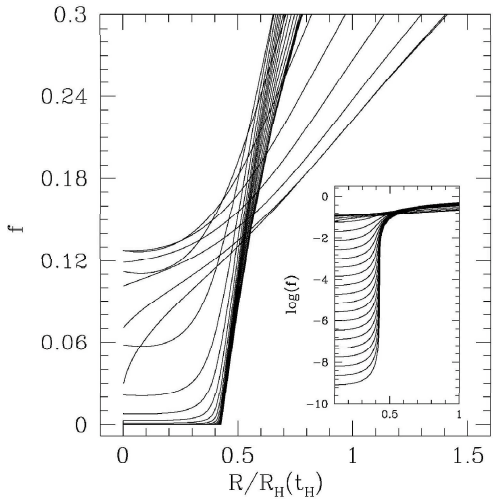

Figure 8: The evolution of the *lapse function*, f, for a mexican–hat perturbation with $\delta - \delta_c = 2.37 \times 10^{-3}$ at the horizon crossing time. The time sequence of the curves goes from bottom to top on the right hand side (Musco et al., 2005).

semi–evacuated region to fall onto the PBH (Musco et al., 2005).

Figure 10 shows the behaviour of the ratio $2m/R_s$ plotted against R_s at successive times. The event horizon corresponds to the asymptotic location of the outermost trapped surface. Remenbering that the BH only forms asymptotically we may introduce as an operational definition for M_{BH} the condition $(1 - 2m/R_s) \leq 10^{-4}$ (Musco et al., 2005).

Finally, Figure 11 shows a plot of m against R_s. Notice that the profiles for m become very flat just outside the BH region at late times. This is a consequence of the very low densities reached there ($< 10^{-4}$ times the background density at the horizon–crossing time) (Musco et al., 2005).

Figures (12), (13), and (14) illustrate further examples of the evolution of slightly supercritical perturbations for the three density perturbation families. The curves display the energy density, ϵ/ϵ_0, at constant proper time, τ, for each mass shell, as a function of the circumferential radius R_s. The initial horizon size, R_h is normalized to unity.

In all cases shown in Figures (12), (13), and (14), a BH with $M_{BH} \approx 0.37 M_H$ forms. The evolution of the three different perturbations exhibits strong similarities: initially, the central overdensity grows in amplitude while the outer underdensity, if present in the initial conditions, gradually widens and levels out. A BH forms in the interior. Some time after the initial formation of an event horizon, material close to the BH but outside the event horizon bounces and launches a compression wave traveling outward. This compression wave is connected to the BH by a rarefaction region that evacuates the immediate

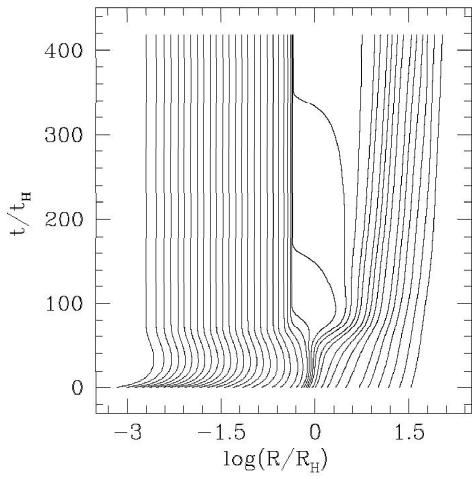

Figure 9: The fluid element worldlines for a mexican–hat perturbation with $\delta - \delta_c = 2.37 \times 10^{-3}$ at the horizon crossing time. The time is measured in units of the horizon–crossing time t_H (Musco et al., 2005).

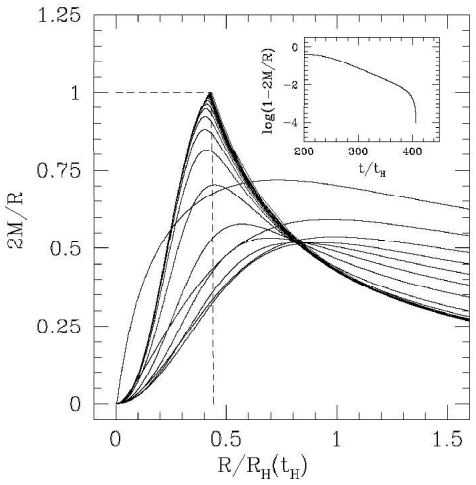

Figure 10: The profile of $2M/R_s$ at different times, with the inset showing the approach of the maximum value of $2M/R_s \to 1$ for a mexican–hat perturbation with $\delta - \delta_c = 2.37 \times 10^{-3}$ at the horizon crossing time. The time sequence of the curves goes from top to bottom on the right hand side (Musco et al., 2005).

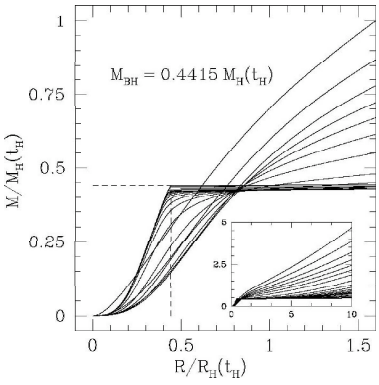

Figure 11: The evolution of the mass–energy for a mexican–hat perturbation with $\delta - \delta_c = 2.37 \times 10^{-3}$ at the horizon crossing time. The time sequence of the curves goes from top to bottom on the right hand side (Musco et al., 2005).

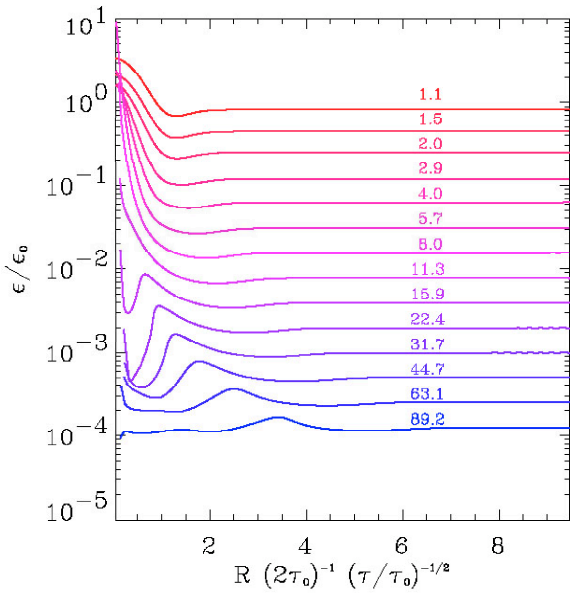

Figure 12: Time evolution of a near–critical mexican–hat perturbation with initial $\delta = 0.6780$. A BH with mass $M_{BH} = 0.37 M_H$ forms in the interior (Niemeyer & Jedamzik, 1999a).

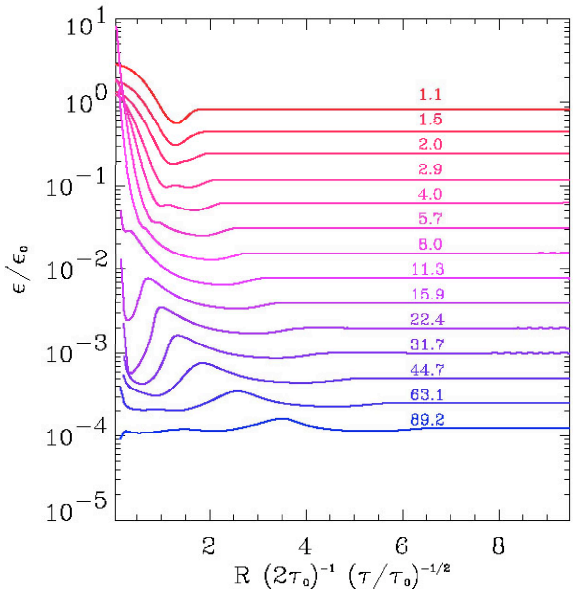

Figure 13: Time evolution of a near–critical polynomial perturbation with initial $\delta = 0.7175$. A BH with mass $M_{BH} = 0.36 M_H$ forms in the interior (Niemeyer & Jedamzik, 1999a).

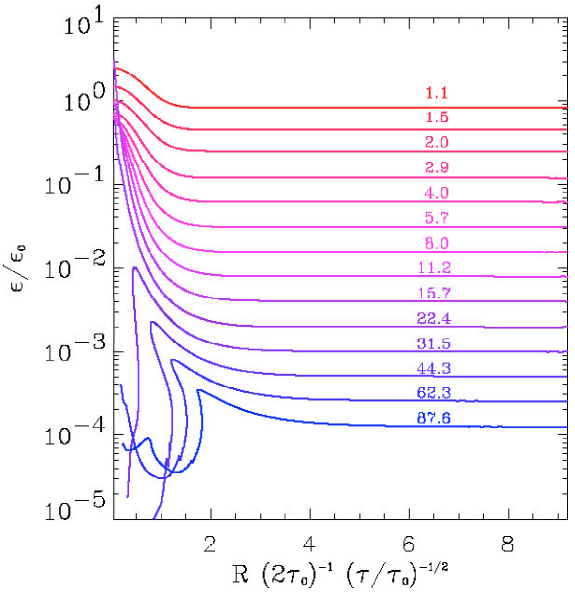

Figure 14: Time evolution of a near–critical Gaussian perturbation with initial $\delta = 0.7015$. A BH with mass $M_{BH} = 0.37 M_H$ forms in the interior (Niemeyer & Jedamzik, 1999a).

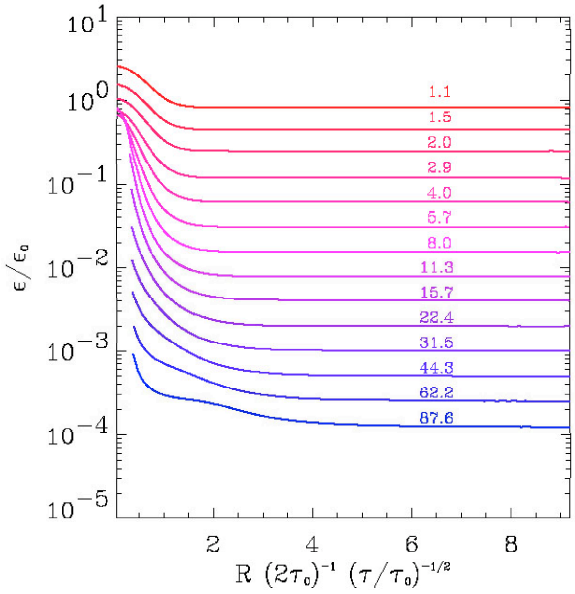

Figure 15: Time evolution of an overcritical Gaussian perturbation with initial $\delta = 0.7196$. A BH with mass $M_{BH} = 2.75M_H$ forms in the interior (Niemeyer & Jedamzik, 1999a).

vicinity of the BH (Niemeyer & Jedamzik, 1999a).

The bounce of material outside the newly formed BH is a feature intrinsic only to BHs very close to the formation threshold ($\delta_c \approx 0.7$). As Figure 15 demonstrates, no bounce occurs if the initial conditions are sufficiently far above the threeshold. In this case a large BH with $M_{BH} = 2.75M_H$ is formed. Here the event horizon reaches further out, encompassing regions where the pressure gradient is smaller, preventing pressure forces from overcoming gravitational attraction (Niemeyer & Jedamzik, 1999a).

Hawke & Stewart (2002) considered another kind of perturbation: the *offset Gaussian curve*. Figures 16 and 17 show the pressure, velocity and mass aspect as function of r at selected times for a supercritical evolution of an initially offset Gaussian perturbation. The initial pressure profile splits into two parts. The part closest to the origin collapses under its own self–gravity. The pressure rapidly grows by four or more orders of magnitude until about $t \approx 4$. The velocity profile is uniformly negative here. Simultaneously, an apparent horizon starts to form, and this is signalled by v falling to $-c$ ($t \approx 4.2$). The matter inside is now trapped.

The other part of the initial profile disperses from the origin. Most of the matter is at the back of the pulse (i.e., closest to the origin), and it disperses with a higher velocity than the rest of the pulse. Initially this pulse is stable and compact. As it travels into the unperturbed region a shock forms because the

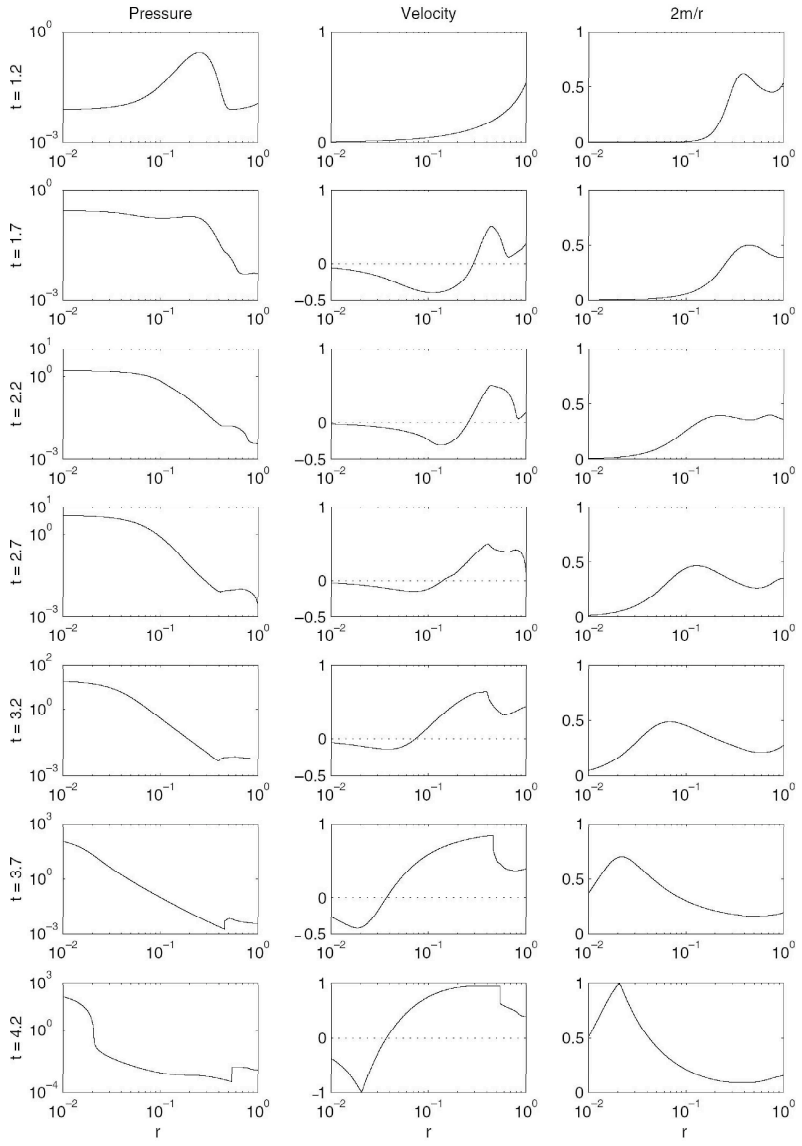

Figure 16: The pressure, velocity and mass aspect as functions of r for selected values of t during a supercritical evolution where the initial pressure profile is an offset Gaussian curve (Hawke & Stewart, 2002).

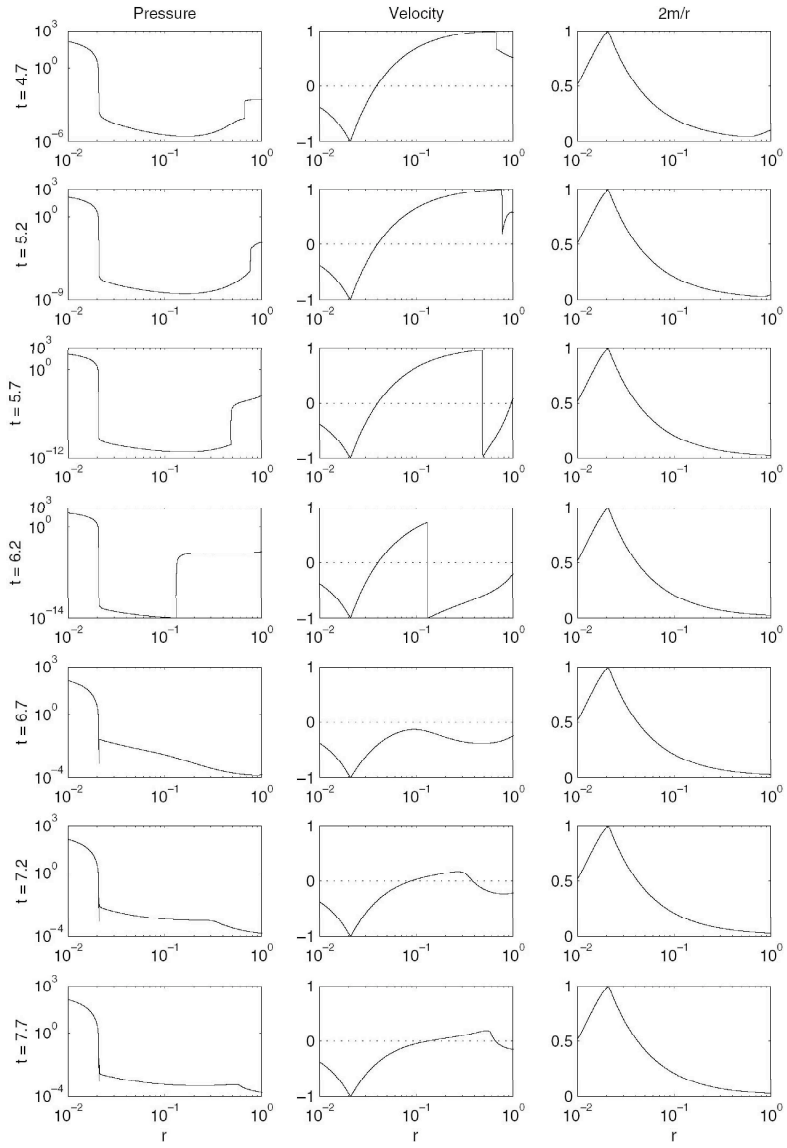

Figure 17: The evolution of Figure 16 continued to later times. The spike in the pressure in the final three plots is not a numerical instability. The apparent horizon has expanded because of the accretion of the infalling shock (Hawke & Stewart, 2002).

pulse moves with a higher velocity than the background material. This occurs between time $t = 4$ and $t = 5$ (Hawke & Stewart, 2002).

In the region between the apparent horizon and the outgoing pulse a void forms. Most of the matter that was formerly in this region has either fallen inside the apparent horizon, or has been washed out by the underlying expansion of the Universe. The pressure in this void may be about 15 orders of magnitude less than that inside the horizon and it is also substantially less than the pressure of the outgoing pulse. In this case, the pressure gradient and the gravitational field of the BH force the outgoing pulse to split again. The majority of the outgoing pulse continues to escape, but some of the matter falls into the BH. As this matter passes through the void a very strong shock forms across which the velocity changes from near c to near $-c$ ($t \approx 5.7$). After the accretion of this matter, the BH very slowly accretes matter from the background, but the relative amount accreted during this last stage appears to be negligible (Hawke & Stewart, 2002).

2.4.2 Evolution of super critical perturbations when $\Lambda > 0$

Let us consider now the effect for PBH formation of including a cosmological constant Λ large enough to affect the dynamics. A cosmological constant is equivalent to a false vacuum with energy density (Musco et al., 2005)

$$\epsilon_v = \frac{\Lambda}{8\pi} \tag{60}$$

and pressure

$$p_v = -\frac{\Lambda}{8\pi} \tag{61}$$

Its effect can be included by adding these terms onto the standard energy density ϵ and pressure p. A positive Λ eventually causes the expansion of the Universe as a whole to start accelerating (this happens when ϵ_v becomes greater than ϵ) and acts against the growth of overdensities. It is convenient to introduce the quantity (Musco et al., 2005)

$$y = \frac{\epsilon_v}{\epsilon_v + \epsilon} = \frac{4}{3}\Lambda M_H^2 \tag{62}$$

where

$$M_H = \frac{4}{3}\pi R_h^3 \left(\epsilon + \epsilon_v\right) \tag{63}$$

and $R_h = 2M_H$. This quantity can be used as a measure of the importance of the Λ term. The qualitative picture of collapses leadind to PBH formation is not changed very greatly by the presence of a Λ term but there are significant differences in the parameters of the scaling law (equation 32). For sufficiently small Λ the parameter γ follows a linear realtionship given by (Musco et al., 2005)

$$\gamma(\Lambda) = \gamma(0) - 8.3y \tag{64}$$

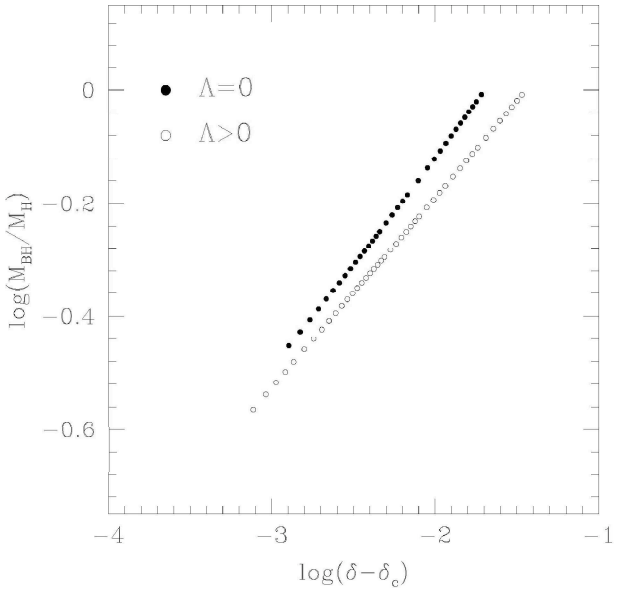

Figure 18: Scaling behaviour for M_{BH} as a function of $\delta - \delta_c$ calculated for growing–mode mexican–hat perturbations specified within the linear regime. The filled circles refer to the case $\Lambda = 0$ and the open circles to the case $\Lambda > 0$ giving $y = 3.0 \times 10^{-3}$ (Musco et al., 2005).

where $\gamma(0)$ is the value of γ when $\Lambda = 0$. The critical amplitude δ_c increases with increasing Λ and follows also a linear relationship (Musco et al., 2005)

$$\delta_c(\Lambda) = \delta_c(0) + 0.98y \tag{65}$$

A positive Λ acts against collapse which means that the PBH masses will be lower and the threshold δ_c will be raised. For a given Λ its influence is greater for larger BH masses than for smaller ones (Musco et al., 2005). Figure 18 shows the scaling behaviour for M_H as a function of the distance $\delta - \delta_c$ for growing–mode mexican–hat perturbations specified within the linear regime considering $\Lambda = 0$ and $\Lambda > 0$.

In Table 3 it is shown the values for γ, K, and δ_c according to various authors (see equation 32). Notice that the value of γ does not depend very significantly of the type of perturbation considered and that the same does not apply to K. Notice also that the critical value δ_c is somewhere between 1/3 (analytical result) and 0.7 (numerical approach).

2.4.3 Evolution of subcritical perturbations

We have a subcritical perturbation when $\delta < \delta_c$. If $\delta \ll \delta_c$ the perturbation initially grows but then it vanishes into the surrounding medium. Near critical perturbations ($\delta <\approx \delta_c$) may have interesting behaviours (Musco et al., 2005).

Table 3: The collapse parameters γ, δ_c and K (see equation 32) obtained from different methods and/or from different density profiles. The references are: (1) Carr (1975), (2) Koike et al. (1995), (3) Niemeyer & Jedamzik (1999a), (4) Hawke & Stewart (2002), (5) Green et al. (2004) and (6) Musco et al. (2005).

Method / Density profile	γ	δ_c	K	Ref.
Analytic	–	$\frac{1}{3}$	–	(1)
Analytic	0.35580192	–	–	(2)
Gaussian perturbation	0.34	0.70	11.9	(3)
Mexican–hat perturbation	0.36	0.67	2.9	(3)
Polynomial perturbation	0.37	0.71	2.4	(3)
Gaussian perturbation	0.35	0.4	–	(4)
Offset Gaussian perturbation	0.36	0.8	–	(4)
Peaks Theory	–	0.3–0.5	–	(5)
Gaussian perturbation	0.36–0.37	0.71	–	(6)
Mexican–hat perturbation	0.36–0.37	0.67	–	(6)
Polynomial perturbation	0.36–0.37	0.71	–	(6)
Mexican–hat perturbation (growing modes)	0.36–0.37	0.43	–	(6)
Polynomial perturbation (growing modes)	0.36–0.37	0.47	–	(6)

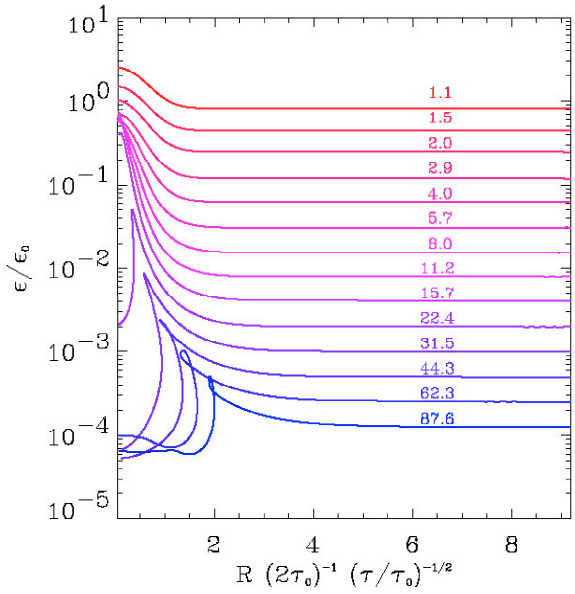

Figure 19: Time evolution of an undercritical Gaussian perturbation with initial $\delta = 0.7006$. No BH is formed (Niemeyer & Jedamzik, 1999a).

In Figure 19 it is shown a situation where no PBH is formed. The initial density perturbation turns into an acoustic wave or wave–package propagating to infinity (Novikov et al., 1979). Rarefaction waves travel from the fitting region toward the center of the disturbance and outward. At a certain epoch the expansion in the inner region is replaced by a contraction. As the contraction proceeds, the pressure gradient rises to the point where the central core is dispersed, and a compression wave travels outward (Nadezhin et al., 1978).

In Figure 20 it is shown the fluid worldlines for a mexican–hat perturbation with $\delta - \delta_c = -3 \times 10^{-3}$. Initially the perturbation grows within the expanding fluid. The contraction is not strong enough to produce a PBH and the fluid bounces out again, expanding until it encounters the surrounding matter which did not participate in the contraction. A compression wave forms where the two regions of fluid meet, while the density becomes very low at the centre of the perturbation. Some matter of the surroundings is sent back into the middle of the rarefaction where it undergoes a second bounce which is much more extreme than the first one (because of the near vacuum state inside the collapsing shell).

The compression wave formed by the second bounce propagates out into the surrounding medium following the first one. Both proceed to damp geometrically and eventually the medium returns to a uniform state. Additional bounces are expected for δ closer to δ_c. No PBH is formed (Musco et al., 2005).

Figures 21 and 22 show the pressure, velocity and mass aspect as functions of r at selected times for a subcritical evolution of an offset Gaussian perturbation.

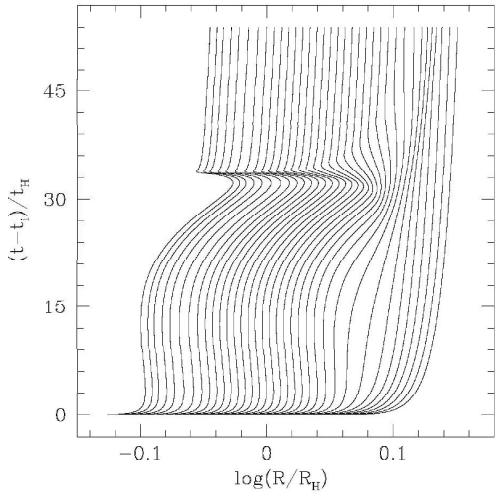

Figure 20: Worldlines for a mexican–hat undercritical perturbation $\delta - \delta_c = -3.0 \times 10^{-3}$. The plot shows alternating collapse and expansion of the perturbed region while the outer material continues to expand uniformly (Musco et al., 2005).

For the subcritical evolution the initial pressure profile again splits into two parts. The outer part disperses as before. The part closest to the origin is initially held by its own self–gravity. However, this is insufficient to maintain its position and it soon disperses, leaving a void near the origin where the pressure drops by around ten orders of magnitude ($t \approx 4.5$). Once again the pressure gradient caused by the formation of this void leads to some of the outgoing material being drawn back in an infalling shock. The amount of matter in the infalling shock is comparable to the supercritical case. This indicates that the amount of accreted matter appears to be independent of the BH mass. This fills the void and reflects from the origin, leaving the FRW background (Hawke & Stewart, 2002).

This behaviour is also shown in the evolution of the velocity profile. The dispersion of the fluid near the origin which occurs between $t = 4$ and $t = 5$ is signalled by the positive velocity near the origin. This grows to form the large outgoing pulse. The infalling shock appears as the large change in velocity at around $t \approx 6$ in the centre of the grid (Hawke & Stewart, 2002).

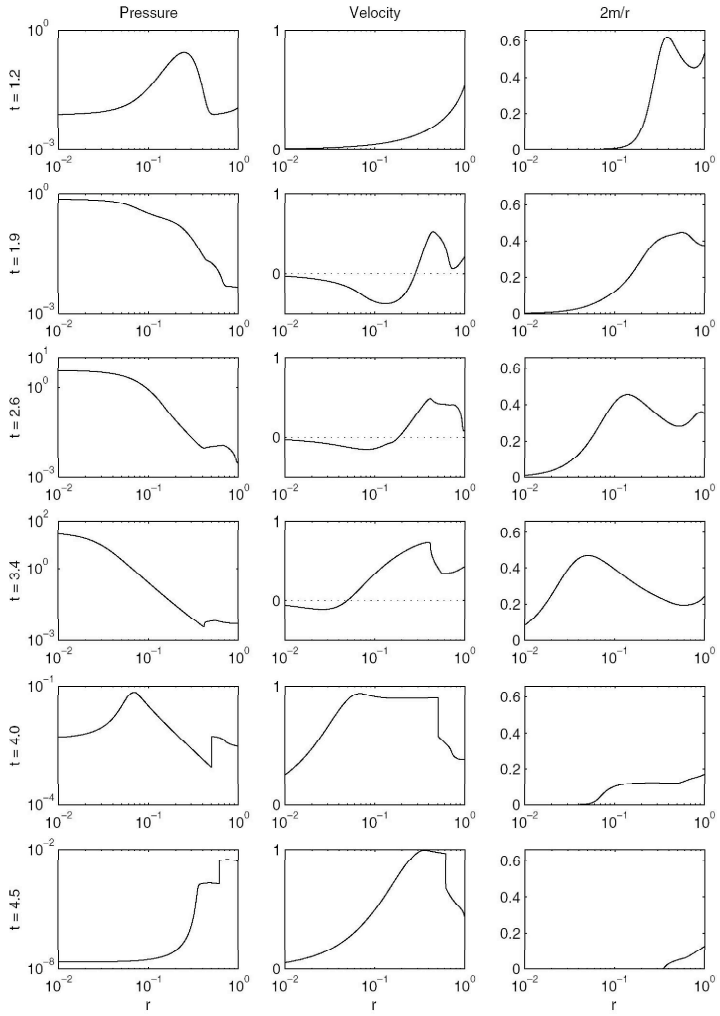

Figure 21: The pressure, velocity and mass aspect as functions of r for selected values of t during a subcritical evolution where the initial pressure profile is an offset Gaussian curve (Hawke & Stewart, 2002).

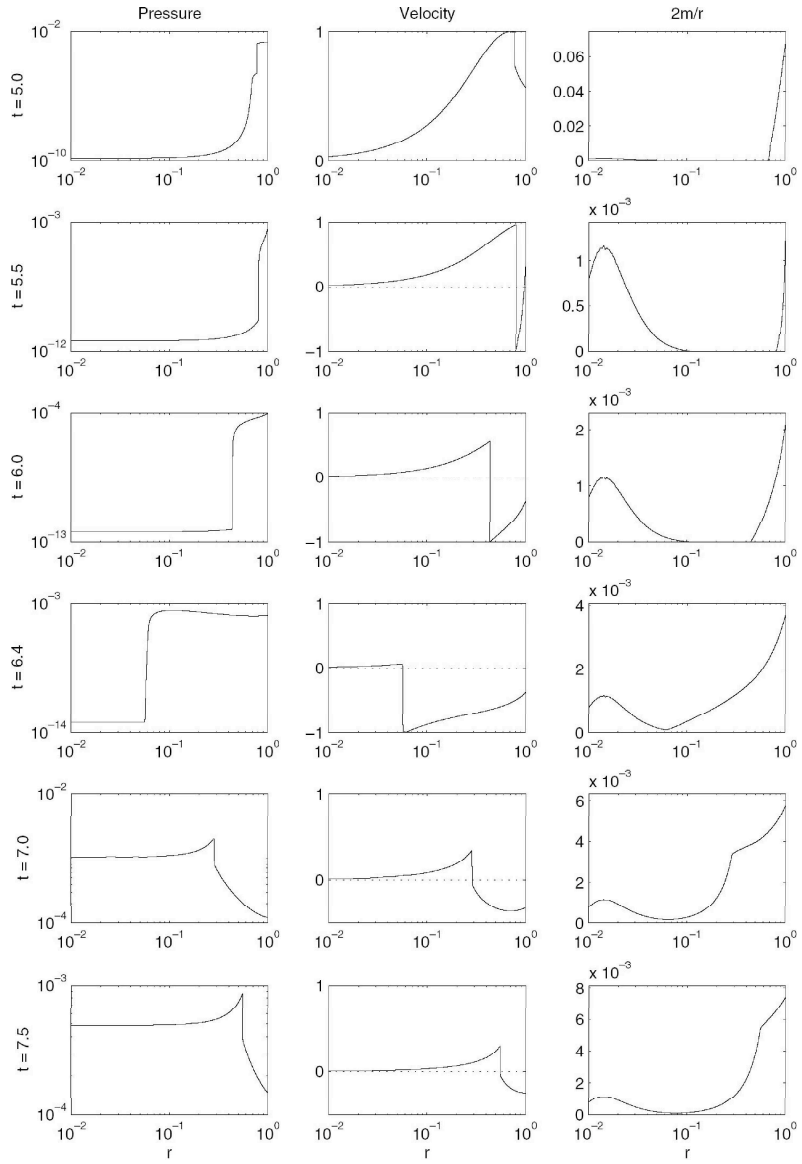

Figure 22: The evolution of Figure 21 continued to later times (Hawke & Stewart, 2002).

3 The probability of PBH formation

If one wants to determine the PBH density in the Universe at the present time, one must be able to evaluate the fraction of the universe going into PBHs at a given epoch. For that we need to know the mass variance (mass dispersion) in the Universe at that particular epoch besides the shape of the primordial fluctuations spectrum.

A correct evaluation of the mass variance in the universe when the PBH forms is crucial. The calculus involves a suitable window function that smoothes the density contrast and a transfer function which takes into account the dynamics of the fluctuations after horizon–entry.

3.1 The primordial power spectrum

The primordial power spectrum of the density contrast is operationally deffined by (e.g. Blais et al., 2003)

$$P(k) = \left\langle |\delta_k|^2 \right\rangle \tag{66}$$

where the brackets can be taken as representing classical averages over small regions of k–space. In fact the brackets refer to quantum expectation values, but as it was already mentioned (Section 2.1) as long as we are interested in PBHs that form for $t \geq 10^{-23}$s then, due to an effective quantum–to–classical transition, it is sufficient to deal with classical averages. The fluctuations as well as their Fourier transforms are all classical stochastic quantities and the power spectrum can be treated as a classical power spectrum (Polarski, 2001).

Notice that what is meant by primordial power spectrum is the power spectrum on *superhorizon scales* (scales much bigger than the Hubble radius for which $k \ll aH$). On these scales, the scale dependence of the power spectrum is unaffected by cosmic evolution. On subhorizon scales this is not the case. For such scales the power spectrum $P(k)$ must involve convolution with a *Transfer Function* $T(k,t)$ (Blais et al., 2003, Section 3.3).

Let us introduce here the quantities $\delta_H^2(k,t)$ and $k^3\phi^2(k,t)$, where ϕ denotes the gauge–invariant gravitational potential, defined as (Bringmann et al., 2002)

$$\delta_H^2(k,t) = \frac{(RH)^4}{k^4}\frac{k^3}{2\pi^2}P(k,t) = \frac{2}{9\pi^2}k^3\phi^2(k,t) \tag{67}$$

which have the peculiarity of being time independent on superhorizon scales being equal in very good approximation to their value at the horizon crossing time t_k. At the horizon crossing time ($t = t_k$ and $k = RH$) we have that

$$\delta_H^2(k,t_k) = \frac{k^3}{2\pi^2}P(k,t_k) = \frac{2}{9\pi^2}k^3\phi^2(k,t_k) \tag{68}$$

Following the literature we will introduce here also the quantity $F(k)$ defined at the horizon crossing time as (e.g. Blais et al., 2003)

$$k^3\phi^2(k,t_k) = \frac{4}{9}F(k) \tag{69}$$

valid as long as $t_e \ll t_k \ll t_{eq}$. The quantity $k_0^3\phi^2(k_0,t_0)$, or equivalently $\delta_H^2(k_0,t_0)$ (where the subscript 0 stands for a quantity evaluated at present time) at the present Hubble radius scale can be derived using the large angular scale CMB anisotropy data. It is that quantity that comes from observations which fixes the overall amplitude of the fluctuations spectrum.

Since the primordial power spectrum is an unknown function one is forced to parametrize it (see e.g. Bridle et al., 2003). The simplest models of inflation predict a *power–law primordial power spectrum* (see Sections 4.1, 4.2 and 4.4). However there are also viable models of inflation which predict primordial power spectra which cannot be parametrized by a simple power law. That is the case of the *Broken scale invariance power spectrum* (see Section 4.3). Mukherjee & Wang (2003) have considered a model independent approach and have shown that, with the present WMAP data, the shape of the reconstructed power spectrum is consistent with scale–invariance, although it allows some indication of a preferred scale at $k \sim 0.01$ Mpc^{-1} ($\sim 10^{-25}$ m^{-1}).

3.2 The fraction of the universe going into PBHs

If the primordial fluctuations obey a Gaussian statistics then the probability P_δ that a spherical region of initial mass m has a density contrast in the range $[\delta, \delta + d\delta]$ will also obey a Gaussian statistics (e.g. Green et al., 2004). Thus we may write (Carr, 1975)

$$P_\delta d\delta = \frac{1}{\sqrt{2\pi}\sigma(m)} \exp\left(-\frac{\delta^2}{2\sigma^2(m)}\right) d\delta \tag{70}$$

which represents a Gaussian normal distribution about zero with standard deviation or mass variance $\sigma(m)$. We may write also $\sigma(m)$ as $\sigma(r)$ where r represents the radius of a spherical region containing the mass M in its interior. The probability $\beta(M_H)$ that a region of comoving size $r = (RH)^{-1}_{t=t_k} = (ck)^{-1}$ (see equation 24) has an averaged density contrast at horizon crossing in the range $\delta_c \leq \delta \leq \delta_{max}$, which is the condition for PBH formation (Section 2.2), is given by (e.g. Bringmann et al., 2002)[2]

$$\beta(M_H) = \frac{1}{\sqrt{2\pi}\sigma(t_k)} \int_{\delta_c}^{\delta_{max}} exp\left(-\frac{\delta^2}{2\sigma^2(t_k)}\right) d\delta \tag{71}$$

where

$$\sigma^2(t_k) = \sigma^2(k) = \sigma^2(r)\big|_{t=t_k} \tag{72}$$

If $\delta_c \gg \sigma(t_k)$ and $\delta_{max} - \delta_c \gg \sigma(t_k)$ we have the approximation (e.g. Bringmann et al., 2002)

$$\beta(M_H) \approx \frac{\sigma(t_k)}{\sqrt{2\pi}\delta_c} \exp\left(-\frac{\delta_c^2}{2\sigma^2(t_k)}\right) \tag{73}$$

[2]Taking into account that M_H represents the horizon mass evaluated at the instant t_k when the fluctuation with wavenumber k crosses the horizon we may write also $\beta(t_k)$ or $\beta(k)$ meaning exactly the same as $\beta(M_H)$. The idea applies also to other quantities (e.g. mass variance).

The value of $\beta(M_H)$ is usually interpreted as giving the probability that a PBH will be formed with a mass $M_{PBH} \geq M_H(t_k)$. Strictly speaking this is not true, since β does not take into account those regions that are underdense on a scale M_H, but nevertheless overdense on some larger scale. In the *Press–Schechter formalism* this seems to be taken care (in some models) by multiplying β with a factor 2. Fortunately, in most cases, β is a very rapidly falling function of mass, so this effect can be neglected. In this case $\beta(M_H)$ does give the probability for PBH formation and thus also the mass fraction of the regions that will evolve into PBHs of mass greater or equal to M_H at time t_k (Blais et al., 2003; Bringmann et al., 2002).

Remenber that for the smallest scales we cannot speak anymore about classical fluctuations (see Section 2.1) and that is why the equations (70), (71) and (73) do not apply anymore on that case. As it was mentioned for all PBHs produced after approximately 10^{-23}s, the quantum–to–classical transition is already extremely effective which means that one can really work to tremendously high accuracy with classical probability distributions (Polarski, 2001).

3.3 The mass variance

The main problem in calculating the production rate for PBHs is the correct evaluation of $\sigma(r)$ at a given epoch (e.g. Blais et al., 2003; Green & Liddle, 1997). The mass variance can be generically written as (e.g. Liddle & Lyth, 1993; Longair, 1998)

$$\sigma^2(r) = \left\langle \left(\frac{\delta M}{M} \right)_r^2 \right\rangle = \frac{1}{(2\pi)^3} \int_0^\infty P(k) d^3k \tag{74}$$

where $P(k)$ is the power spectrum averaged over a small region of k–space. As long as we are interested in $t \geq 10^{-23}$s it will be sufficient to consider classical averages due to the quantum–to–classical transition (Section 2.1). Assuming spherical symmetry, the volume element of k–space d^3k turns out to be $4\pi k^2 dk$ and we are left with

$$\sigma^2(r) = \frac{1}{2\pi^2} \int_0^\infty k^2 P(k) dk \tag{75}$$

If we want to examine specific mass ranges, we have to smooth the density distribution, introducing a suitable window function W (e.g. Green & Liddle, 1997). Different window functions have been proposed in the literature, namely the top–hat window function (e.g. Blais et al., 2003) and the Gaussian window function (e.g. Green et al., 2004).

The choice of a suitable window function turns out to be a very important problem. It must be done in accordance with the results one uses. For example, if one uses $\delta_c \approx 0.7$ as found by Niemeyer & Jedamzik (1999a) then one must also use the top–hat window function in order to be consistent with their numerical results (Bringmann et al., 2002).

Despiste the fact that a Gaussian window would be more convenient for theoretical calculations (e.g. Liddle & Lyth, 1993) it would erroneously yeld too

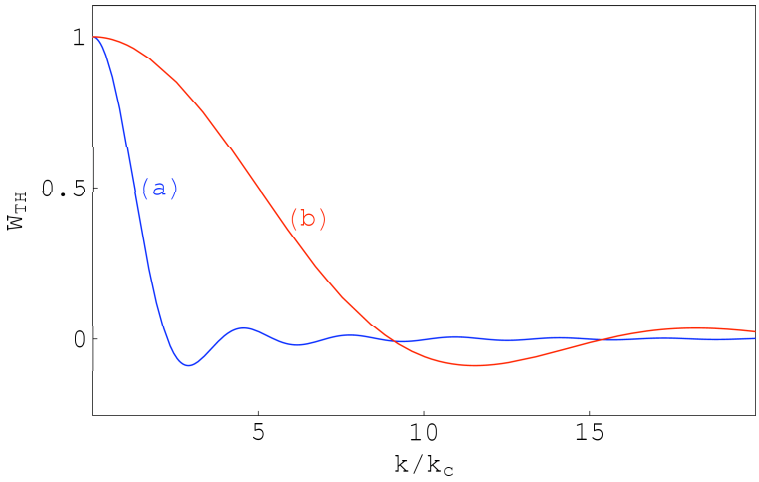

Figure 23: The Fourier transform of the top–hat window function (equation 76) with (a) $r = 2k_c$ and (b) $r = k_c/2$ where k_c is an arbitrary wavenumber.

small values for the mass variance (Blais et al., 2003). Actually the top–hat window function is accepted as the most physical choice to study the formation of PBHs. With this choice the smoothed density contrast δ describes directly the average density contrast in the region relevant to PBH formation (Blais et al., 2003), i.e., it is sensitive to scales well within the horizon (Green et al., 2004). Thus, we will addopt a top–hat window function. The Fourier transform of the top–hat window function divided by the probed volume $V_W = \frac{4}{3}\pi r^3$ is given by (e.g. Blais et al., 2003; Bringmann et al., 2002)

$$W_{TH}(kr) = \frac{3}{(kr)^3}\left(\sin(kr) - kr\cos(kr)\right) \tag{76}$$

In Figure 23 we have examples of typical curves for the window function defined by equation (76). The mass variance can now be rewritten in order to accomodate (76) as (e.g. Blais et al., 2003; Bringmann et al., 2002)

$$\sigma^2(r) = \frac{1}{2\pi^2}\int_0^\infty k^2 W_{TH}^2(kr)P(k)dk \tag{77}$$

There is a natural upper cut–off in k–space for the power spectrum, namely k_e, corresponding to the Hubble radius at the end of inflation t_e. In fact the smallest scale generated by inflation (Blais et al., 2003). The lower limit can be taken zero if we assume that the number of e–folds during inflation (cf. equations (4) and (5)) amply solves the cosmological horizon problem (Bringmann et al., 2002). Thus we will rewrite equation (77) as

$$\sigma^2(r) = \frac{1}{2\pi^2}\int_0^{k_e} k^2 W_{TH}^2(kr)P(k)dk \tag{78}$$

Considering that k represents the scale entering the horizon at time t_k and that k' represents all scales, i.e $0 \leq k' \leq k_e$ we will introduce here the variable $x = k'/k$ such that $0 \leq x \leq k_e/k$ and $x = 1$ at horizon crossing. Considering this variable change, equation (78) becomes

$$\sigma^2(r) = \frac{1}{2\pi^2} \int_0^{\frac{k_e}{k}} k^3 x^2 W_{TH}^2(x) P(kx) dx \tag{79}$$

Considering the same variable change in equation (67) we have that

$$P(kx, t) = \frac{2\pi^2 kx}{(RH)^4} \delta_H^2(kx, t) \tag{80}$$

Inserting this into equation (79) we have

$$\sigma^2(r) = \int_0^{\frac{k_e}{k}} \frac{k^4 x^3}{(RH)^4} \delta_H^2(kx, t) W_{TH}^2(x) dx \tag{81}$$

But we are interested in the instant $t = t_k$ when the fluctuation with wavenumber k enters the horizon. Thus, inserting (24) into equation (81) we have that

$$\sigma^2(k) = \int_0^{\frac{k_e}{k}} x^3 \delta_H^2(kx, t_k) W_{TH}^2(x) dx \tag{82}$$

With the help of the relation (69) we can write (82) also in the form

$$\sigma^2(k) = \frac{8}{81\pi^2} \int_0^{\frac{k_e}{k}} x^3 F(kx) W_{TH}^2(x) dx \tag{83}$$

On superhorizon scales ($ck \ll RH$) the scale dependence of the power spectrum is unnafected by cosmic evolution. However on subhorizon scales the power spectrum must involve convolution with a Transfer function $T(k, t)$ (e.g. Blais et al., 2003) appropriate to the type of perturbation (i.e. adiabatic or isocurvature perturbations [3]).

The transfer function must be taken at the time t_k of interest and not today. That is because at each stage of the cosmological evolution, the correct use of the transfer function takes into account the dynamics of the fluctuations after horizon–entry. This leads effectivelly to very different spectra on small scales at different times. The transfer function is defined through (Blais et al., 2003)

$$T^2(k, t) = \frac{P(k, t)}{P(k, t_u)} \frac{P(0, t_u)}{P(0, t)} \tag{84}$$

where t_u represents some initial time when all scales are outside the Hubble radius, i.e., when $ck < RH$. Taking as a reference the end of inflation we will

[3] Isocurvature perturbations correspond to perturbations in the local equation of state, while adiabatic perturbations correspond to perturbations in the local energy density, and thus the local curvature. However at the time of PBH creation (which corresponds to the time we need to evaluate the transfer function) the fluctuations can be classified as either adiabatic or isocurvature (Chisholm, 2006).

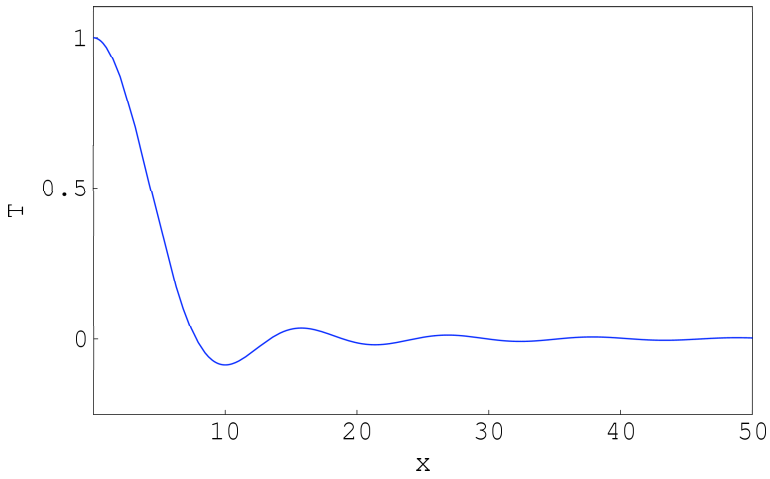

Figure 24: The transfer function (equation 85) as a function of $x = k/k_c$ where k_c is some arbitrary wavenumber.

consider $t_u = t_e$. Notice that when $k \to 0$ (superhorizon scales) we have that $T(k,t) \to 1$ as expected. The transfer function can be computed analytically yelding (Blais et al., 2003)

$$T^2(kx, t_k) = W_{TH}^2(c_s x) = W_{TH}^2\left(\frac{x}{\sqrt{3}}\right) \tag{85}$$

where $c_s = 1/\sqrt{3}$ denotes the speed of sound in the radiation dominated era. We see that actually $T^2(kx, t_k)$ does not depend on the wavenumber k. This will be true for scales very deep inside the radiation era ($t_e \ll t_k \ll t_{eq}$, $k_e \gg k \gg k_{eq}$), which are the ones we are interested in (Blais et al., 2003). In Figure 24 it is represented the characteristic curve for the transfer function (85). We are now in position to write an accurate general formula for the mass variance valid when the fluctuation with wavenumber k enters the horizon (Blais et al., 2003)

$$\sigma^2(k) = \frac{8}{81\pi^2}\int_0^{\frac{k_e}{k}} x^3 F(kx) W_{TH}^2(x) W_{TH}^2(c_s x) dx \tag{86}$$

It may be useful to consider the following relation where all the quantities are evaluated at the time t_k (Blais et al., 2003; Bringmann et al., 2002)

$$\sigma^2(t_k) = \alpha^2(k)\delta_H^2(k, t_k) \tag{87}$$

with the function $\alpha(k)$ given by (e.g. Blais et al., 2003)

$$\alpha^2(k) = \int_0^{\frac{k_e}{k}} x^3 \frac{\delta_H^2(kx)}{\delta_H^2(k)} W_{TH}^2(x) W_{TH}^2(c_s x) dx \tag{88}$$

or, equivalently (e.g. Polarski, 2002)

$$\alpha^2(k) = \int_0^{\frac{k_e}{k}} x^3 \frac{F(kx)}{F(k)} W_{TH}^2(x) W_{TH}^2(c_s x) dx \tag{89}$$

It is crucial to distinguish both quantities $\sigma^2(t_k)$ and $\delta_H^2(k, t_k)$. As seen from equation (87) the quantity $\sigma^2(t_k)$, which depends on the averaging, is correctly related to the non–averaged quantity $\delta_H^2(k, t_k)$ in a non–trivial way by means of the function $\alpha(k)$. The quantity $\delta_H^2(k, t_k)$ can be reconstructed at the time t_k from its present value $\delta_H^2(k_0, t_0)$. This is not the case for the quantity $\sigma^2(t_k)$ because the deformation of the power spectrum is different at the time t_k and today (Polarski, 2002).

The problem in evaluating $\alpha(k)$ comes from the evolution of the perturbations for scales k' inside the Hubble radius: $k = RH \leq k' \leq k_e$ or equivalently $1 \leq x \leq \frac{k_e}{k}$. This small scale evolution is encoded in the transfer function $T(k, t)$. Clearly, an accurate value of $\alpha(k)$ can be obtained only numerically and with an explicit knowledge of $T(k, t)$ (Bringmann et al., 2002).

It is clear at this point that the problem in evaluating $\beta(k)$ is transfered to the evaluation of the function $\alpha(k)$. Knowing $\alpha(k)$ (equation 88) it is straightforward to find $\sigma(k)$ (equation 87) and $\beta(k)$ (equation 71) as long as we have the needed observational input and a suitable expression for the primordial power spectrum $P(k)$.

3.4 Mass variance in the presence of Λ

Recent supernovae observations strongly suggest that we live in a presently accelerating universe, i.e., in a universe with a positive *Cosmological Constant* Λ (e.g. Polarski, 2002). The total matter density value is (e.g. Spergel et al., 2006)

$$\Omega_{m,0} = \frac{\rho_{m,0}}{\rho_{cr,0}} \approx 0.24 \tag{90}$$

and the dark energy density is (e.g. Polarski, 2002; Spergel et al., 2006)

$$\Omega_{\Lambda,0} = \frac{\Lambda}{3H_0^2} = 1 - \Omega_{m,0} \approx 0.76 \tag{91}$$

For a correct calculation of the mass variance at early times we must take into account the existence of a $\Lambda > 0$. However as long as we are interested in times $t_k \ll t_{eq}$ and in universes where Ω_Λ domination occurs late it turns out that the transfer function at time t_k does not depend on Λ and the same must apply therefore to the quantity $\alpha(k)$ (Polarski, 2002).

Thus, we can conclude that the influence of a cosmological constant on the mass variance $\sigma(k)$ and consequently on the probability $\beta(k)$ comes solely from its influence on the quantity $\delta_H^2(k, t_k)$ (cf. equation 87, Polarski (2002)). It can be shown that in a flat universe, a cosmological constant with $\Omega_{\Lambda,0} \approx 0.7$ will

have the effect of decreasing the mass variance $\sigma(k)$ in about 15%, (see Polarski (2002) for more details)

$$\sigma^2(t_k)\left|_{\Omega_{\Lambda,0}=0.7} \simeq 0.85\sigma^2(t_k)\right|_{\Omega_{m,0}=1} \tag{92}$$

When dealing with a flat universe with $\Omega_{m,0} < 1$, we have the relation (Polarski, 2002)

$$\delta_H^2(k_0, t_0) = \frac{k_0^3}{2\pi^2} P(k_0, t_0) = \frac{2}{9\pi^2}\Omega_{m,0}^{-2} k_0^3 \phi^2(k_0, t_0) \tag{93}$$

where all quantities are evaluated at the present time t_0. In the following sections, unless information in contrary, we will be considering that $\Omega_{\Lambda,0} \approx 0.76$.

4 Reconstructing the primordial spectrum

The simplest models of inflation predict a scale–free power law primordial spectrum (Section 4.1). Although this kind of spectrum explains quite well the formation of LSS, according to it the fraction of the Universe going into PBHs is pratically zero (Section 5.1).

If we want to keep the hyphothesis of PBH formation we must consider a spectrum with more power in the smaller scales. Thus we have introduced the scale–free power spectrum with a pure step (Section 4.2), which is a phenomenological variant of the scale–free power law spectrum, and in a more natural basis the Broken Scale Invariance spectrum which cannot be parametrized by a simple power law (Section 4.3). A very promissing spectrum is the so called running–tilt power spectrum (Section 4.4) which relays in recent observations of the anisotropy on the CMB.

4.1 Scale–free power law spectrum

The fact that gravity does not have a characteristic scale, leads us to postulate for the fluctuations a power–law spectrum (e.g. Combes et al., 2002; Bringmann et al., 2002; Green & Liddle, 1997; Longair, 1998)

$$P(k,t) = A(t)k^n \tag{94}$$

where n is the so called *spectral index* and $A(t)$ is a function of time. The simplest case for the power spectrum, which is usually considered, is the one which is *scale–free*, i.e., the case where n is equal to a constant. This choice is made in the assumption that the spectrum of the initial fluctuations must have been very broad with no prefered scales (e.g. Longair, 1998).

Harrison (1970) and Zeldovich (1970) argued that in order to explain the development of primordial fluctuations into protogalaxies, n must exactly, or very closely, equal unity and that we should have at the horizon crossing time

$$P(k,t_k) \sim k^{-3} \tag{95}$$

That is because in that case the density contrast $\delta(m)$ has the same amplitude on all scalles when the perturbations came throuhg the horizon (e.g. Carr, 1975; Longair, 1998; Combes et al., 2002). When $n = 1$, the power spectrum (94) is called the *Harrison–Zeldovich Spectrum* (e.g. Longair, 1998). In this particular case when the fluctuation enters the horizon we have (e.g. Bringmann et al., 2002)

$$A(t_k) \sim k^{-4} \tag{96}$$

In the more general case we may write the power spectrum as (e.g. Narlikar, 2002)

$$P(k,t_k) \sim k^{n-4} \tag{97}$$

The value of the constant of proportionality in equation (97) depends on the kind of universe we are dealing with (radiation dominated universe or matter dominated universe). Thus, we may write the power spectrum (97) as

$$P(k,t_k) = \Gamma^2(\theta)k^{n-4} \tag{98}$$

where $\Gamma(\theta)$ is a function of the adiabatic index θ (see equation 2) given by the expression (see Liddle & Lyth (1993) for more details)

$$\Gamma(\theta) = \frac{2(1+\theta)}{5+3\theta} \tag{99}$$

In the case of a radiation dominated universe ($\theta = 1/3$) we have $\Gamma(1/3) = 4/9$ and in the case of a matter dominated universe ($\theta = 0$) we have $\Gamma(0) = 2/5$. We can now relate, with the help of equations (98), (99) and (67) the value of $\delta_H(k_r)$ evaluated at some instant during the radiation dominated era with the value of $\delta_H(k_c)$ evaluated at some instant t_{k_c}, where k_c is some suitable pivot scale. Doing so we obtain the following result

$$\delta_H^2(k_r,t_{k_r}) = \Theta^2(k_c)\delta_H^2(k_c,t_{k_c})\left(\frac{k_r}{k_c}\right)^{n-1} \tag{100}$$

where we have considered

$$\Theta(k_c) = \frac{\Gamma(\frac{1}{3})}{\Gamma(\theta_{k_c})} = \begin{cases} \frac{10}{9} & k_c < k_{eq} \\ 1 & k_c \geq k_{eq} \end{cases} \tag{101}$$

The amplitude of the density perturbation spectrum at some pivot scale k_c is given, according to WMAP observations, by (e.g. Easther, 2005; Verde et al., 2003)

$$\delta_H^2(k_c) = \left(\frac{5}{3}\right)^2 \frac{800\pi^2}{T^2}A(k_c) \tag{102}$$

where T is the CMB temperature in units of μK (i.e., $T = 2.725 \times 10^6\ \mu K$ – (e.g. Verde et al., 2003)) and $A(k_c)$ is the normalization of the amplitude at the pivot scale k_c. Inserting the CMB temperature into equation (102) we obtain (e.g. Easther, 2005)

$$\delta_H^2(k_c) = 2.95 \times 10^{-9}A(k_c) \tag{103}$$

Two important pivot scales often used are the one corresponding to the present ($k_c = k_0$) for which equation (100) becomes (Bringmann et al., 2002)

$$\delta_H^2(k_r,t_{k_r}) = \left(\frac{10}{9}\right)^2 \delta_H^2(k_0,t_{k_0})\left(\frac{k_r}{k_0}\right)^{n-1} \tag{104}$$

and the one corresponding to the last scatering surface ($k_c = k_{eq}$) for which equation (100) becomes (e.g. Düchting, 2004)

$$\delta_H^2(k_r,t_{k_r}) = \delta_H^2(k_{eq},t_{k_{eq}})\left(\frac{k_r}{k_{eq}}\right)^{n-1} \tag{105}$$

Another pivot scale that have been used more recently is $k_c = 0.002\text{Mpc}^{-1} \approx 6.5 \times 10^{-26}\text{m}^{-1}$ (e.g. Spergel et al., 2003). It may be useful to relate the value of $\delta_H^2(k_0, t_{k_0})$ with the value of $\delta_H^2(k_c, t_{k_c})$ where k_c represents some pivot scale in the past. Remenbering that for a scale–free power law spectrum n is a constant and considering that $k_c < k_{eq}$ (i.e. considering k_c within the matter dominated stage) we have from equations (100) and (104) that

$$\delta_H^2(k_0, t_{k_0}) = \delta_H^2(k_c, t_{k_c}) \left(\frac{k_0}{k_c}\right)^{n-1} \tag{106}$$

It is clear from equations (100), (104) or (105) that in the case of a scale–free power spectrum the quantity δ_H behaves at horizon crossing like (e.g. Bringmann et al., 2002)

$$\delta_H^2(k, t_k) \propto k^{n-1} \tag{107}$$

or, equivalently, like

$$k^3 \phi^2(k, t_k) \propto k^{n-1} \tag{108}$$

Noticing, with the help of equation (104), that in the case of a scale–free power law spectrum we have

$$\frac{\delta_H^2(kx)}{\delta_H^2(k)} = x^{n-1} \tag{109}$$

we can write the function $\alpha(k)$ (equation 88) in the form (e.g. Blais et al., 2003)

$$\alpha^2(k) = \int_0^{\frac{k_e}{k}} x^{n+2} W_{TH}^2(x) W_{TH}^2(c_s x) dx \tag{110}$$

The mass variance $\sigma(k)$ can be determiend with the help of equation (87) with $\alpha(k)$ given by equation (110) and δ_H given by equation (104). It may be useful to express the mass variance in terms of masses instead of wavenumbers. Making use of equations (24), (8), (9), (11) and (12) we have that

$$\frac{k}{k_0} = \frac{R(t_k)H(t_k)}{R(t_0)H(t_0)} = \frac{3}{4}\left(\frac{t_0}{t_{eq}}\right)^{1/3}\left(\frac{t_{eq}}{t_k}\right)^{1/2} \tag{111}$$

Taking now into account that $M_H(t) \sim t$ (cf. equation 17) and considering the result (111), equation (104) and equation (87) it turns out that the mass variance can be written as (e.g. Blais et al., 2003; Bringmann et al., 2002)

$$\sigma^2(t_k) = \frac{100}{81}\alpha^2(k)\delta_H^2(t_0)\left(\frac{3}{4}\right)^{n-1}\left[\frac{M_H(t_0)}{M_H(t_{eq})}\right]^{\frac{n-1}{3}}\left[\frac{M_H(t_{eq})}{M_H(t_k)}\right]^{\frac{n-1}{2}} \tag{112}$$

In the case $n = 1$ (Harrison–Zeldovich spectrum) this simplifies considerably and we are left with

$$\sigma^2(t_k) = \frac{100}{81}\alpha^2(k)\delta_H^2(t_0) \tag{113}$$

Notice that we are assuming here that $\Lambda = 0$. If $\Lambda > 0$, as it is suggested by recent observations, the values for the mass variance as given by equations (112) and (113) are over estimated by a factor of about 15% (see Section 3.4).

4.2 Scale–free power law spectrum with a pure step

We will consider now a primordial power spectrum with a pure step at some wavelength $k = k_s$, with the corresponding time of re–entrance satisfying $t_{k_s} < t_{eq}$ (i.e. $k_s > k_{eq}$). The basic idea is to replace equation (100) by (Blais et al., 2003)

$$\delta(k_r, t_{k_r}) = \Theta^2 \delta^2(k_c, t_{k_c}) \left(\frac{k}{k_c}\right)^{n-1} \times \begin{cases} 1 & \text{for} \quad k < k_s \\ p^{-2} & \text{for} \quad k \geq k_s \end{cases} \tag{114}$$

where Θ is given by equation (101) and the ratio of the power on large scales to that on small scales is given by the parameter p^2. Note that aside from the step the spectrum as a constant spectral index n. Equations (112) and (113) continue to be valid but now with $\alpha(k)$ given by (Blais et al., 2003)

$$\begin{aligned} &\alpha^2(k) = \textstyle\int_0^{\frac{k_s}{k}} x^{n+2} W_{TH}^2(c_s x) W_{TH}^2(x) dx \\ &+p^{-2} \textstyle\int_{\frac{k_s}{k}}^{\frac{k_e}{k}} x^{n+2} W_{TH}^2(c_s x) W_{TH}^2(x) dx \end{aligned} \tag{115}$$

Notice that, as must be the case, the effect of the step disappears both for $k_s \to k_e$ and $k_s \to 0$.

4.3 Broken Scale Invariance spectrum

A more natural primordial power spectrum is the so called *Broken Scale Invariance* (BSI) spectrum which is produced during the inflationary era (notice that the scale–free power law spectrum with a pure step is purely phenomenological).

A BSI primordial spectrum is based in an inflationary model with a jump in the first derivative of the inflaton potential $V(\phi)$ at some scale k_s. An exact analytical expression has been derived for this kind of spectrum by Starobinsky (1992). At re–entrance inside the Hubble radius during the radiation dominated stage, the BSI spectrum is given, for $t_e \ll t_k \ll t_{eq}$, by (e.g. Blais et al., 2003)

$$F(k) = \frac{9 H_s^6}{2 A_-^2} f(k) \tag{116}$$

where

$$\begin{aligned} f(k) &= 1 - 3(p-1)\tfrac{1}{y}\left(\left(1 - \tfrac{1}{y^2}\right)\sin(2y) + \tfrac{2}{y}\cos(2y)\right) \\ &+\tfrac{9}{2}(p-1)^2 \tfrac{1}{y^2}\left(1 + \tfrac{1}{y^2}\right)\left(1 + \tfrac{1}{y^2} + \left(1 - \tfrac{1}{y^2}\right)\cos(2y) - \tfrac{2}{y}\sin(2y)\right) \end{aligned} \tag{117}$$

with

$$y = \frac{k}{k_s} \tag{118}$$

$$p = \frac{A_-}{A_+} \tag{119}$$

$$H_s^2 = \frac{8\pi G V(\phi_s)}{3} \tag{120}$$

where ϕ denotes the gravitational potential and the quantities A_- and A_+ are the inflaton potential derivatives on both sides of the jump.

The expression for $F(k)$ depends, besides the overall normalization, only on the parameters p and k_s. The shape of the spectrum depends only on y and the scale k_s only determines the location of the step. The strenght of the jump is given by p (Blais et al., 2003). The typical form of the spectrum is depicted in Figures 47 ($p < 1$) and 48 ($p > 1$). The asymptotic behaviour of $F(k)$ is given by (Blais et al., 2003)

$$F(0) = \frac{9H_s^6}{2A_+^2} \tag{121}$$

$$F(\infty) = \frac{9H_s^6}{2A_-^2} = \frac{F(0)}{p^2} \tag{122}$$

and approaches the scale invariant Harrison–Zeldovich spectrum on large and small scales, but with different amplitudes (e.g. Düchting, 2004). Combining equations (122) and (116) we have

$$F(k) = \frac{F(0)}{p^2} f(k) \tag{123}$$

Equation (69) gives the relation between $F(k)$ and $\phi(k)$ at the horizon crossing time t_k as long as $t_e \ll t_k \ll t_{eq}$. If we want to relate these quantities on larger scales, such as k_0 we should consider instead the relation (Blais et al., 2003)

$$k_0^3 \phi^2(k_0, t_0) = \frac{9\pi^2}{2} \delta_H^2(t_0) = \frac{9}{25} F(k_0) \approx \frac{9}{25} F(0) \tag{124}$$

According to this we have

$$F(0) = \frac{25\pi^2}{2} \delta_H^2(0) \tag{125}$$

where $\delta_H^2(0) \approx \delta_H^2(k_0)$ is the observational input from the CMB radiation as in the scale–free power spectrum. Inserting this result into equation (123) we obtain

$$F(k) = \frac{25\pi^2}{2p^2} \delta_H^2(0) f(k) \tag{126}$$

Taking the last result into account we have from equations (68), (69) and (126) that

$$\delta_H^2(t_k, k) = \frac{100}{81} \frac{\delta_H^2(0)}{p^2} f(k) \tag{127}$$

Inserting this result into equation (87) we obtain for the mass variance the expression

$$\sigma^2(k) = \frac{100}{81}\frac{\delta_H^2(0)}{p^2} f(k)\alpha^2(k) \tag{128}$$

where $f(k)$ is given by equation (117) and $\alpha^2(k)$ is given by

$$\alpha^2(k) = \int_0^{\frac{k_e}{k}} x^3 \frac{f(kx)}{f(k)} W_{TH}^2(x) W_{TH}^2(c_s x) dx \tag{129}$$

4.4 Running–tilt power law spectrum

Inflationary models predict that the spectral index of fluctuations n should be a slowly varying function of scale (i.e. $n = n(k)$). Fits of observations of LSS and CMB usually employ a power law spectrum

$$P(k) = P(k_c)\left(\frac{k}{k_c}\right)^{n(k)} \tag{130}$$

where k_c is some pivot scale and $n(k)$ represents the running of the spectral index. We may write $n(k)$ in the form (e.g. Düchting, 2004)

$$n(k) = n_0 + \sum_{i\geq 1} \frac{n_i}{(i+1)!}\left(\ln\frac{k}{k_c}\right)^i \tag{131}$$

The value of n_0 depends on the pivot scale used, and represents the *tilt* of the spectrum. It is given by (e.g. Spergel et al., 2003)

$$n_0 = n_s(k) = \frac{d\ln(P(k))}{d\ln(k)} \tag{132}$$

The value of n_1 represents the *running of tilt* of the spectrum for the chosen pivot scale. It is given by (e.g. Düchting, 2004)

$$n_1 = \alpha_s(k) = \frac{dn_s(k)}{d\ln(k)} \tag{133}$$

Typical *slow–roll* models predict that the running of the spectal index α_s is unobservably small. However this issue has generated recent interest after the WMAP team claim that $\alpha_s < 0$ was favored over $\alpha_s = 0$ (e.g. Tegmark et al., 2004). The evidence for running come predominantly from the very largest scales multipoles. Excluding $l < 5$ multipoles from the WMAP temperature we obtain $\alpha_s \approx 0$ (Bridle et al., 2003). At this moment we only have observational values for n_0 and n_1. A definitve measurement of n_1 and possibly of n_2 and n_3 is expected from the Planck satellite and other upcoming surveys (e.g. Düchting, 2004).

Notice that we can continue to apply for the calculus of $\alpha^2(k)$ and $\sigma^2(k)$ equations (110) and (112), as long as we consider a variable spectral index as the one given by equation (131).

5 Results

In this Section we integrate the equations in order to find the fraction of the universe going into PBHs at different epochs $\beta(k)$. We have considered all the four primordial spectrum models presented in Section 4. In all cases the basic observational input is the numerical value of $\delta_H^2(k_0, t_0)$ which is found using the CMB anisotropy data for large angular scales. In the case of a scale–free power law spectrum we have that $\beta(k) \approx 0$ at all epochs (Section 5.1).

For the remaining models (pure step power spectrum, BSI and running–tilt power spectrum) we have also to give values to two aditional parameters (see Sections 4.2, 4.3 and 4.4). In each case we tried to find out the values leading to a bigger value of $\beta(k)$.

5.1 Scale–free power law spectrum

The observational input needed in equations (112) and (113) is the numerical value of $\delta_H^2(k_0, t_0)$ which is found using the CMB anisotropy data for large angular scales. Once $\delta_H^2(k_0, t_0)$ is a known number, the overall normalization of the spectrum is fixed (Blais et al., 2003).

We will consider here the case $n = 0.951$ which corresponds to the best fit of the results obtained by the WMAP mission[4] (Spergel et al., 2006) and the case $n = 1$ which corresponds to the Harisson–Zeldovich spectrum.

For the case $n = 1$ we have from the COBE data that (e.g. Polarski, 2002)

$$k_0^3 \phi^2(k_0, t_0) = 0.86 \times 10^{-8} A_0^2(\{n_i\}) \tag{134}$$

The exact amplitude depends on the cosmological parameter of order unity $A_0(\{n_i\})$. For a power law spectrum with spectral index n at least on large scales, the quantity A_0 is chosen such that (Polarski, 2002)

$$A_0^2(n = 1) \simeq \begin{cases} 1 & \Omega_{m,0} = 0.3 \\ 1.94 & \Omega_{m,0} = 1 \end{cases} \tag{135}$$

Thus, considering a flat critical density universe with $\Omega_{m,0} = 0.3$ we have, according to equations (93), (134), and (135) that for $n = 1$

$$\delta_H^2(k_0, n = 1) \approx 2.152 \times 10^{-9} \tag{136}$$

On the other hand for the case $n = 0.951$ we have $A = 0.75$ for the pivot scale $k_c = 0.002\text{Mpc}^{-1} \approx 6.5 \times 10^{-26}\text{m}^{-1}$ (Spergel et al., 2003). Inserting the value of A into equation (103) we obtain $\delta_H^2(k_c) \approx 2.21 \times 10^{-9}$. With the help of equation (106) we have that

$$\delta_H^2(k_0, n = 0.951) \approx 2.45 \times 10^{-9} \tag{137}$$

We will know evaluate the integral (110). The value of $x_{max} = k_e/k$ depends on the moment that we are interested in. For instance if we want to determine

[4] Using WMAP data only the best fit value for the spectral index, in the context of a power law flat ΛCDM model, is $n = 0.951^{+0.015}_{-0.019}$(Spergel et al., 2006).

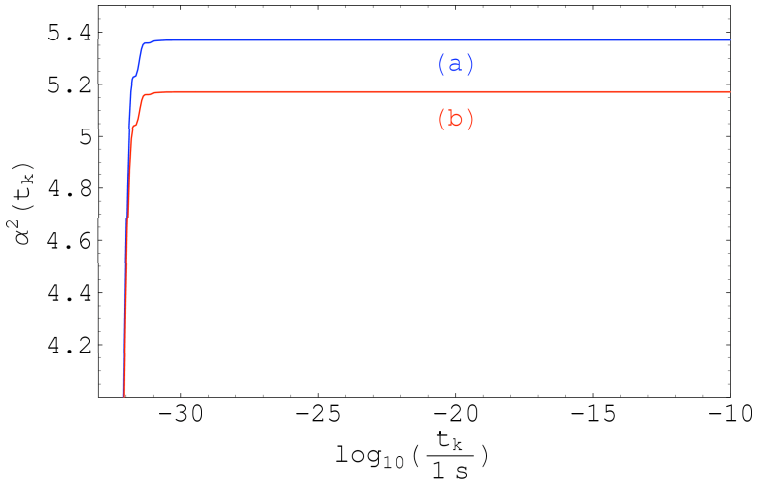

Figure 25: The $\alpha^2(t_k)$ function for a scale–free power law spectrum (equation 110) with: (a) $n = 1$ and (b) $n = 0.951$. As long as we are interested in $t \geq 10^{-23}$s we can consider the value of $\alpha^2(t_k)$ as constant ($\alpha^2(t_k) \approx 5.37$ for $n = 1$ and $\alpha^2(t_k) \approx 5.17$ for $n = 0.951$).

the value of $\alpha(k)$ right at the end of inflation we should take $x_{max} = 1$ ($k = k_e$). On the other hand if we are interested in the present value of $\alpha(k)$ we should take $x_{max} = k_e/k_0 \sim 10^{24}$ (cf. Table 2).

Let us consider first the case $n = 1$. In Figure 25 it is shown the plot of the function for $k_e \leq k \leq k_0$. Notice that in the limit $x_{max} \to \infty$ (or equivalently $k \to 0$) we have the value

$$\alpha^2(0, n = 1) \approx 5.36981 \tag{138}$$

Numerical calculations and inspection of Figure 25 show that this value is very accurately aproximated already for relatively small values of x_{max}. For example when $x_{max} = 50$, which corresponds to $k = k_e/50 \sim 10^{-4}$ m^{-1}, we have already $\alpha^2(k, n = 1) \approx 5.36981$. This happens well before the quantum–to–classical transition ($k \sim 10^{-7}$ m^{-1}, cf. Table 2) and as long as we are interested in events that took place after that particular epoch we may consider (cf. Blais et al., 2003)

$$\alpha^2(k, n = 1) \approx \alpha^2(0, n = 1) \approx 5.36981 \tag{139}$$

In the case $n = 0.951$ we have a similar situation (cf. Figure 25) but now with

$$\alpha^2(k, n = 0.951) \approx \alpha^2(0, n = 0.951) \approx 5.17079 \tag{140}$$

We are now in position to determine the value of the mass variance $\sigma(k)$. We will consider only scales that enter the horizon after the quantum–to–classical transition for which the value of $\alpha^2(k)$ can be taken as a constant as we have

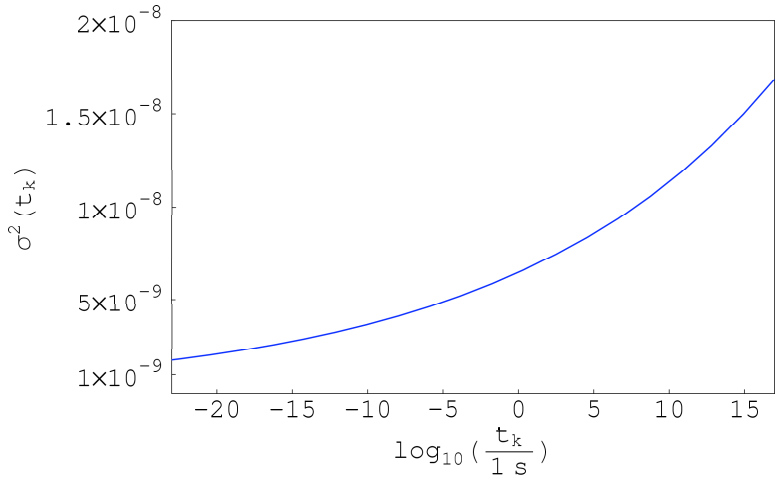

Figure 26: The function $\sigma^2(t_k)$ for a scale–free power law spectrum (equation 112) with $n = 0.951$, from $t_* = 10^{-23}$s to $t_0 = 10^{17}$s. During this period $\sigma^2(t_k)$ increased only by an order of magnitude.

already mentioned. For the case $n = 1$ inserting the corresponding values of $\alpha^2(k)$ and $\delta_H^2(k_0)$ into equation (113) we obtain the constant value

$$\sigma^2(k, n = 1) \approx 1.43 \times 10^{-8} \tag{141}$$

In the case $n = 0.951$ the mass variance is a function of time (or, equivalently, a function of k) as it is clear from equation (112). In Figure 26 it is shown the behaviour of $\sigma^2(k)$ from $t = 10^{-23}$s ($\sigma^2(k) \approx 1.76 \times 10^{-9}$) up to the present ($\sigma^2(k_0) \approx 1.73 \times 10^{-8}$). Notice that in that period the value of $\sigma^2(k)$ was increased only by an order of magnitude. Notice also that the value obtained for σ_0 is of the same order for both cases ($n = 1$ and $n = 0.951$) and that it agrees as expected with the value presented in the literature (e.g. Bringmann et al. (2002), $\sigma^2(t_0) \simeq 10^{-8}$). Knowing the value of the mass variance we can now turn our attention into the function $\beta(k)$ which gives the fraction of the universe going into PBHs at the instant t_k. Assuming $\delta_c = 1/3$ and remenbering the magnitude of the values obtained for the mass variance it is obvious that we can use equation (73). We find out that, for all the times of interest, we have

$$\beta(k) \approx 0 \tag{142}$$

That is because $(\delta_c^2/2\sigma^2) \sim 10^{15}$ and $\exp(-10^{15}) \approx 0$. In order to obtain more interesting values we got to move to a *blue spectrum*, i.e., to a spectrum with $n > 1$. In order to know the allowed range of values that n can assume we must take into account the observational constraints on the value of $\beta(k)$. For example, from the gravitational constraint, which states that the present PBH mass density must not exceed the present density of the universe, we have (e.g.

Blais et al., 2003)

$$\Omega_{PBH,0}(M)h^2 = 6.35 \times 10^{16}\beta(M)\left(\frac{10^{15}g}{M}\right)^{1/2} \tag{143}$$

where $h = 0.73$ (Spergel et al., 2006) represents the Hubble parameter. Inserting this constraint into equation (71) and numerically solving in order to obtain $\sigma(k)$ it is possible to estimate the maximum value allowed for the spectral index n which turns out to be sensitive to the assumed value of δ_c. If $\delta_c = 1/3$ we have $n \leq 1.33$ (Blais et al., 2003). Let us consider, as an example, the extreme case $n = 1.33$. For of a flat critical universe $\Omega_{m,0} = 1$ we have the normalization (e.g. Blais et al., 2003)

$$\delta_H^2(t_0) = \frac{2}{9\pi^2}1.67 \times 10^{-8} \times \exp\left[-0.959(n-1) - 0.169(n-1)^2\right] \tag{144}$$

which gives

$$\delta_H^2(t_0, n = 1.33, \Omega_{m,0} = 1) \approx 2.8 \times 10^{-10} \tag{145}$$

Inserting this last result into the expression of $\sigma^2(k)$ (equation 112)[5] we can determine $\beta(k)$ at different epochs. In Figure 27 we have the corresponding curve of $\beta(k)$ which shows some interesting values for the considered interval. Notice however that as far as we are assuming a scale–free spectrum ($n = constant$) we cannot just move into a blue spectrum ($n > 1$) because we now from recent observations, for example at the pivot scale $k_c = 0.05$ Mpc^{-1}, that $n < 1$ (Spergel et al., 2006).

The idea is to use a power spectrum model with more power in the smaller scales which are the ones relevant to PBH formation. With this purpose we have already introduced three alternatives: the scale–free power spectrum with a pure step (Section 4.2), the Broken Scale Invariance spectrum (Section 4.3) and the Running–tilt spectrum (Section 4.4)). In the following sections we will be determining the allowed values of $\beta(k)$ for such kinds of spectrum.

5.2 Scale–free power law spectrum with a pure step

The observational inputs needed in the pure step case are the numerical values of $\delta_H^2(k_0, t_0)$ and the spectral index n which are equal to the ones used in the free–scale power law spectrum with no step (Section 5.1). In addition we have also to give values to the parameters k_s (location of the step) and p (height of the step).

Considering that PBHs form tipically with masses of the order of the horizon mass at the epoch of formation we will have $M_{PBH} \sim M_H(t_k)$. Thus, give a location for the step k_s is equivalent to give the order of the maximum mass allowed for the PBHs. We will take as an upper constraint the value $M_{PBH} =$

[5] Notice that the obtained values of $\sigma^2(k)$ will correspond to a flat universe with $\Omega_{m,0} = 1$. The obtained values for the mass variance should be decreased by about 15% in order to have results consistent with a $\Omega_{m,0} = 0.3$ universe (cf. Section 3.4).

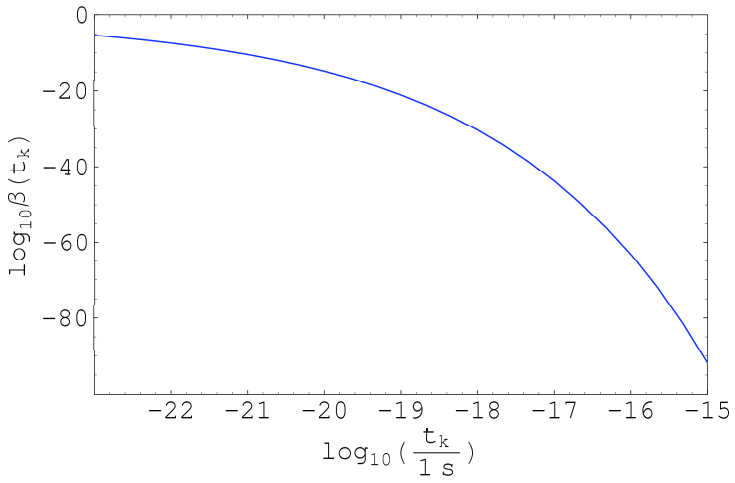

Figure 27: The $\beta(k)$ function (equation 71) for a scale–free power law spectrum with $n = 1.33$.

$10^{10}M_{\odot}$ ($k_s \approx 1.2\times10^{-21}\mathrm{m}^{-1}$, cf. Table 2) which corresponds to the mass of the biggest SMBH known candidates (e.g. Kormendy, 2004). As a lower limit we will consider the value $M_{PBH} = 5.0\times10^{-19}M_{\odot} \approx 10^{15}\mathrm{g}$ ($k_s \approx 1.7\times10^{-7}\mathrm{m}^{-1}$, cf. Table 2) which corresponds to PBHs that are exploding by the present time (e.g. Green & Liddle, 1997). Besides these two values we will consider also $M_{PBH} = 5.0\times10^{-6}M_{\odot}$ ($k_s \approx 5.5\times10^{-14}\mathrm{m}^{-1}$), $M_{PBH} = 5.0\times10^{-2}M_{\odot}$ ($k_s \approx 5.5\times10^{-16}\mathrm{m}^{-1}$), $M_{PBH} = 3M_{\odot}$ ($k_s \approx 7.1\times10^{-17}\mathrm{m}^{-1}$) and $M_{PBH} = 10^{6}M_{\odot}$ ($k_s \approx 1.2\times10^{-19}\mathrm{m}^{-1}$) (cf. Table 2 and Section 2.1).

We are interested in having a spectrum with more power in the smaller scales because that will offer the possibility to produce more instead of less PBHs on small scales. Thus we will consider only the case $0 < p \leq 1$ (Blais et al., 2003). If $p = 1$ we recover the scale–free power law spectrum with no step and if $p = 0$ the entire universe is converted into BHs. In Figure 28 we have the typical curve for the power law spectrum with a pure step for the case $0 < p < 1$.

We know from observational constraints the maximum values allowed for $\beta(M_H)$ for different mass ranges (see e.g. Green & Liddle, 1997; Carr, 2005). These values are the ones represented in Figure 29. As it is clear the strongest constraint on $\beta(M)$ comes from $M_H \sim 10^{15}\mathrm{g}$ with $\beta(10^{15}\mathrm{g}) \sim 10^{-28}$. Inserting this observational constraint into equation (71) we may numerically find, for a given δ_c and for a given k_s, the corresponding minimum value for the parameter p. For $\delta_c = 1/3$ we find out that the minimum value allowed for p varies between 0.00136 ($t_s = 10^{-23}\mathrm{s}$, $k_s = 1.78\times10^{-7}\mathrm{m}^{-1}$) and 0.00139 ($t_s = 2\times10^{5}\mathrm{s}$, $k_s = 1.2\times10^{-21}\mathrm{m}^{-1}$). In face of these results we will neglect the dependence of p_{min} on k_s and consider that $p_{min}(\delta_c = 1/3) \approx 0.0014$. For the rest of the cases of interest to us we find out that p_{min} is pratically constant for $t_s > 10^{-20}\mathrm{s}$ beeing only a bit smaller when $t_s = 10^{-23}\mathrm{s}$. In Table 4 we have the obtained

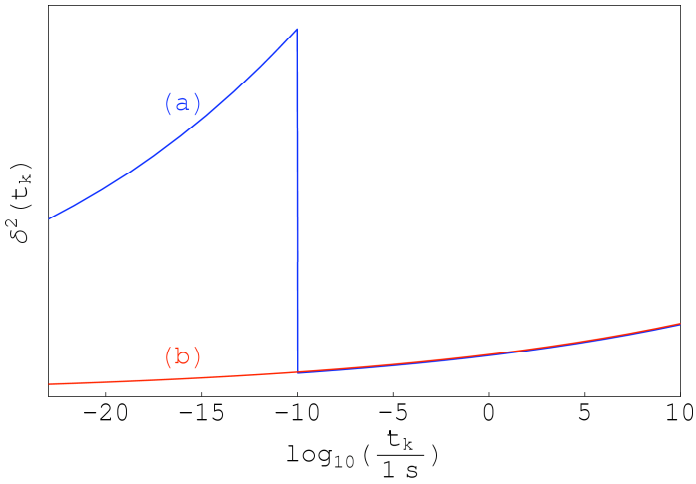

Figure 28: Typical form of the scale–free power law spectrum with $n = 0.951$ and: (a) $0 < p < 1$ and $t_{k_s} = 10^{-10}$s; (b) $p = 1$ (no step at all).

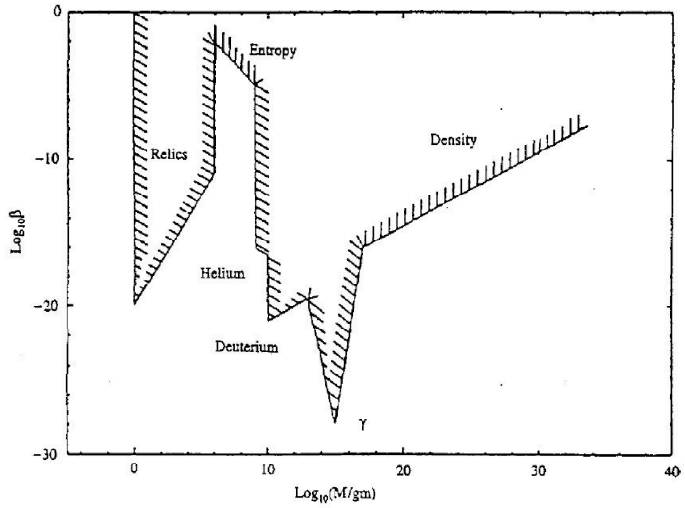

Figure 29: Observational constraints on the fraction of the universe going into PBHs, $\beta(M)$, as a function of the horizon mass M_H. The strongest constraint ($\beta \sim 10^{-28}$) comes from $M_H \sim 10^{15}$g (e.g. Carr, 2005).

Table 4: The minimum values allowed for the parameter p as a function of δ_c for the scale–free power law spectrum with a pure step. Notice that for $t_s > 10^{-20}$s the mimimum values allowed for p are pratically constant in all cases.

δ_c	p_{min}	
	$t_s = 10^{-23}$s	$t_s > 10^{-20}$s
1/3	0.0014	0.0014
0.4	0.0011	0.0012
0.5	0.00091	0.00093
0.6	0.00076	0.00077
0.7	0.00065	0.00066

results. In Figure 30 we have plotted the relation $p_{min}(\delta_c)$ for $t_s > 10^{-20}$s. We find out that this relation is quit well interpolated by a cubic polynomial.

Let us now analise the behaviour of the function $\alpha^2(k)$ (equation 115). In Figure 31 we have the curve of $\alpha^2(k)$ for $p = 1$ (no step) and for $p = 0.75$ with a step located at $t_s = 10^{-10}$s ($k_s \approx 5.5 \times 10^{-14}\mathrm{m}^{-1}$). Notice that, in the case $p = 0.75$, the function rapidly grows up to its maximum value ($\alpha^2(0)p^{-2} \approx 5.17p^{-2}$, cf. equation 140) right after inflation, remaining there until it gets near the step, then it decreases quite rapidly (but not instantaneously) to the asymptotic value $\alpha^2(0) \approx 5.17$ (cf. equation 140) which is commom to the case $p = 1$.

We will consider now the function $\sigma^2(k)$ (equation 112) for different values of k_s and p. But first let us remember that, as it was already explained, we are interested only in PBHs which form after $t \geq 10^{-23}$s. Thus, if the step occurs for $t_s \ll 10^{-23}$s it will have no action on the values of $\beta(k)$ of interest (i.e. we will have for all epochs $\beta(k) \approx 0$ as in the scale–free power law spectrum with no step, Section 5.1).

In Figure 32 we have the representation of $\sigma^2(k)$ with $t_s = 6 \times 10^{-5}$s ($k_s = 7.10 \times 10^{-17}\mathrm{m}^{-1}$) and with p assuming the values 0.1, 0.01 and 0.0014. On the other hand in Figure 33 we have $\sigma^2(k)$ with $p = 0.0014$ and with t_s assuming the values $t_s = 10^{-23}$s ($k_s = 1.7 \times 10^{-7}\mathrm{m}^{-1}$), 6×10^{-5}s ($k_s = 7.1 \times 10^{-17}\mathrm{m}^{-1}$) and 20s ($k_s = 1.2 \times 10^{-19}\mathrm{m}^{-1}$). In both cases we can see that the effect of the step on the mass variance is already significant at $t = 10^{-23}$s and keeps its value (to roughly one order of magnitude) until $t \sim 10t_s$ (i.e. for $t \sim 10t_s$ the action

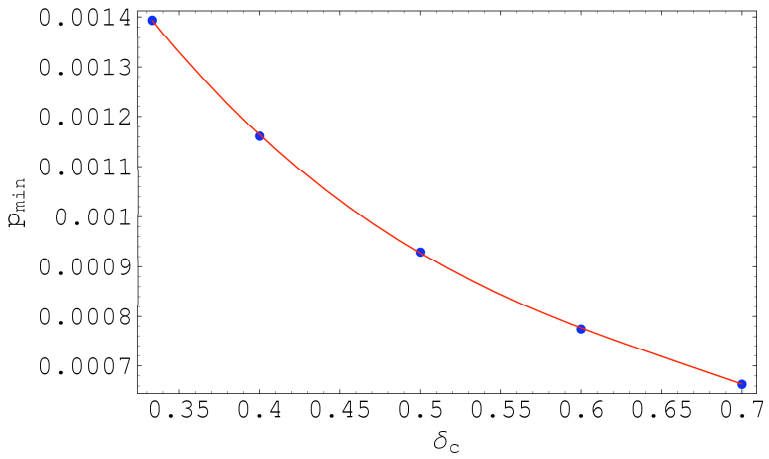

Figure 30: The minimum values allowed for p as a function of the critical threshold δ_c for the scale–free power law spectrum with a pure step when $t_s > 10^{-20}$s. The blue dots represent the evaluated cases and the red line represents the cubic polynomial interpolation ($p_{min}(\delta_c) = -0.008008\delta_c^3 + 0.01632\delta_c^2 - 0.01217\delta_c + 0.003933$).

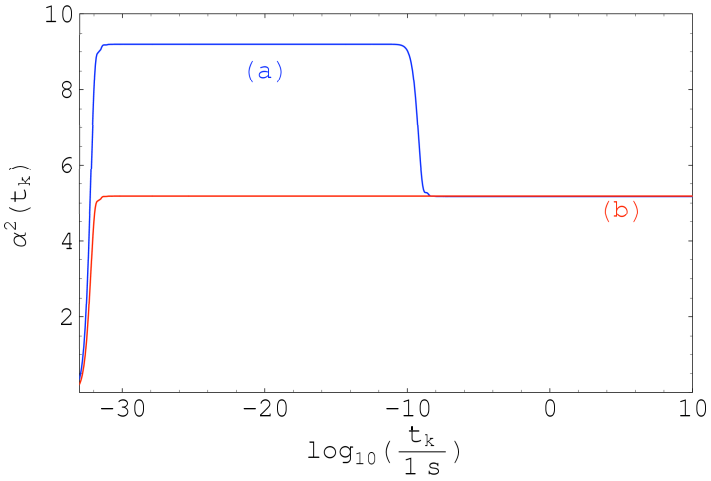

Figure 31: The function $\alpha^2(k)$ for a scale–free power law spectrum with $n = 0.951$ and (a) a pure step located at $t_s = 10^{-10}$s with $p = 0.75$ and (b) no step at all ($p = 1$).

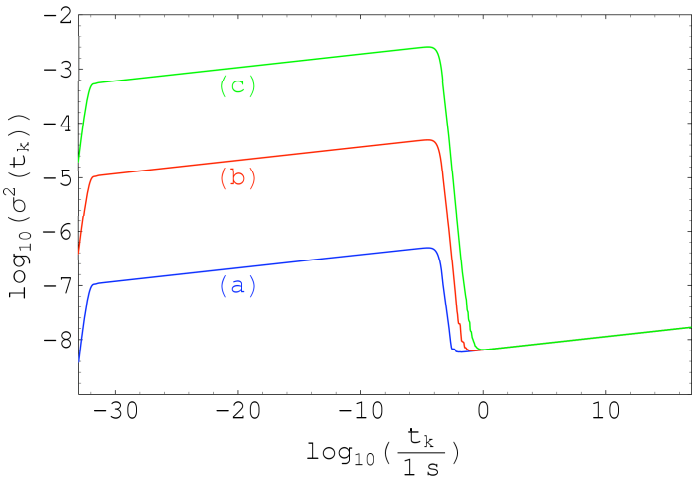

Figure 32: The function $\sigma^2(k)$ for a scale–free power law spectrum with a pure step. The location of the step is $t_s = 6 \times 10^{-5}$s ($k_s = 7.10 \times 10^{-17}\mathrm{m}^{-1}$) and the height of the step is (a) $p = 0.1$, (b) $p = 0.2$ and (c) $p = 0.0014$.

of the step still is very significant). At that point the value of $\sigma^2(k)$ decreases rapidly reaching a minimum value and then it increases again reaching at the present the value $\sigma_0^2 \sim 10^{-8}$.

Let us now turn our attention to the function $\beta(k)$. We want to explore the influence of p, t_s and δ_c on the values of $\beta(k)$. We will start with $p = 0.0014$ and with δ_c assuming the values 1/3 and 0.7. In Figure 34 we have the curve of $\beta(k)$ for $t_s = 10^{-23}$s ($k_s = 1.7 \times 10^{-7}\mathrm{m}^{-1}$) which corresponds to have the step right at the end of inflation. When $\delta_c = 1/3$ we have $\beta(k) \sim 10^{-30}$ near the step but if $\delta_c = 0.7$ then $\beta(k)$ will be of order 10^{-125}. Notice that although $p = 0.0014$ corresponds to the minimum value allowed for p when $\delta_c = 1/3$ that is not the case when $\delta_c = 0.7$. In that case we have $p_{min}(0.7) \approx 0.00065$ (see Table 4).

Keeping $p = 0.0014$ we have in Figures 35, 36, 37, 38 and 39 the curves of $\beta(k)$ for the remaining cases: $t_s = 10^{-10}$s ($k_s = 5.5 \times 10^{-14}\mathrm{m}^{-1}$), $t_s = 10^{-6}$s ($k_s = 5.5 \times 10^{-16}\mathrm{m}^{-1}$), $t_s = 6 \times 10^{-5}$s ($k_s = 7.1 \times 10^{-17}\mathrm{m}^{-1}$), $t_s = 20$s ($k_s = 1.2 \times 10^{-19}\mathrm{m}^{-1}$) and $t_s = 2 \times 10^{5}$s ($k_s = 1.2 \times 10^{-21}\mathrm{m}^{-1}$). Notice that $\beta(k)$ starts always as a growing function attaining its maximum value near the step and then it decreases very rapidly. This behaviour was hidden in the case $t_s = 10^{-23}$s (cf. Figure 34) because we are considering only $t \geq 10^{-23}$s.

We will increase now the value of p and see what happens to $\beta(k)$. In Figures 40, 41 and 42 we have the curve of $\beta(k)$ for the case $p = 0.01$. It is notorius that the obtained values for $\beta(k)$ are smaller by several orders of magnitude when compared with the ones obtained for the case $p = 0.0014$ (e.g. compare Figures 35 and 41).

With the data obtained from Figures 35 to 39 it is possible to find a relation

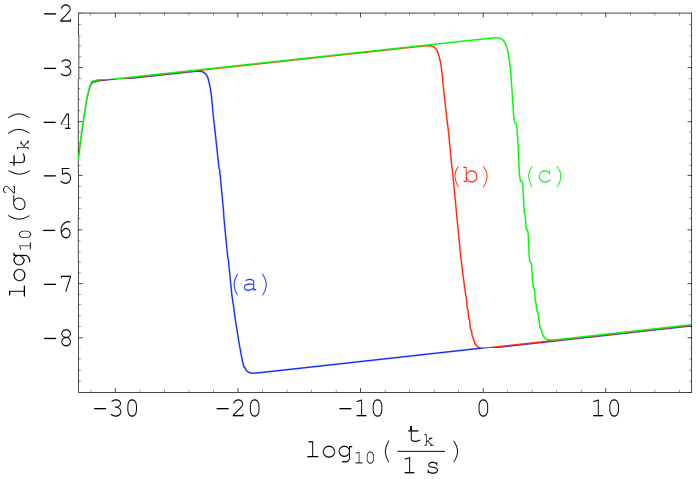

Figure 33: The function $\sigma^2(k)$ for a scale–free power law spectrum with a pure step. The height of the step is $p = 0.0014$ and the location of the step is (a) $t_s = 10^{-23}$s ($k_s = 1.7 \times 10^{-7}\mathrm{m}^{-1}$), (b) 6×10^{-5}s ($k_s = 7.1 \times 10^{-17}\mathrm{m}^{-1}$) and (c) 20s ($k_s = 1.2 \times 10^{-19}\mathrm{m}^{-1}$).

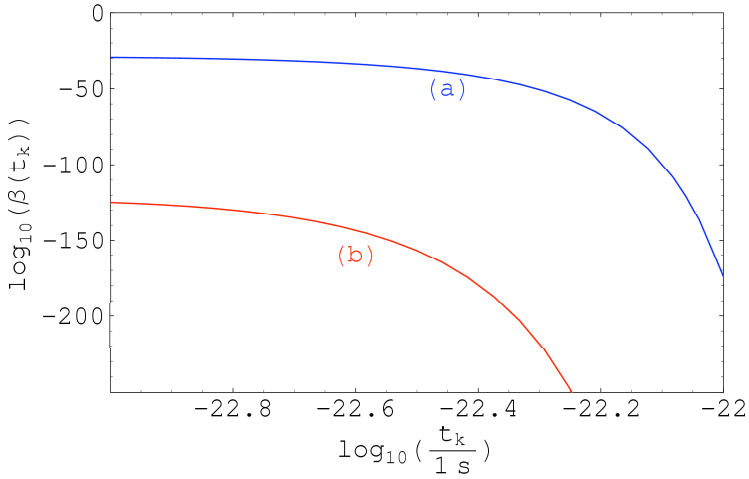

Figure 34: The function $\beta(k)$ for a scale–free power law spectrum with a pure step located at $t_s = 10^{-23}$s ($k_s = 1.7 \times 10^{-7}\mathrm{m}^{-1}$) with $p = 0.0014$ and with (a) $\delta_c = 1/3$ and (b) $\delta_c = 0.7$. When $t_k = 10^{-23}$s we have the values (a) $\beta(k) \sim 10^{-30}$ and (b) $\beta(k) \sim 10^{-125}$.

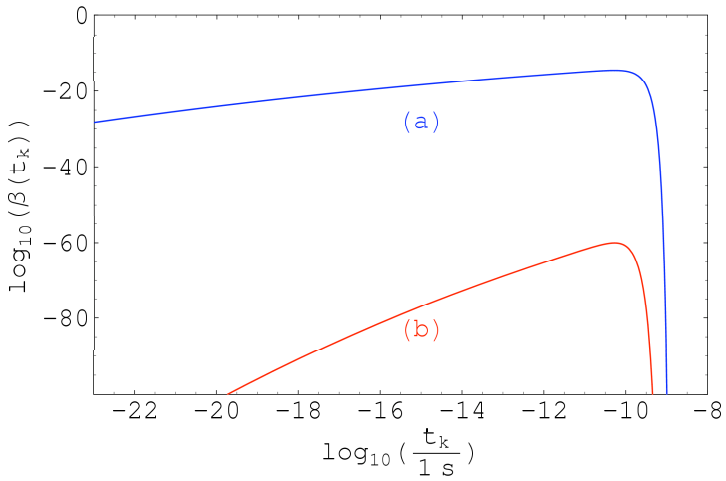

Figure 35: The function $\beta(k)$ for a scale–free power law spectrum with a pure step located at $t_s = 10^{-10}$s ($k_s = 5.5 \times 10^{-14}\mathrm{m}^{-1}$) with $p = 0.0014$ and with (a) $\delta_c = 1/3$ and (b) $\delta_c = 0.7$. The maximum values of $\beta(k)$ are (a) $\beta_{max} \sim 10^{-14}$ and (b) $\beta_{max} \sim 10^{-60}$ and they are located at $t_k \approx 10^{-10.3}$s.

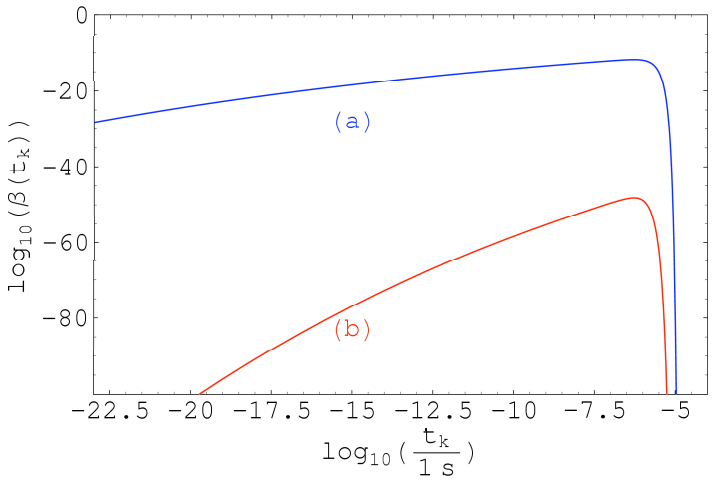

Figure 36: The function $\beta(k)$ for a scale–free power law spectrum with a pure step located at $t_s = 10^{-6}$s ($k_s = 5.5 \times 10^{-16}\mathrm{m}^{-1}$) with $p = 0.0014$ and with (a) $\delta_c = 1/3$ and (b) $\delta_c = 0.7$. The maximum values of $\beta(k)$ are (a) $\beta_{max} \sim 10^{-12}$ and (b) $\beta_{max} \sim 10^{-48}$ and they are located at $t_k \approx 10^{-6.3}$s.

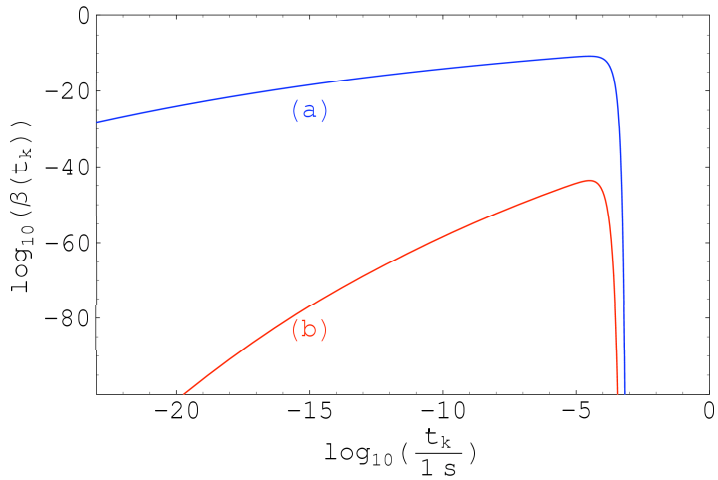

Figure 37: The function $\beta(k)$ for a scale–free power law spectrum with a pure step located at $t_s = 6 \times 10^{-5}$s ($k_s = 7.1 \times 10^{-17}\mathrm{m}^{-1}$) with $p = 0.0014$ and with (a) $\delta_c = 1/3$ and (b) $\delta_c = 0.7$. The maximum values of $\beta(k)$ are (a) $\beta_{max} \sim 10^{-11}$ and (b) $\beta_{max} \sim 10^{-44}$ and they are located at $t_k \approx 10^{-4.5}$s.

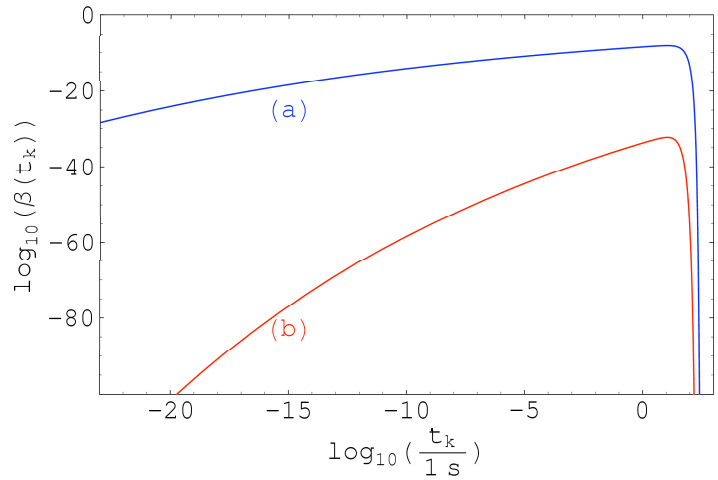

Figure 38: The function $\beta(k)$ for a scale–free power law spectrum with a pure step located at $t_s = 20$s ($k_s = 1.2 \times 10^{-19}\mathrm{m}^{-1}$) with $p = 0.0014$ and with (a) $\delta_c = 1/3$ and (b) $\delta_c = 0.7$. The maximum values of $\beta(k)$ are (a) $\beta_{max} \sim 10^{-8}$ and (b) $\beta_{max} \sim 10^{-32}$ and they are located at $t_k \approx 10^{-1.1}$s.

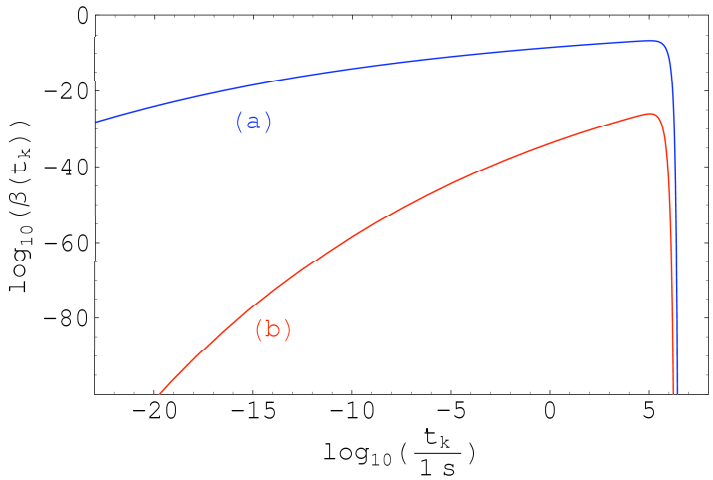

Figure 39: The function $\beta(k)$ for a scale–free power law spectrum with a pure step located at $t_s = 2\times10^5$s ($k_s = 1.2\times10^{-21}\mathrm{m}^{-1}$) with $p = 0.0014$ and with (a) $\delta_c = 1/3$ and (b) $\delta_c = 0.7$. The maximum values of $\beta(k)$ are (a) $\beta_{max} \sim 10^{-7}$ and (b) $\beta_{max} \sim 10^{-26}$ and they are located at $t_k \approx 10^{-5.1}$s.

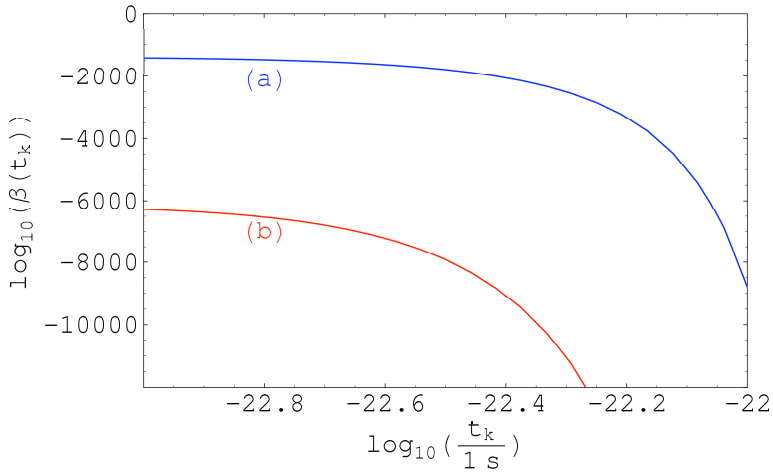

Figure 40: The function $\beta(k)$ for a scale–free power law spectrum with a pure step located at $t_s = 10^{-23}$s ($k_s = 1.7\times10^{-7}\mathrm{m}^{-1}$) with $p = 0.01$ and with (a) $\delta_c = 1/3$ and (b) $\delta_c = 0.7$. When $t_s = 10^{-23}$s we have the values (a) $\beta(k) \sim 10^{-1400}$ and (b) $\beta(k) \sim 10^{-6200}$.

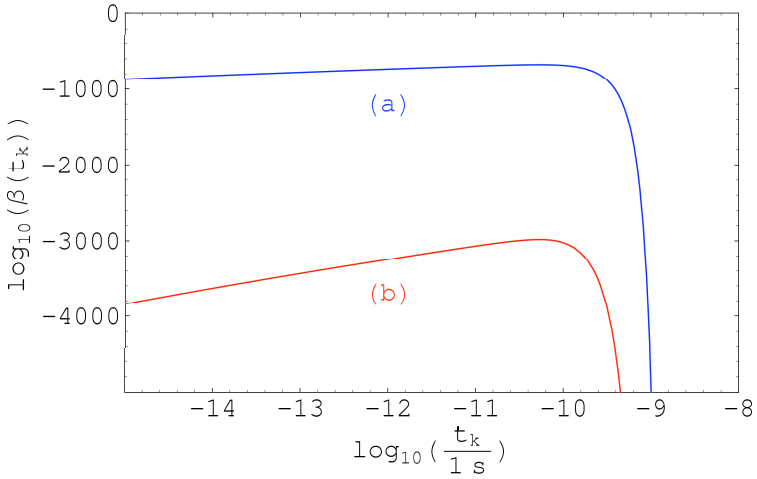

Figure 41: The function $\beta(k)$ for a scale–free power law spectrum with a pure step located at $t_s = 10^{-10}$s ($k_s = 5.5 \times 10^{-14}\mathrm{m}^{-1}$) with $p = 0.01$ and with (a) $\delta_c = 1/3$ and (b) $\delta_c = 0.7$. The maximum values of $\beta(k)$ which are (a) $\beta_{max} \sim 10^{-678}$ and (b) $\beta_{max} \sim 10^{-2983}$ are located at $t_k \approx 10^{-10.3}$s.

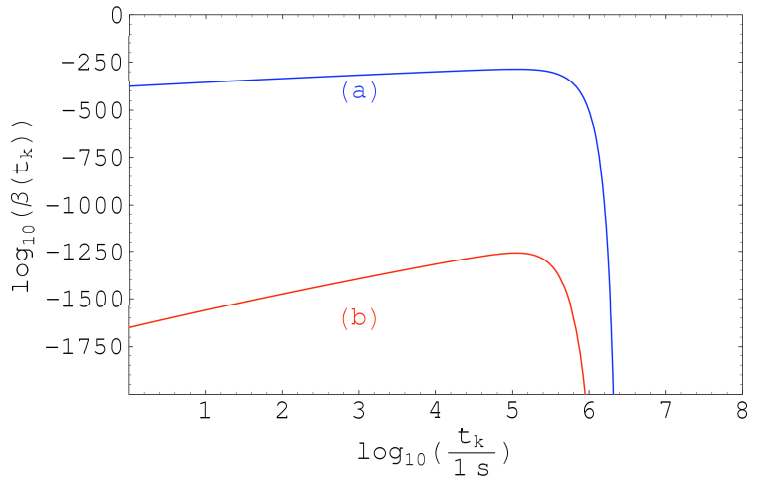

Figure 42: The function $\beta(k)$ for a scale–free power law spectrum with a pure step located at $t_s = 2 \times 10^{5}$s ($k_s = 1.2 \times 10^{-21}\mathrm{m}^{-1}$) with $p = 0.01$ and with (a) $\delta_c = 1/3$ and (b) $\delta_c = 0.7$. The maximum values of $\beta(k)$ which are (a) $\beta_{max} \sim 10^{-286}$ and (b) $\beta_{max} \sim 10^{-1258}$ are located at $t_k \approx 10^{5.1}$s.

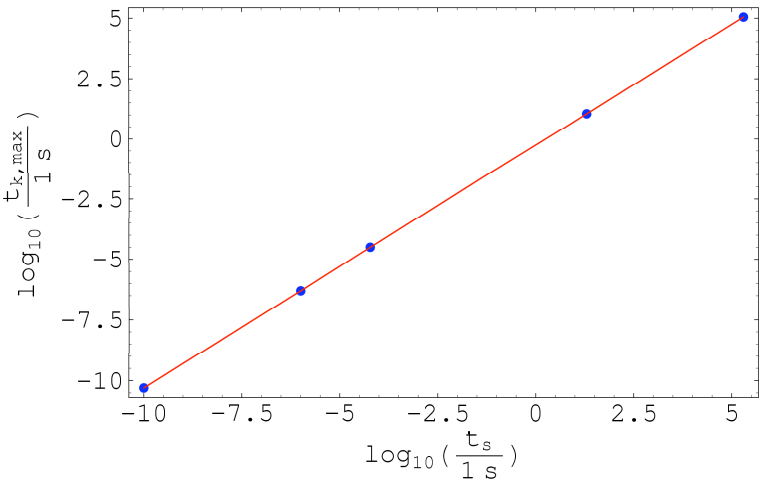

Figure 43: The relation between $t_{k_{max}}$ (corresponding to the instant for which $\beta(k)$ gets its maximum) and t_s (corresponding to the location of the pure step) for a scale–free power law spectrum with a pure step.

between the location of the step and the location of the maximum value allowed for $\beta(k)$. The location of β_{max} depends only on the value of t_s (the value of β_{max} depends also on the values of p and δ_c). In Figure 43 it is represented the dependence between $t_{k_{max}}$ (the instant corresponding to β_{max}) and t_s. This linear relation can be written as

$$t_{k_{max}} \approx 0.54 t_s \tag{146}$$

In Figures 34 to 42 it is clear the dependence of $\beta(k)$ on the parameter δ_c. For example, if the correct value of δ_c is 0.7 instead of 1/3 (see Section 2.2) then the values allowed for $\beta(k)$ will be much smaller (considering the same value of p in both cases). For example for $t_s = 20$s and $p = 0.0014$ (Figure 38) we have $\beta_{max}(k) \sim 10^{-8}$ when $\delta_c = 1/3$ and $\beta_{max}(k) \sim 10^{-32}$ when $\delta_c = 0.7$.

In Figure 44 we have the curve of $\beta(k)$ when $t_s = 10^{-6}$s and with δ_c assuming the values $1/3$, 0.4 and 0.7. In each case it was considered the minimum value allowed for p (cf. Figure 30). Notice that previously we have considered the cases $\delta_c = 1/3$ and $\delta_c = 0.7$ but with the same value of p for both (e.g. Figure 36). The example of Figure 44 shows that when one combines a given δ_c with the respective value of p_{min} (cf. Figure 30) the obtained results for $\beta(k)$ are very similar.

In Figure 45 we have the relation between β_{max} and the location of the step t_s when $p = 0.0014$ and $\delta_c = 1/3$. In Figure 46 we have the same situation but now with $\delta_c = 0.7$. This relation is well interpolated by a quadratic polynomial.

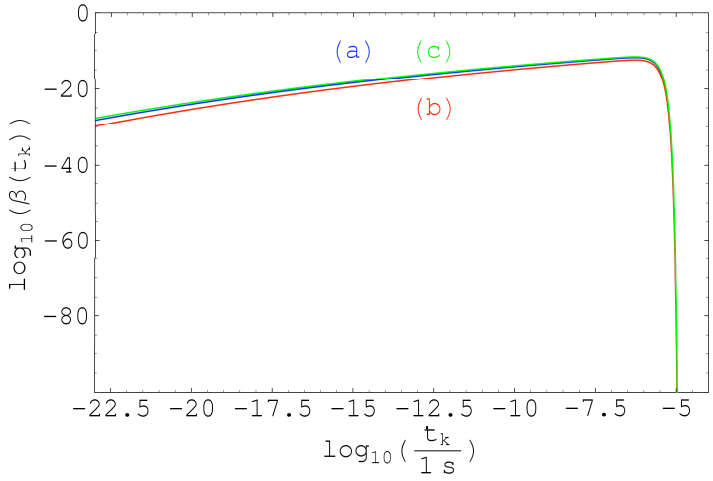

Figure 44: The function $\beta(k)$ for a scale–free power law spectrum with a pure step located at $t_s = 10^{-6}$s ($k_s = 5.5 \times 10^{-16}\mathrm{m}^{-1}$) with (a) $\delta_c = 1/3$, $p = p_{min}(1/3) \approx 0.0014$, (b) $\delta_c = 0.4$, $p = p_{min}(0.4) \approx 0.0012$ and (c) $\delta_c = 0.7$, $p = p_{min}(0.7) \approx 0.00066$. The maximum values of $\beta(k)$ are for all cases of order 10^{-12} and they are located at $t_k \approx 10^{-6.3}$s.

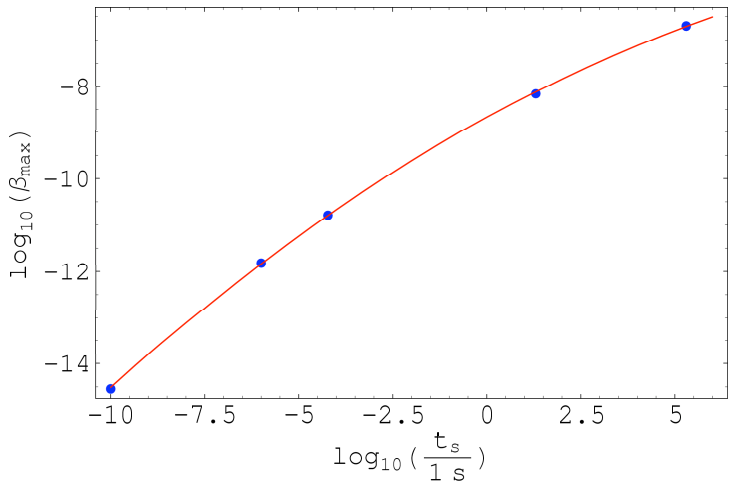

Figure 45: The relation between β_{max} and t_s for a scale–free power law spectrum with a pure step when $p = 0.0014$ and $\delta_c = 1/3$. The blue dots represent the obtained values (see Figures 35 to 39) and the red line represents the quadratic interpolation $\beta_{max} = 10^{-8.67+0.44x-0.014x^2}$ where $x = \log_{10} t_s$.

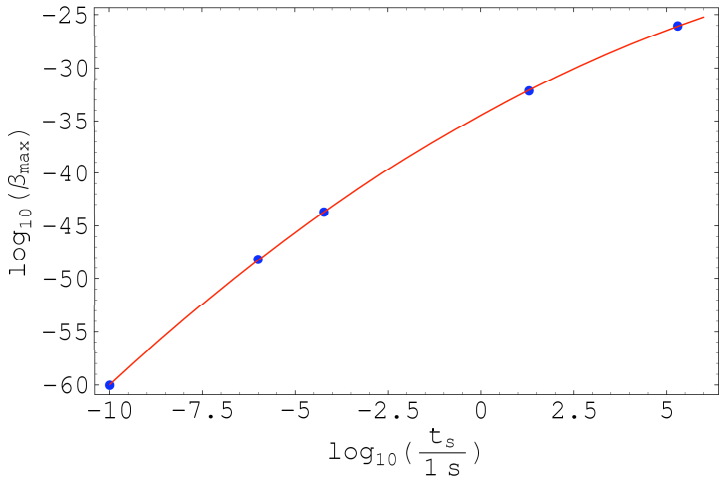

Figure 46: The relation between β_{max} and t_s for a scale–free power law spectrum with a pure step when $p = 0.0014$ and $\delta_c = 0.7$. The blue dots represent the obtained values (see Figures 35 to 39) and the red line represents the quadratic interpolation $\beta_{max} = 10^{-34.5+1.92x-0.063x^2}$ where $x = \log_{10} t_s$.

5.3 Broken Scale Invariance spectrum

The observational input needed in equation (128) is the numerical value of $\delta_H(k_0, t_0)$ which may be taken from CMB measurements. We will consider once again the value given in equation (137) because when one goes to large scales the BSI spectrum approaches the scale invariant Harrison–Zeldovich spectrum (e.g. Düchting, 2004).

We are left with the two free parameters k_s (the location of the jump) and p (the strenght of the jump). For the value of k_s we will consider the same values as in the pure step case (cf. Section 5.2, Table 2).

The typical form of the spectrum is depicted in Figures 47 ($p < 1$) and 48 ($p > 1$). When compared to a pure step (Figure 28), we see that the BSI spectrum is a step dressed up with a rich structure, in particular large oscilations confined to the neighborhood of the step. For the case $p > 1$ the BSI spectrum has a flat upper plateau on larger scales and a sharp decrease on smaller scales with large oscilations. In the case $p < 1$ we have instead an increase in small scales. Thus, the case of interest to us is the one with $p < 1$ due to the increase of power in small scales (Blais et al., 2003).

In order to find the minimum value permited for p we will proceed as in the pure step case (see Section 5.2). Thus, inserting the observational constraint $\beta(10^{15}\text{g}) \sim 10^{-28}$ into equation (71) we may numerically find, for a given δ_c and for a given k_s, the corresponding minimum value for the parameter p. In Figure 49 we have the relation between p_{min} and t_s (or, equivalently k_s) for the case $\delta_c = 1/3$. Notice that for $t_s > 10^{-20}$s the minimum value allowed for p is

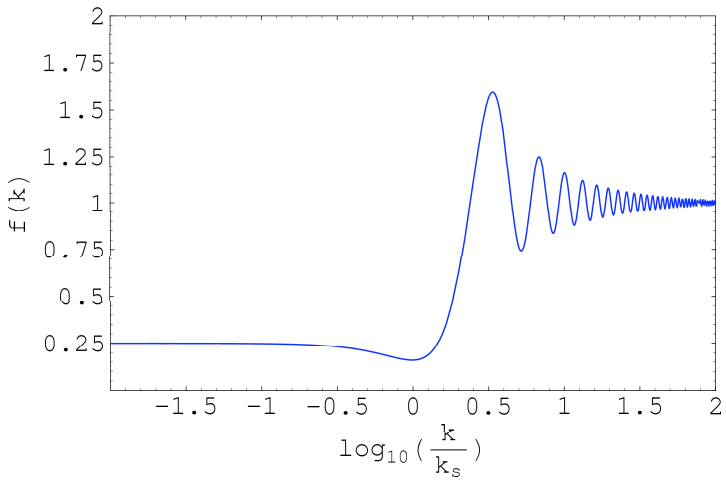

Figure 47: Typical form of the BSI spectrum (equation 117) with the parameter $p < 1$. The jump scale k_s and the large scale normalization are arbitrary.

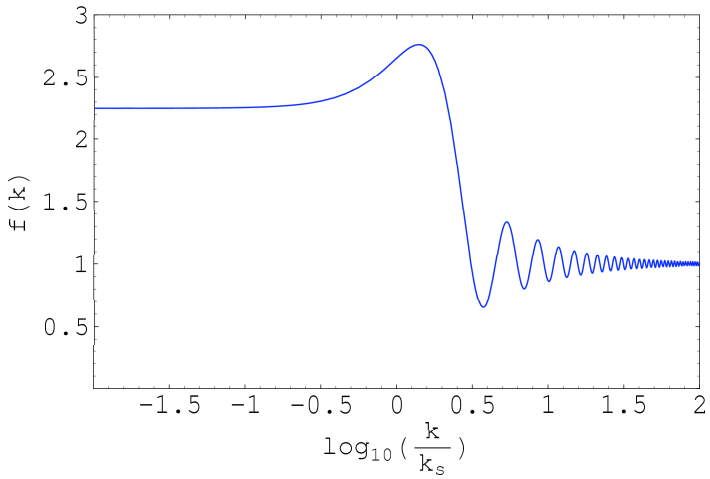

Figure 48: Typical form of the BSI spectrum (equation 117) with the parameter $p > 1$. The jump scale k_s and the large scale normalization are arbitrary.

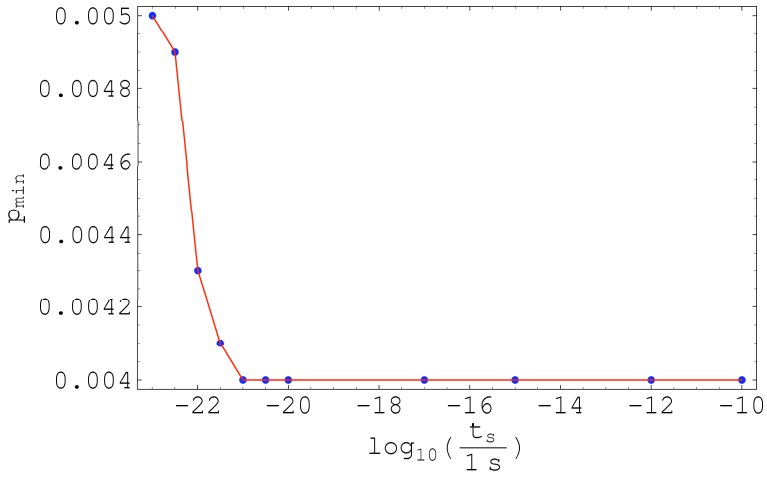

Figure 49: The dependence between the mimimum value allowed for p and the value of the parameter t_s for the BSI spectrum when $\delta_c = 1/3$. Notice that for $t_s > 10^{-20}$s the minimum value allowed for p is pratically constant.

pratically constant. A similar behaviour is achieved when we consider the other values of δ_c of interest to us. Notice that, with the exception of $t_s = 10^{-23}$s, the values of t_s of interest to us are all above 10^{-20}s. In Table 5 we have some of the obtained results. We find out that the relation $p_{min}(\delta_c)$ is quit well interpolated by a cubic polynomial for both cases, $t_s = 10^{-23}$s and $t_s > 10^{-23}$s, as it is shown in Figure 50.

Notice that, although we have used the same observational constraint here and in the pure step case (Section 5.2), we have obtained different minimum values for the parameter p. That is because we are dealing with different models.

Let us consider now the function $\alpha^2(k)$ (equation 129). In Figure 51 we have the curve of $\alpha^2(k)$ for $k_s = 5.5 \times 10^{-14}\text{m}^{-1}$ ($t_s = 10^{-10}$s) with $p = 0.0040$ and $p = 0.0020$. The two curves are very similar despiste the fact that the peak is not located at the same place for both cases. In Figure 52 we have the curve of $\alpha^2(k)$ when $p = 0.0050$ for $k_s = 1.7 \times 10^{-7}\text{m}^{-1}$ ($t_s = 10^{-23}$s) and in Figure 53 the curve of $\alpha^2(k)$ when $p = 0.0040$ for $k_s = 1.2 \times 10^{-19}\text{m}^{-1}$ ($t_s = 20$s). In these three examples it is evident the non–trivial shape of the function $\alpha^2(k)$ specially when one gets near the peak.

In Figures 54, 55 and 56 we have the curves of $\sigma^2(k)$ for the same cases considered for the function $\alpha^2(k)$ (Figures 51, 52 and 53). It is notorious that the rich structure of the BSI spectrum (Figure 47), which was still present in the $\alpha^2(k)$ (cf. Figures 51, 52 and 53), nearly completely disappeared due to the effects of the filtering. Nevertheless, and most importantly, what remains is a noticeable peak. Notice also that in each case $\sigma^2(k)$ decreases quite rapidly after the peak and then it evolves to the present value $\sigma_0^2 \sim 10^{-8}$.

Let us now turn our attention to the function $\beta(k)$. We want to explore the

Table 5: The minimum values allowed for the parameter p as a function of δ_c for the BSI spectrum. Notice that for $t_s > 10^{-20}$s the mimimum values allowed for p are pratically constant for all cases.

δ_c	p_{min}	
	$t_s = 10^{-23}$s	$t_s > 10^{-20}$s
1/3	0.0050	0.0040
0.4	0.0041	0.0033
0.5	0.0033	0.0026
0.6	0.0028	0.0022
0.7	0.0024	0.0019

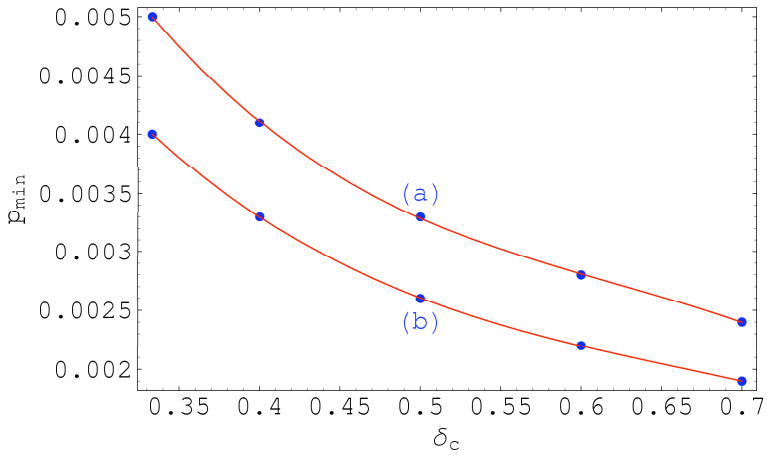

Figure 50: The minimum values allowed for p as a function of the critical threshold δ_c for a BSI spectrum when (a) $t_s = 10^{-23}$s and (b) $t_s > 10^{-20}$s. The blue dots represent the evaluated cases and the red line represents the cubic polynomial interpolation (a) $p_{min}(\delta_c) = -0.04712\delta_c^3 + 0.08810\delta_c^2 - 0.05881\delta_c + 0.01656$ and (b) $p_{min}(\delta_c) = -0.02897\delta_c^3 + 0.05768\delta_c^2 - 0.04116\delta_c + 0.01238$.

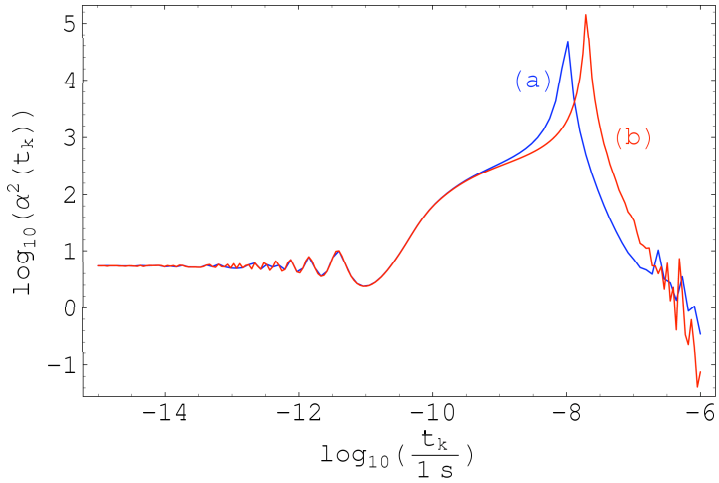

Figure 51: The function $\alpha^2(k)$ for the BSI spectrum when $k_s = 5.5 \times 10^{-14}\mathrm{m}^{-1}$ ($t_s = 10^{-10}$s) and (a) $p = 0.0040$, (b) $p = 0.0020$.

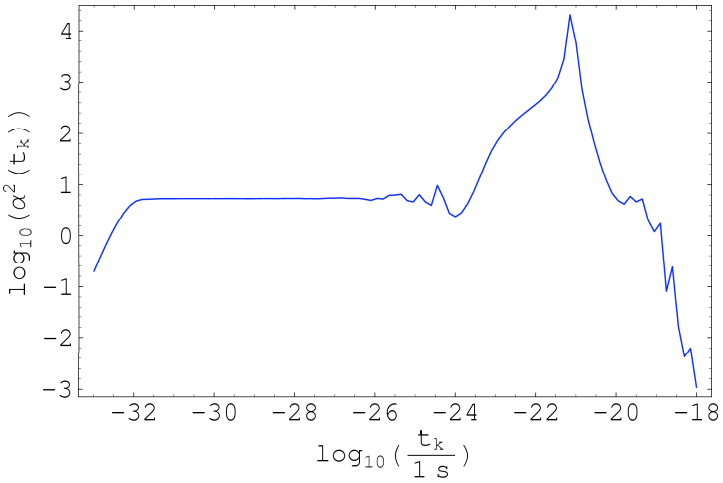

Figure 52: The function $\alpha^2(k)$ for the BSI spectrum when $k_s = 1.7 \times 10^{-7}\mathrm{m}^{-1}$ ($t_s = 10^{-23}$s) and $p = 0.0050$.

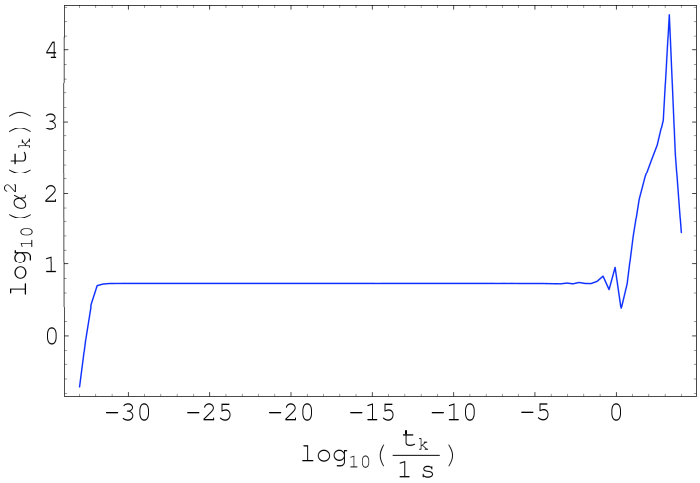

Figure 53: The function $\alpha^2(k)$ for the BSI spectrum when $k_s = 1.2 \times 10^{-19}\mathrm{m}^{-1}$ ($t_s = 20\mathrm{s}$) and $p = 0.0040$.

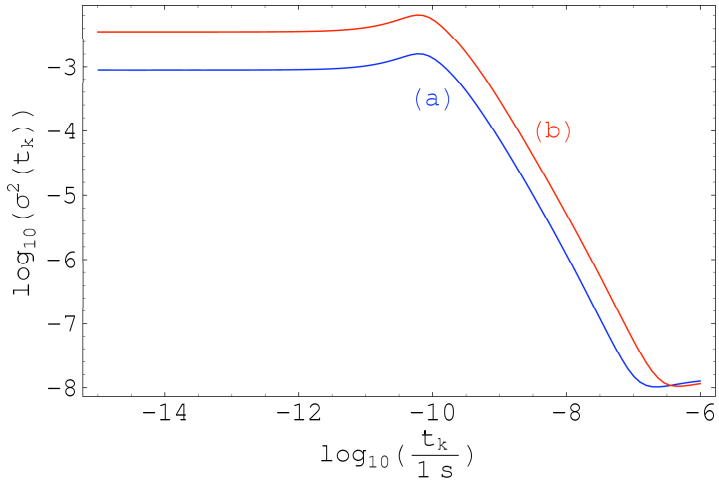

Figure 54: The function $\sigma^2(k)$ for the BSI spectrum when $k_s = 5.5 \times 10^{-14}\mathrm{m}^{-1}$ ($t_s = 10^{-10}\mathrm{s}$) and (a) $p = 0.0040$, (b) $p = 0.0020$.

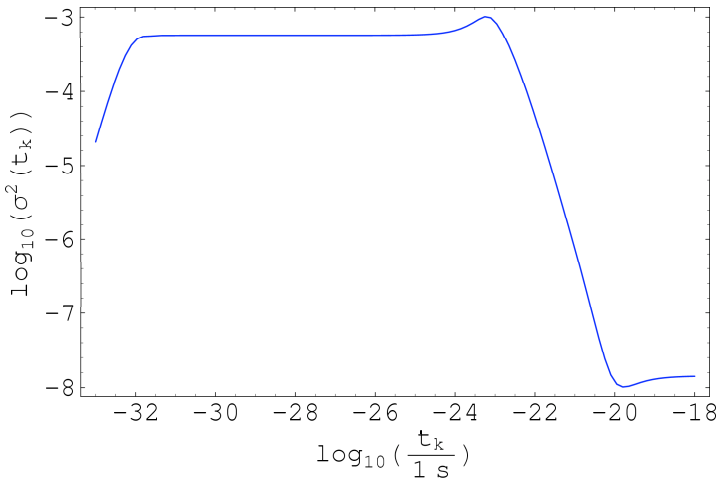

Figure 55: The function $\sigma^2(k)$ for the BSI spectrum when $k_s = 1.7 \times 10^{-7}\mathrm{m}^{-1}$ ($t_s = 10^{-23}\mathrm{s}$) and $p = 0.0050$.

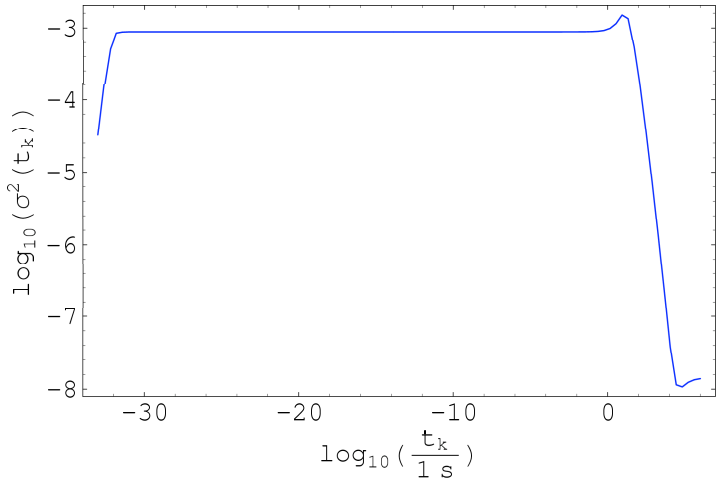

Figure 56: The function $\sigma^2(k)$ for the BSI spectrum when $k_s = 1.2 \times 10^{-19}\mathrm{m}^{-1}$ ($t_s = 20\mathrm{s}$) and $p = 0.0040$.

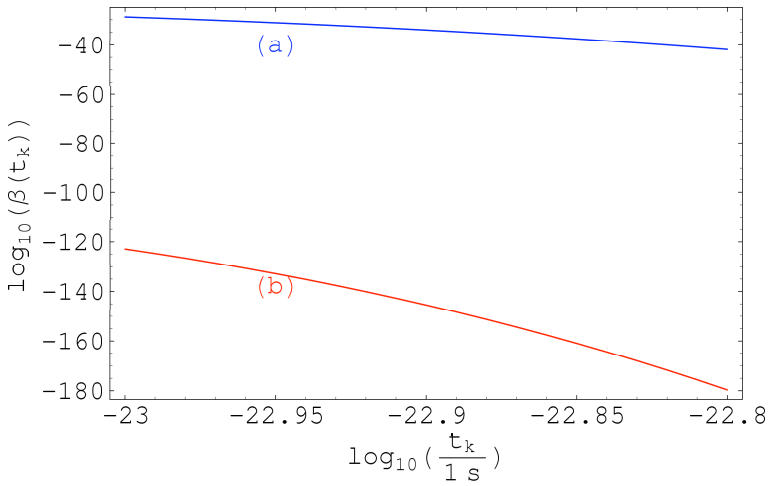

Figure 57: The function $\beta(k)$ for the BSI spectrum for $t_s = 10^{-23}$s ($k_s = 1.7 \times 10^{-7}\text{m}^{-1}$) with $p = 0.0050$ and with (a) $\delta_c = 1/3$ and (b) $\delta_c = 0.7$. When $t_k = 10^{-23}$s we have the values (a) $\beta(k) \sim 10^{-28}$ and (b) $\beta(k) \sim 10^{-123}$.

influence of p, t_s and δ_c on the values of $\beta(k)$. In Figure 57 we have the curve of $\beta(k)$ for $t_s = 10^{-23}$s ($k_s = 1.7 \times 10^{-7}\text{m}^{-1}$; which corresponds to have the jump right at the end of inflation) and $p = 0.0050$. When $\delta_c = 1/3$ we have $\beta(k) \sim 10^{-28}$ near the step but if $\delta_c = 0.7$ then the corresponding value of $\beta(k)$ will be of order 10^{-123}. Notice that although $p = 0.0050$ corresponds to the minimum value allowed for p when $\delta_c = 1/3$ that is not the case when $\delta_c = 0.7$. In that case we have $p_{min}(0.7) \approx 0.0024$ (see Table 5).

Considering $p = 0.0040$ we have in Figures 58, 59, 60, 61 and 62 the curves of $\beta(k)$ for the remaining cases: $t_s = 10^{-10}$s ($k_s = 5.5 \times 10^{-14}\text{m}^{-1}$), $t_s = 10^{-6}$s ($k_s = 5.5 \times 10^{-16}\text{m}^{-1}$), $t_s = 6 \times 10^{-5}$s ($k_s = 7.1 \times 10^{-17}\text{m}^{-1}$), $t_s = 20$s ($k_s = 1.2 \times 10^{-19}\text{m}^{-1}$) and $t_s = 2 \times 10^{5}$s ($k_s = 1.2 \times 10^{-21}\text{m}^{-1}$). Notice that $\beta(k)$ starts always as a growing function attaining its maximum value near t_s and then it decreases very rapidly. This behaviour was hidden in the case $t_s = 10^{-23}$s (cf. Figure 57) because we are considering only $t \geq 10^{-23}$s.

It seems that the order of β_{max} does not depend on the location of k_s. From Figures 58 to 62 we sse that for $\delta_c = 1/3$ and $p = 0.0040$ we have always $\beta_{max} \sim 10^{-16}$ and for $\delta_c = 0.7$ and $p = 0.0040$ we have always $\beta_{max} \sim 10^{-68}$. This was not the case for the pure step power law spectrum with a pure step (cf. Figures 45 and 46).

We will increase now the value of p and see what happens to $\beta(k)$. In Figures 63, 64 and 65 we have the curve of $\beta(k)$ for the case $p = 0.01$. It is notorius that the obtained values for $\beta(k)$ are smaller by several orders of magnitude when compared with the ones obtained previously (Figures 57 to 62).

With the data obtained from Figures 58 to 62 it is possible to find a relation between the location of the step and the location of the maximum value allowed

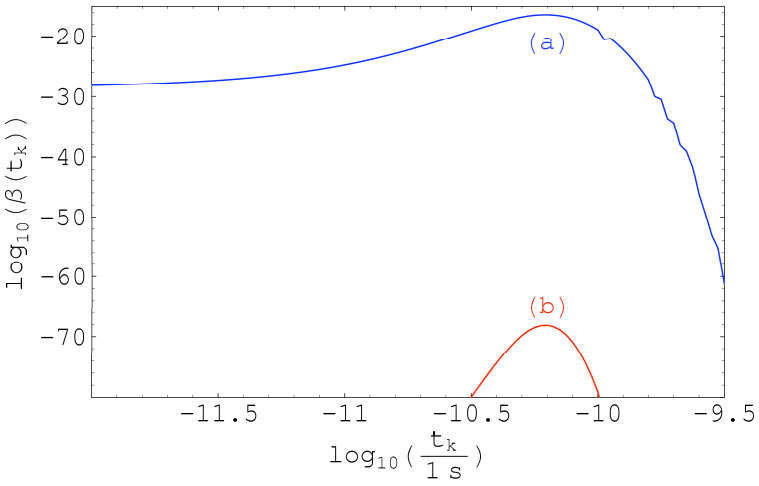

Figure 58: The function $\beta(k)$ for the BSI spectrum when $k_s = 5.5 \times 10^{-14}\mathrm{m}^{-1}$ ($t_s = 10^{-10}$s) with $p = 0.0040$ and with (a) $\delta_c = 1/3$ and (b) $\delta_c = 0.7$. The maximum values attained by $\beta(k)$ are (a) $\beta_{max} \sim 10^{-16}$ and (b) $\beta_{max} \sim 10^{-68}$ and they are located at $t_k \approx 10^{-10.2}$s.

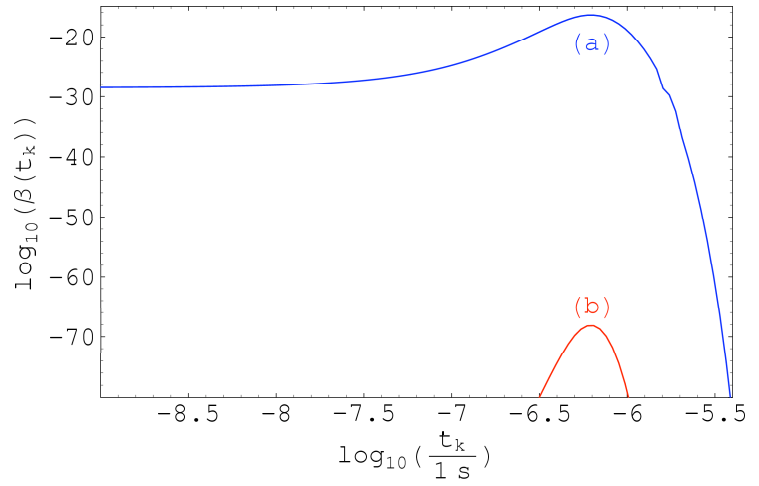

Figure 59: The function $\beta(k)$ for the BSI spectrum when $k_s = 5.5 \times 10^{-16}\mathrm{m}^{-1}$ ($t_s = 10^{-6}$s) with $p = 0.0040$ and with (a) $\delta_c = 1/3$ and (b) $\delta_c = 0.7$. The maximum values attained by $\beta(k)$ are (a) $\beta_{max} \sim 10^{-16}$ and (b) $\beta_{max} \sim 10^{-68}$ and they are located at $t_k \approx 10^{-6.2}$s.

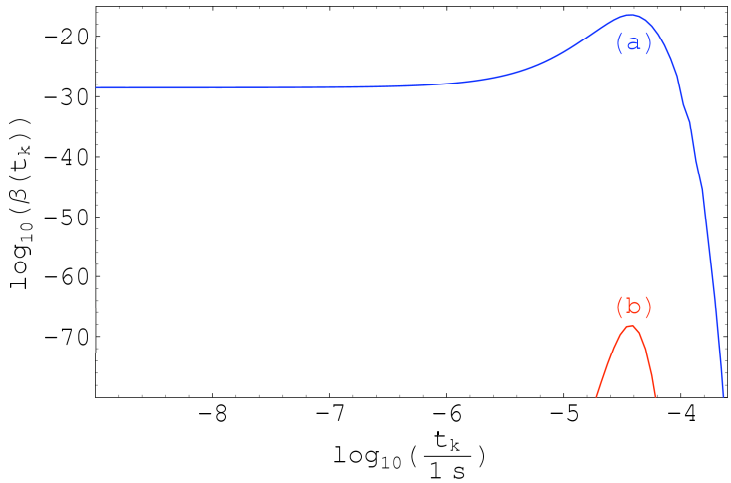

Figure 60: The function $\beta(k)$ for the BSI spectrum when $k_s = 7.1 \times 10^{-17}\mathrm{m}^{-1}$ ($t_s = 6 \times 10^{-5}\mathrm{s}$) with $p = 0.0040$ and with (a) $\delta_c = 1/3$ and (b) $\delta_c = 0.7$. The maximum values attained by $\beta(k)$ are (a) $\beta_{max} \sim 10^{-16}$ and (b) $\beta_{max} \sim 10^{-68}$ and they are located at $t_k \approx 10^{-4.4}\mathrm{s}$.

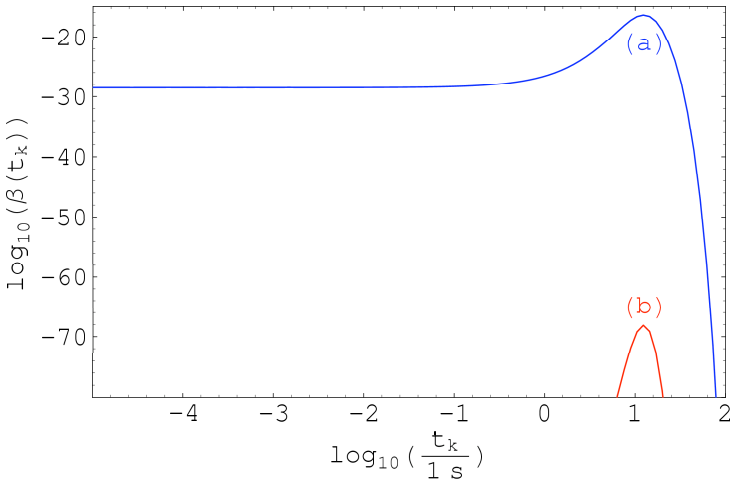

Figure 61: The function $\beta(k)$ for the BSI spectrum when $k_s = 1.2 \times 10^{-19}\mathrm{m}^{-1}$ ($t_s = 20\mathrm{s}$) with $p = 0.0040$ and with (a) $\delta_c = 1/3$ and (b) $\delta_c = 0.7$. The maximum values attained by $\beta(k)$ are (a) $\beta_{max} \sim 10^{-16}$ and (b) $\beta_{max} \sim 10^{-68}$ and they are located at $t_k \approx 10^{1.1}\mathrm{s}$.

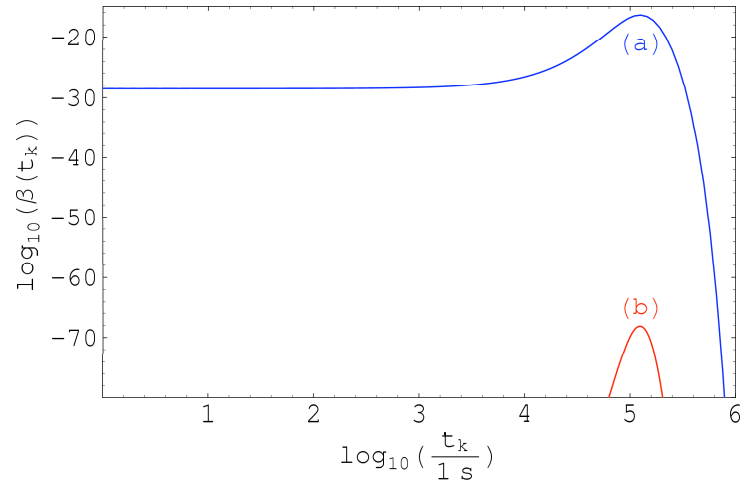

Figure 62: The function $\beta(k)$ for the BSI spectrum when $k_s = 1.2 \times 10^{-21}\mathrm{m}^{-1}$ ($t_s = 2 \times 10^5\mathrm{s}$) with $p = 0.0040$ and with (a) $\delta_c = 1/3$ and (b) $\delta_c = 0.7$. The maximum values attained by $\beta(k)$ are (a) $\beta_{max} \sim 10^{-16}$ and (b) $\beta_{max} \sim 10^{-68}$ and they are located at $t_k \approx 10^{5.1}\mathrm{s}$.

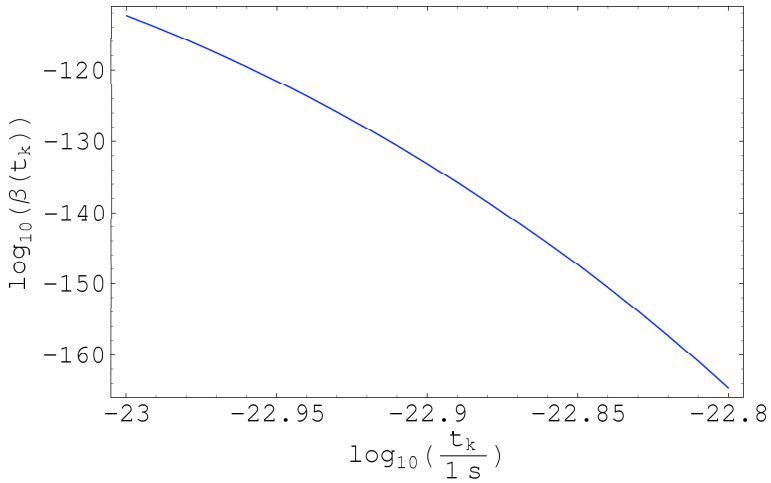

Figure 63: The function $\beta(k)$ for the BSI spectrum for $t_s = 10^{-23}\mathrm{s}$ ($k_s = 1.7 \times 10^{-7}\mathrm{m}^{-1}$) with $p = 0.01$ and with $\delta_c = 1/3$. When $t_k = 10^{-23}\mathrm{s}$ we have $\beta(k) \sim 10^{-112}$.

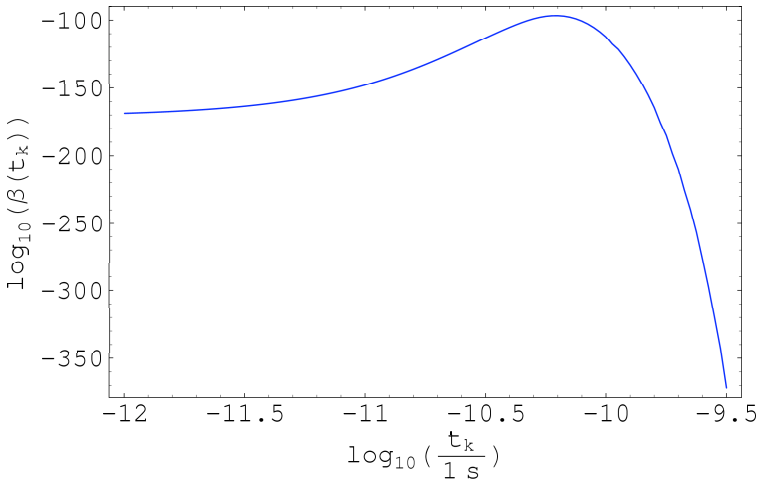

Figure 64: The function $\beta(k)$ for the BSI spectrum when $k_s = 5.5 \times 10^{-14}\mathrm{m}^{-1}$ ($t_s = 10^{-10}$s) with $p = 0.01$ and $\delta_c = 1/3$. The maximum value attained by $\beta(k)$ is $\beta_{max} \sim 10^{-97}$ located at $t_k \approx 10^{-10.2}$s. The case $\delta_c = 0.7$ (not represented) gives $\beta_{max} \sim 10^{-421}$.

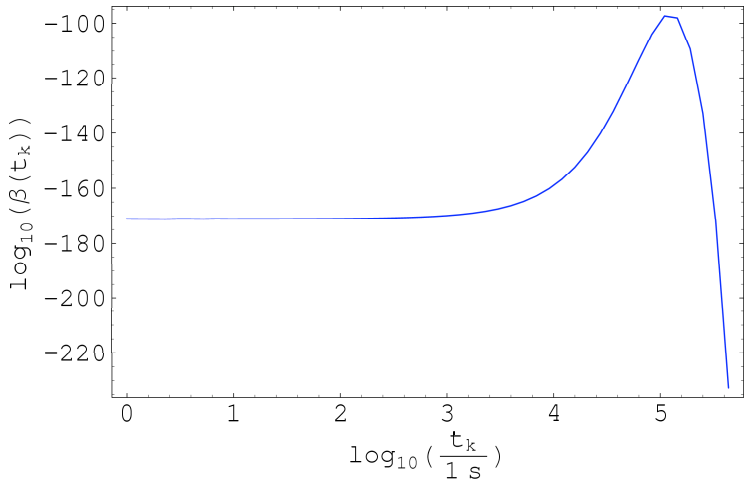

Figure 65: The function $\beta(k)$ for the BSI spectrum when $k_s = 1.2 \times 10^{-21}\mathrm{m}^{-1}$ ($t_s = 2 \times 10^{5}$s) with $p = 0.01$ and $\delta_c = 1/3$. The maximum value attained by $\beta(k)$ is $\beta_{max} \sim 10^{-97}$ located at $t_k \approx 10^{5.1}$s. The case $\delta_c = 0.7$ (not represented) gives $\beta_{max} \sim 10^{-421}$.

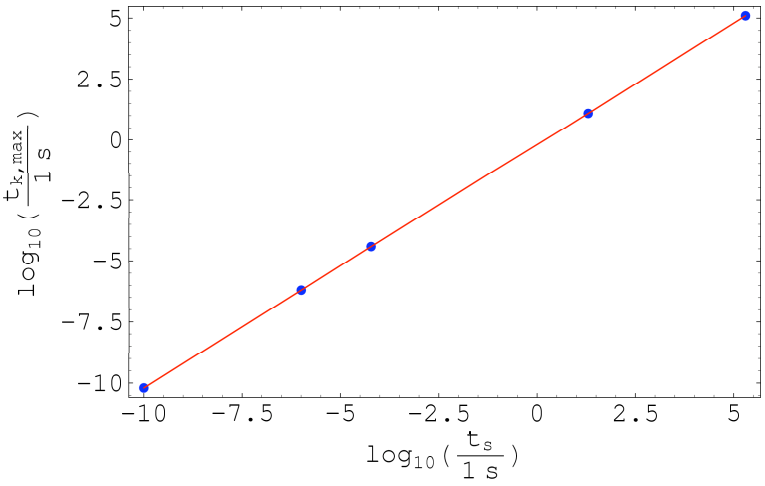

Figure 66: The relation between $t_{k_{max}}$ (corresponding to the instant for which $\beta(k)$ gets its maximum) and t_s for the BSI spectrum.

for $\beta(k)$. The location of β_{max} depends only on the value of t_s (the value of β_{max} depends also on the values of p and δ_c). In Figure 66 it is represented the dependence between $t_{k_{max}}$ (the instant corresponding to β_{max}) and t_s. This linear relation can be written as

$$t_{k_{max}} \approx 0.63 t_s \tag{147}$$

which is very similar to the result obtained for the pure step power spectrum (cf. equation 146).

In Figure 67 we have the curve of $\beta(k)$ when $t_s = 10^{-6}$s and with δ_c assuming the values $1/3$, 0.4 and 0.7. In each case it was considered the correspondent minimum value allowed for p (cf. Table 5). Notice that previously we have considered the cases $\delta_c = 1/3$ and $\delta_c = 0.7$ but with the same value of p for both (e.g. Figure 59). The example of Figure 67 shows that when one combines a given δ_c with the respective value of p_{min} (cf. Table 5) the obtained results for $\beta(k)$ are very similar.

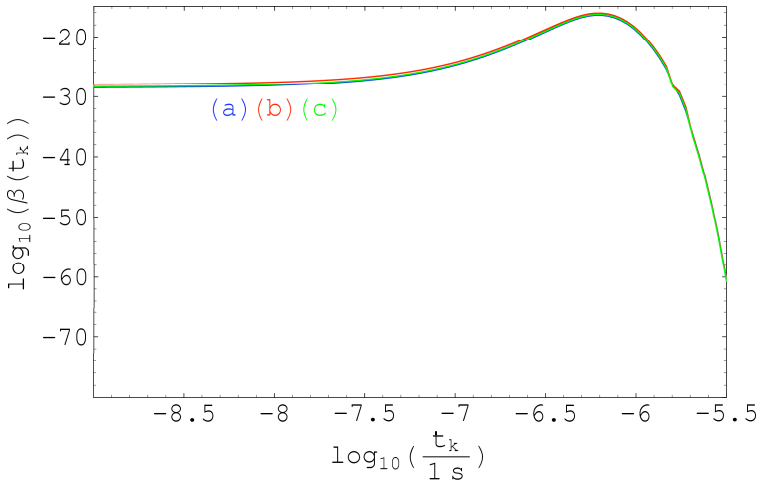

Figure 67: The function $\beta(k)$ for the BSI spectrum with $t_s = 10^{-6}$s ($k_s = 5.5 \times 10^{-16}\text{m}^{-1}$) and (a) $\delta_c = 1/3$, $p = p_{min}(1/3) \approx 0.0040$, (b) $\delta_c = 0.4$, $p = p_{min}(0.4) \approx 0.0033$ and (c) $\delta_c = 0.7$, $p = p_{min}(0.7) \approx 0.0019$. The maximum values of $\beta(k)$ are of the same order for all cases ($\beta_{max} \sim 10^{-16}$) and they are located at $t_k \approx 10^{-6.2}$s.

5.4 Running–tilt power law spectrum

The observational input needed for the running–tilt power spectrum are, besides the value of $\delta_H^2(k_0, t_{k_0})$, the values for the parameters n_i evaluated at some pivot scale k_c. According to the most recent results from the WMAP mission we have (e.g. Spergel et al., 2006)

$$n_0 = n_s(k_c) = 0.951^{+0.015}_{-0.019} \tag{148}$$

$$n_1 = \alpha_s(k_c) = -0.055^{+0.029}_{-0.035} \tag{149}$$

where the pivot scale is $k_c = 0.002\text{Mpc}^{-1} \approx 6.5 \times 10^{-26}\text{m}^{-1}$. The values for the other parameters (i.e. the values of n_i, $i \geq 2$) are unknown at the present. A definitive measurement of n_1, and possibly also of n_2 and n_3 is expected from upcoming surveys such as the Planck satellite mission (e.g. Düchting, 2004).

Here we will consider for n_0 and n_1 the values obtained from the WMAP mission and we will look for some sets of values for n_2 and n_3 leading to a blue spectrum ($n(k) > 1$) because that is the case which favours PBH production. The remaining n_i (n_i, $i \geq 4$) will be set to zero. Within this assumption equation (131) can be written as

$$n(k) = n_0 + \frac{n_1}{2} \ln \frac{k}{k_c} + \frac{n_2}{6} \left(\ln \frac{k}{k_c} \right)^2 + \frac{n_3}{24} \left(\ln \frac{k}{k_c} \right)^3 \tag{150}$$

According to the observational constraints the maximum value allowed for $n(k)$ should be somewhere between 1.2 and 1.4 (e.g. Green & Liddle, 1997). Thus, for a given pair of values n_2 and n_3 we will consider that we have a blue spectrum if

$$1 < n(k) \leq 1.4 \tag{151}$$

We must ensure also that $\beta(10^{15}\text{g})$ does not exceed the value 10^{-28}. Thus, inserting the observational constraint $\beta(10^{15}\text{g}) \sim 10^{-28}$ into equation (71) we may numerically find, for a given δ_c, the corresponding value for the spectral index $n(k)$. For example, when $\delta_c = 1/3$ we have $n(10^{15}\text{g}) \approx 1.2412$, which is the highest value allowed for $n(10^{15}\text{g})$. In Table 6 we have the results for other values of δ_c.

If $n_2 = 0$ and $n_3 = 0$ we will have $n(k) < 1$ for all epochs as it is clear from Figure 68. Giving other values to n_2 and n_3 we may find situations for which condition (151) holds. Provided that $4n_2^2 - 9n_1n_3 > 0$ the function (150) shows a maximum and a minimum located at

$$k_\mp = k_c \exp\left(-\frac{4n_2}{3n_3} \mp \frac{2}{3n_3} \sqrt{4n_2^2 - 9n_1n_3} \right) \tag{152}$$

Fixing a value to $k_\mp$ we find the following linear relation between n_2 and n_3

$$n_3 = \frac{-4(3n_1 + 2n_2 \ln \frac{k_\mp}{k_c})}{3(\ln \frac{k_\mp}{k_c})^2} \tag{153}$$

Table 6: The maximum value allowed for the spectral index $n(10^{15}\mathrm{g})$ as a function of δ_c for the running–tilt power spectrum.

δ_c	$n(10^{15}\mathrm{g})$
1/3	1.2412
0.4	1.2493
0.5	1.2591
0.6	1.2671
0.7	1.2739

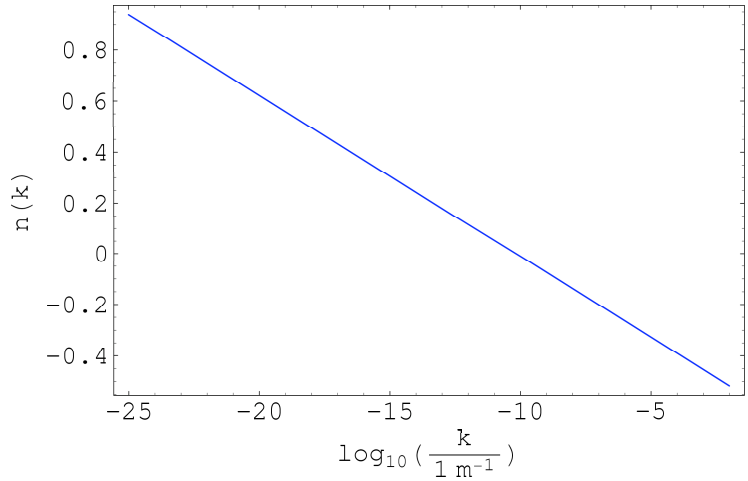

Figure 68: The function $n(k)$ (equation 150) with $n_2 = n_3 = 0$. We have that $n(k) < 1$ for all the epochs of interest.

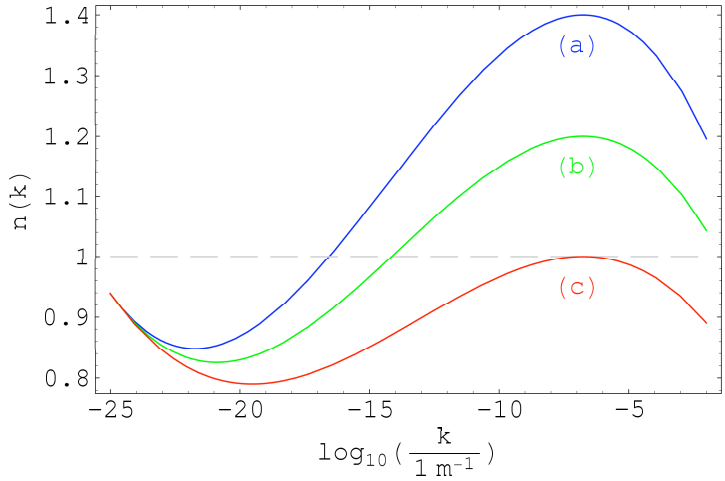

Figure 69: The function $n(k)$ (equation 150) with a maximum located at $k_+ = 1.7 \times 10^{-7}\mathrm{m}^{-1}$. The cases represented correspond to (a) $n(k_+) = 1.4$, $n_2 = 0.00123$, $n_3 = -0.000650$; (b) $n(k_+) = 1.2$, $n_2 = 0.0103$, $n_3 = -0.000524$ and (c) $n(k_+) = 1$, $n_2 = 0.00827$, $n_3 = -0.000398$.

Considering $d^2n(k)/dk^2 = 0$ with n_3 replaced by the expression (153) we find out that $n(k)$ has an inflexion point located at

$$n_{2_{inf}} = -\frac{3n_1}{\ln \frac{k_\mp}{k_c}} \tag{154}$$

Taking into account that $n_1 < 0$ and that $\ln \frac{k_\mp}{k_c} > 0$ [6] it turns out that $n(k)$ will have a maximum (k_+) if $n_2 > n_{2_{inf}}$ and a minimum (k_-) if $n_2 < n_{2_{inf}}$. We are interested in the case of the existence of a maximum and on the possible values of n_2 that verify condition (151). To find out those values we will consider $n(k_+) = 1$ and $n(k_+) = 1.4$ with n_3 replaced by the expression (153).

We will consider for k_+ the same values that we have atributted to k_s in the pure step and BSI spectrums (cf. Section 5.2, Section 5.3, Table 2). In Table 7 we have, for each case, the values of n_2 and n_3 such that $n(k_+) = 1$, $n(k_+) = 1.2$, $n(k_+) = 1.3$ and $n(k_+) = 1.4$. In Figures 69 to 74 we have the curves of $n(k)$ for all the cases considered in Table 7.

It is clear that we must exclude the cases $n(k_+) = 1.3$ and $n(k_+) = 1.4$ when $k_+ = 1.7 \times 10^{-7}\mathrm{m}^{-1}$ ($t_{k_+} = 10^{-23}\mathrm{s}$). That is because on that cases we will have $\beta(10^{-23}\mathrm{s}) \gg 10^{-28}$ which does not agree with observation. As we have already seen $n(1.7 \times 10^{-7}\mathrm{m}^{-1})$ should not exceed 1.24121 (see Figure 69).

In Figure 75 we have examples of the typical form for the running–tilt power spectrum (equation 104 with n replaced by $n(k)$) in comparisson to the scale–

[6] We will always have $\ln \frac{k_\mp}{k_c} > 0$ because the values of $k_\mp$ we are interested in are by far greater than the pivot scale $k_c \approx 6.5 \times 10^{-26}\mathrm{m}^{-1}$.

Table 7: The values for the parameters n_2 and n_3 leading to a maximum of the spectral index $n(k)$ located at k_+. We have considered maximum values of $n(k)$ equal to 1, 1.2, 1.3 and 1.4.

	$n(k_+) = 1$		$n(k_+) = 1.2$	
$k_+(\mathrm{m}^{-1})$	n_2	n_3	n_2	n_3
1.7×10^{-7}	0.00827	-0.000398	0.0103	-0.000524
5.5×10^{-14}	0.0132	-0.000989	0.0180	-0.00145
5.5×10^{-16}	0.0161	-0.00146	0.0230	-0.00226
7.1×10^{-17}	0.0179	-0.00178	0.0262	-0.00285
1.2×10^{-19}	0.0271	-0.00395	0.0444	-0.00715
1.2×10^{-21}	0.0427	-0.00932	0.0800	-0.0194
	$n(k_+) = 1.3$		$n(k_+) = 1.4$	
$k_+(\mathrm{m}^{-1})$	n_2	n_3	n_2	n_3
1.7×10^{-7}	0.0113	-0.000587	0.0123	-0.000650
5.5×10^{-14}	0.0203	-0.00168	0.0227	-0.00192
5.5×10^{-16}	0.0265	-0.00267	0.0299	-0.00307
7.1×10^{-17}	0.0304	-0.00338	0.0345	-0.00391
1.2×10^{-19}	0.0530	-0.00875	0.0617	-0.0103
1.2×10^{-21}	0.0987	-0.0245	0.117	-0.0296

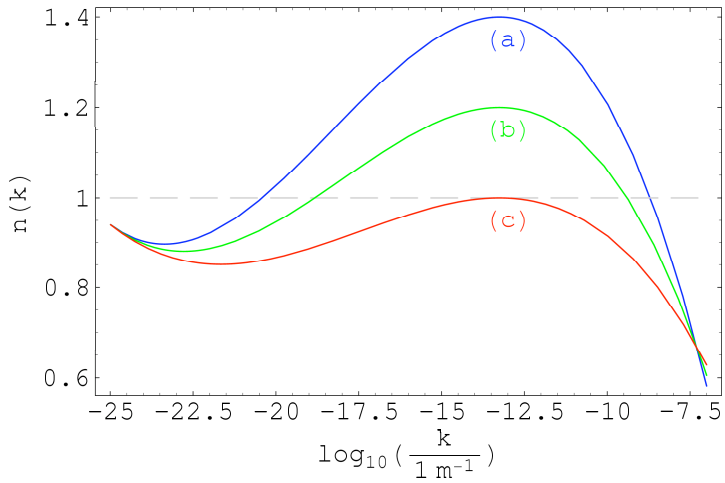

Figure 70: The function $n(k)$ (equation 150) with a maximum located at $k_+ = 5.5 \times 10^{-14}\mathrm{m}^{-1}$. The cases represented correspond to (a) $n(k_+) = 1.4$, $n_2 = 0.0227$, $n_3 = -0.00192$; (b) $n(k_+) = 1.2$, $n_2 = 0.0180$, $n_3 = -0.00145$ and (c) $n(k_+) = 1$, $n_2 = 0.0132$, $n_3 = -0.000989$.

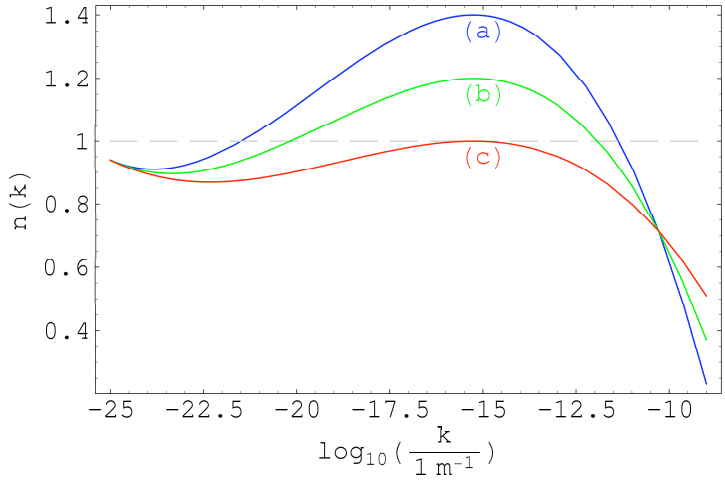

Figure 71: The function $n(k)$ (equation 150) with a maximum located at $k_+ = 5.5 \times 10^{-16}\mathrm{m}^{-1}$. The cases represented correspond to (a) $n(k_+) = 1.4$, $n_2 = 0.0299$, $n_3 = -0.00307$; (b) $n(k_+) = 1.2$, $n_2 = 0.0230$, $n_3 = -0.00226$ and (c) $n(k_+) = 1$, $n_2 = 0.0161$, $n_3 = -0.00146$.

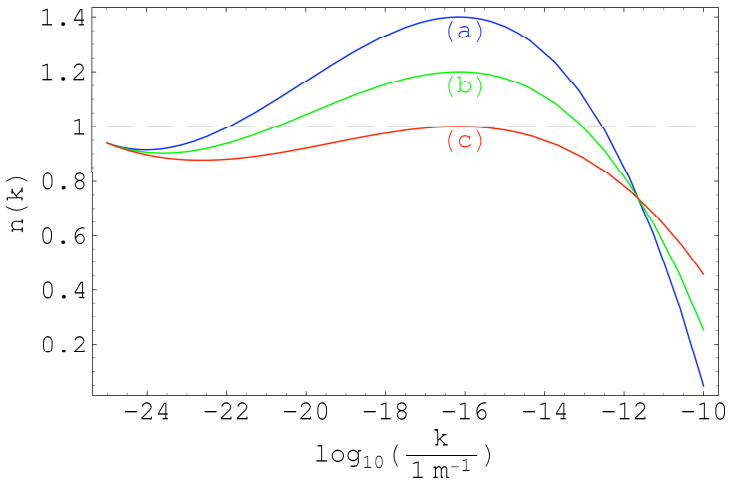

Figure 72: The function $n(k)$ (equation 150) with a maximum located at $k_+ = 7.1 \times 10^{-17}\mathrm{m}^{-1}$. The cases represented correspond to (a) $n(k_+) = 1.4$, $n_2 = 0.0345$, $n_3 = -0.00391$; (b) $n(k_+) = 1.2$, $n_2 = 0.0262$, $n_3 = -0.00285$ and (c) $n(k_+) = 1$, $n_2 = 0.0179$, $n_3 = -0.00178$.

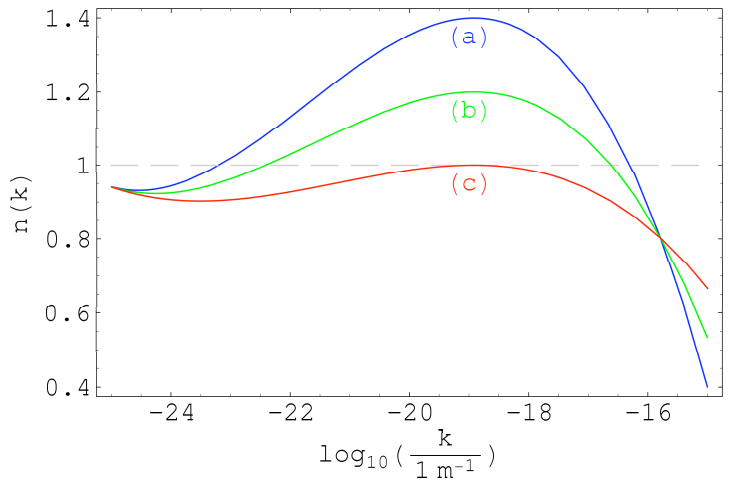

Figure 73: The function $n(k)$ (equation 150) with a maximum located at $k_+ = 1.2 \times 10^{-19}\mathrm{m}^{-1}$. The cases represented correspond to (a) $n(k_+) = 1.4$, $n_2 = 0.0617$, $n_3 = -0.0103$; (b) $n(k_+) = 1.2$, $n_2 = 0.0444$, $n_3 = -0.00715$ and (c) $n(k_+) = 1$, $n_2 = 0.0271$, $n_3 = -0.00395$.

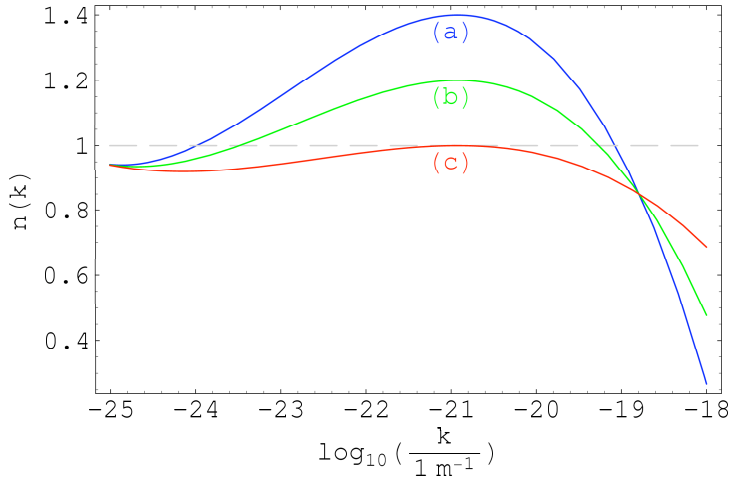

Figure 74: The function $n(k)$ (equation 150) with a maximum located at $k_+ = 1.2 \times 10^{-21}\mathrm{m}^{-1}$. The cases represented correspond to (a) $n(k_+) = 1.4$, $n_2 = 0.117$, $n_3 = -0.0296$; (b) $n(k_+) = 1.2$, $n_2 = 0.00800$, $n_3 = -0.0194$ and (c) $n(k_+) = 1$, $n_2 = 0.0427$, $n_3 = -0.00932$.

free power spectrum (Section 4.1).

Let us now analise the behaviour of the function $\alpha^2(k)$ (equation 110 with the spectral index given by equation 150). In Figure 76 we have the curve of $\alpha^2(k)$ when $n(k_+) = 1.4$ with k_+ assuming the values $5.5 \times 10^{-14}\mathrm{m}^{-1}$ ($t_{k_+} = 10^{-10}$s), $5.5 \times 10^{-16}\mathrm{m}^{-1}$ ($t_{k_+} = 10^{-6}$s) and $1.2 \times 10^{-19}\mathrm{m}^{-1}$ ($t_{k_+} = 20$s). In Figure 77 we have the curve of $\alpha^2(k)$ for $k_+ = 5.5 \times 10^{-16}\mathrm{m}^{-1}$ ($t_{k_+} = 10^{-6}$s) now with $n(k_+)$ assuming the values 1.2, 1.3 and 1.4.

Let us now turn our attention to the function $\sigma^2(k)$ (equation 112). In Figures 78 and 79 we have the curve of $\sigma^2(k)$ for the same examples that we have considered for $\alpha^2(k)$ (Figures 76 and 77). Notice that any peculiar features present in the curves of $\alpha^2(k)$ are smeared out when one gets to the $\sigma^2(k)$ function. It is clear from Figures 78 and 79 that when $t \sim 10^{12}$s the value of $\sigma^2(k)$ is already very close to the present value $\sigma_0^2 \sim 10^{-8}$.

We will consider now the function $\beta(k)$. We want to explore the influence of k_+, $n(k_+)$ and δ_c on the values of $\beta(k)$ (remember that the influence of k_+ is incorporated into the parameters n_2 and n_3).

In Figures 80 to 84 we explore the case $n(k_+) = 1.4$ when $t_{k_+} = 10^{-10}$s ($k_+ = 5.5 \times 10^{-14}\mathrm{m}^{-1}$), $t_{k_+} = 10^{-6}$s ($k_+ = 5.5 \times 10^{-16}\mathrm{m}^{-1}$), $t_{k_+} = 6 \times 10^{-5}$s ($k_+ = 7.1 \times 10^{-17}\mathrm{m}^{-1}$), $t_{k_+} = 20$s ($k_+ = 1.2 \times 10^{-19}\mathrm{m}^{-1}$) and $t_{k_+} = 2 \times 10^{5}$s ($k_+ = 1.2 \times 10^{-21}\mathrm{m}^{-1}$). In Figures 80 and 81 we have considered both $\delta_c = 1/3$ and $\delta_c = 0.7$. On the remaining cases (Figures 82 to 84) we have considered only the curve of $\beta(k)$ with $\delta_c = 1/3$. That was because, on that cases, the obtained values for $\beta(k)$ when $\delta_c = 0.7$ were much smaller than the ones obtained with $\delta_c = 1/3$ (see Figure captions). Notice that $\beta(k)$ starts as a growing function,

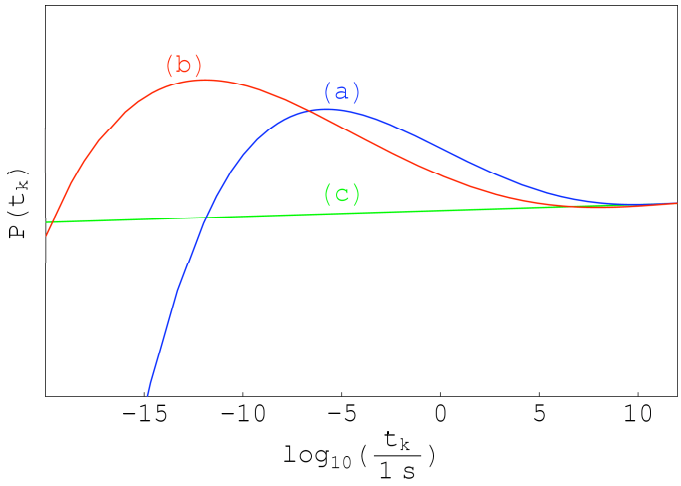

Figure 75: Typical form of the running–tilt power spectrum (curves (a) and (b)) in comparisson with the scale–free power law spectrum (curve (c)). The curve (a) corresponds to $k_+ = 7.1 \times 10^{-17}\mathrm{m}^{-1}$ with $n(k_+) = 1.4$ and the curve (b) corresponds to $k_+ = 5.5 \times 10^{-14}\mathrm{m}^{-1}$ with $n(k_+) = 1.4$ (cf. Table 7). The curve (c) represents the scale–free power law spectrum with $n(k) = 0.951$.

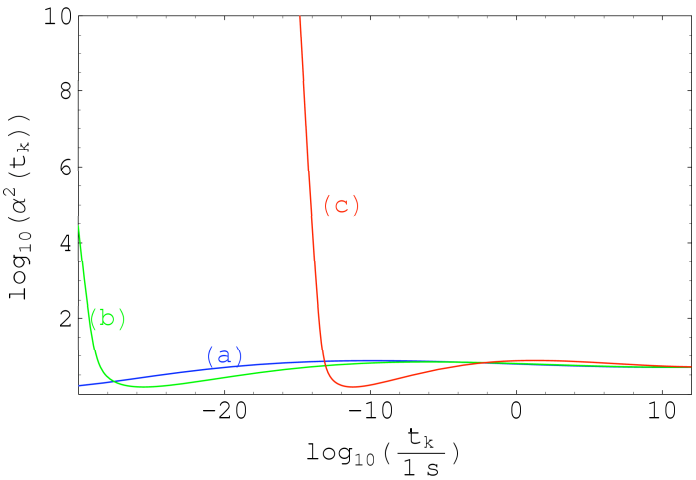

Figure 76: The function $\alpha^2(k)$ for the running–tilt power spectrum when the spectral index has the maximum value $n(k_+) = 1.4$ with (a) $k_+ = 5.5 \times 10^{-14}\mathrm{m}^{-1}$ ($t_{k_+} = 10^{-10}$s), (b) $k_+ = 5.5 \times 10^{-16}\mathrm{m}^{-1}$ ($t_{k_+} = 10^{-6}$s) and (c) $k_+ = 1.2 \times 10^{-19}\mathrm{m}^{-1}$ ($t_{k_+} = 20$s).

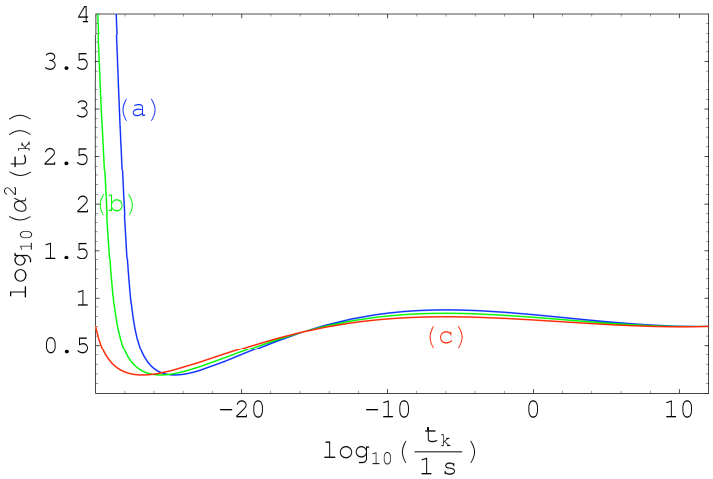

Figure 77: The function $\alpha^2(k)$ for the running–tilt power spectrum when the spectral index presents a maximum located at $k_+ = 5.5 \times 10^{-16}\mathrm{m}^{-1}$ ($t_{k_+} = 10^{-6}$s) with (a) $n(k_+) = 1.4$, (b) $n(k_+) = 1.3$ and (c) $n(k_+) = 1.2$.

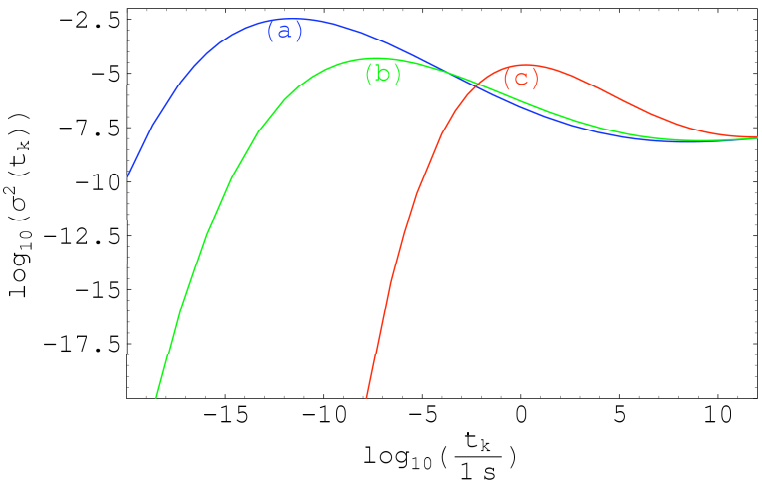

Figure 78: The function $\sigma^2(k)$ for the running–tilt power spectrum when the spectral index presents the maximum value $n(k_+) = 1.4$ with (a) $k_+ = 5.5 \times 10^{-14}\mathrm{m}^{-1}$ ($t_{k_+} = 10^{-10}$s), (b) $k_+ = 5.5 \times 10^{-16}\mathrm{m}^{-1}$ ($t_{k_+} = 10^{-6}$s) and (c) $k_+ = 1.2 \times 10^{-19}\mathrm{m}^{-1}$ ($t_{k_+} = 20$s).

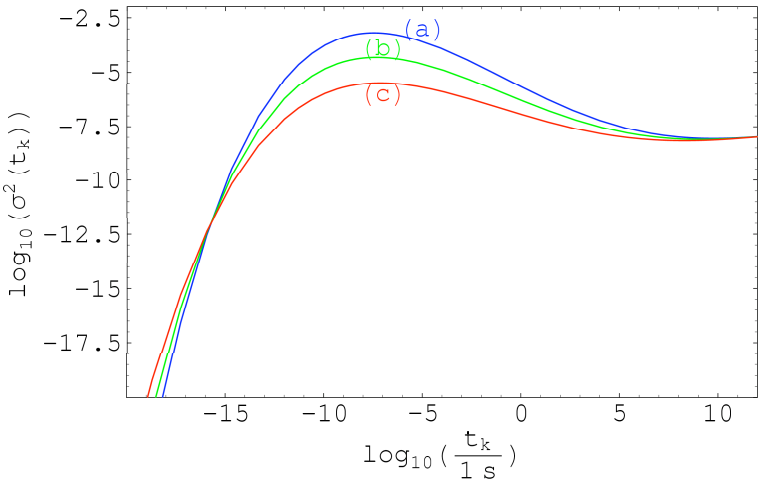

Figure 79: The function $\sigma^2(k)$ for the running–tilt power spectrum when the spectral index presents a maximum located at $k_+ = 5.5 \times 10^{-16}\mathrm{m}^{-1}$ ($t_{k_+} = 10^{-6}$s) with (a) $n(k_+) = 1.4$, (b) $n(k_+) = 1.3$ and (c) $n(k_+) = 1.2$.

attains its maximum value around the peak of $n(k)$ which is located at t_{k_+} and then it decreases to negligible values.

In Figures 85 and 86 we explore the case $n(k_+) = 1.3$ when $t_{k_+} = 10^{-10}$s ($k_+ = 5.5 \times 10^{-14}\mathrm{m}^{-1}$) and $t_{k_+} = 10^{-6}$s ($k_+ = 5.5 \times 10^{-16}\mathrm{m}^{-1}$). We have not considered further cases because, as it is clear, when one moves to shorter wavelenghts the obtained values for $\beta(k)$ will be smaller, by several orders of magnitude, and in the case $k_+ = 5.5 \times 10^{-16}\mathrm{m}^{-1}$ (Figure 86) we already have $\beta_{max} \sim 10^{-495}$ with $\delta_c = 1/3$.

In Figures 87 and 88 we explore the case $n(k_+) = 1.2$ when $t_{k_+} = 10^{-23}$s ($k_+ = 1.7 \times 10^{-7}\mathrm{m}^{-1}$) and $t_{k_+} = 10^{-10}$s ($k_+ = 5.5 \times 10^{-14}\mathrm{m}^{-1}$) with $\delta_c = 1/3$. Notice that although this value of $n(k_+)$ is well inside the range of values that lead to a blue spectrum (see condition 151) the obtained values for $\beta(k)$ are very small which makes the PBH production highly improbable.

We will consider also the case when $\beta(10^{-23}\mathrm{s}) \approx 10^{-28}$. As we have already seen this happens for $n(1.7 \times 10^{-7}\mathrm{m}^{-1}) \approx 1.2412$ when $\delta_c = 1/3$ (cf. Table 6). In that case we obtain from equation (150) the relation

$$n_3 \approx 0.000457871 - 0.0942809 n_2 \tag{155}$$

Inserting a given $k_\mp$ into equation (153) we find a second relation between n_2 and n_3. We will consider two examples. First, when $k_\mp = 1.7 \times 10^{-7}\mathrm{m}^{-1}$ ($t_{k_\mp} = 10^{-23}$s) we have

$$n_3 \approx 0.000122329 - 0.0628813 n_2 \tag{156}$$

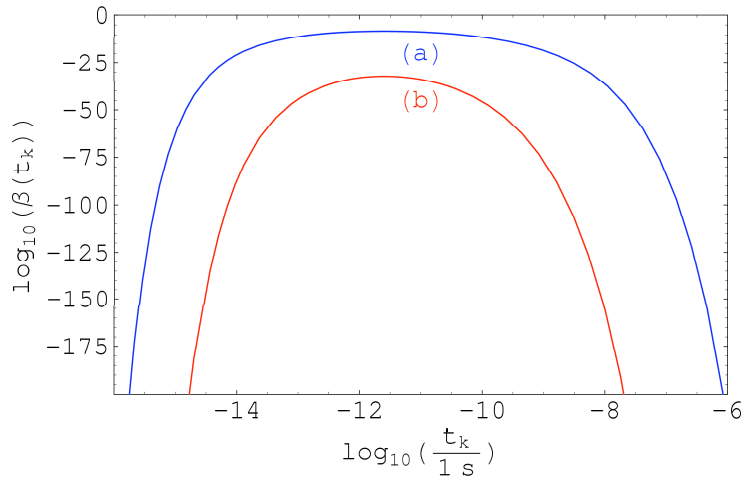

Figure 80: The function $\beta(k)$ for the running–tilt power spectrum when the maximum value of the spectral index is $n(k_+) = 1.4$ with $k_+ = 5.5 \times 10^{-14}\mathrm{m}^{-1}$ ($t_{k_+} = 10^{-10}$s) and (a) $\delta_c = 1/3$, (b) $\delta_c = 0.7$. The maximum values attained by $\beta(k)$ are (a) $\beta_{max} \sim 10^{-8}$ and (b) $\beta_{max} \sim 10^{-32}$ located at $t_k \approx 10^{-11.6}$s.

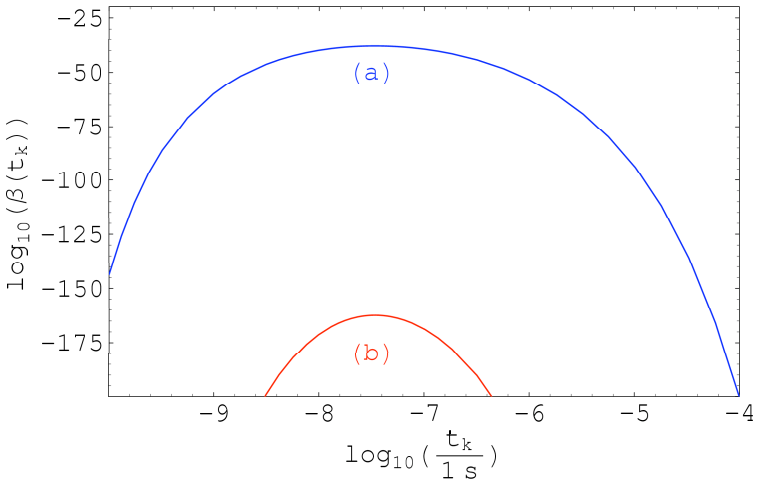

Figure 81: The function $\beta(k)$ for the running–tilt power spectrum when the maximum value of the spectral index is $n(k_+) = 1.4$ with $k_+ = 5.5 \times 10^{-16}\mathrm{m}^{-1}$ ($t_{k_+} = 10^{-6}$s) and (a) $\delta_c = 1/3$, (b) $\delta_c = 0.7$. The maximum values attained by $\beta(k)$ are (a) $\beta_{max} \sim 10^{-38}$ and (b) $\beta_{max} \sim 10^{-162}$ located at $t_k \approx 10^{-7.5}$s.

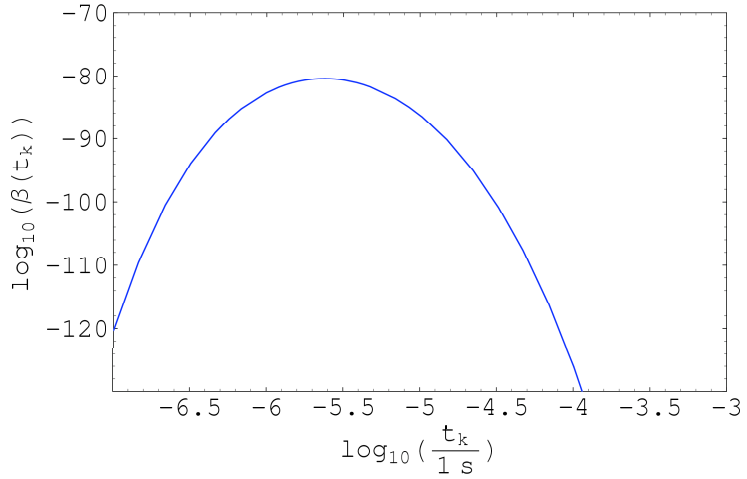

Figure 82: The function $\beta(k)$ for the running–tilt power spectrum when the maximum value of the spectral index is $n(k_+) = 1.4$ with $k_+ = 7.1 \times 10^{-17}\mathrm{m}^{-1}$ ($t_{k_+} = 6 \times 10^{-5}$s) and $\delta_c = 1/3$. The maximum value attained by $\beta(k)$ is $\beta_{max} \sim 10^{-80}$ located at $t_k \approx 10^{-5.6}$s. The case $\delta_c = 0.7$ (not represented) gives $\beta_{max} \sim 10^{-349}$.

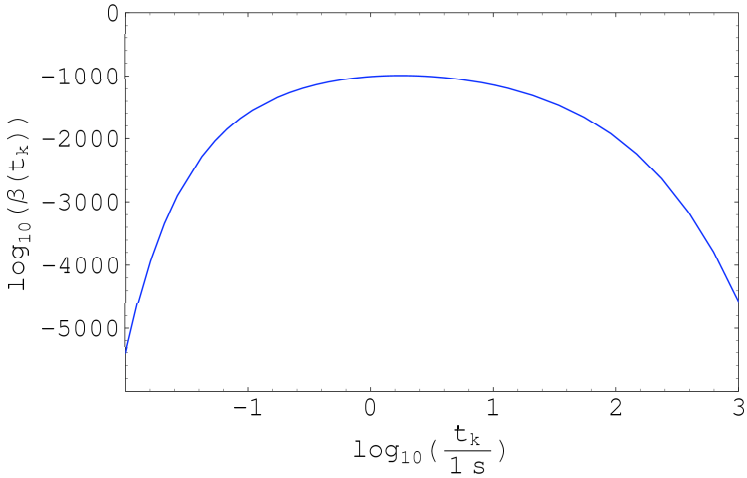

Figure 83: The function $\beta(k)$ for the running–tilt power spectrum when the maximum value of the spectral index is $n(k_+) = 1.4$ with $k_+ = 1.2 \times 10^{-19}\mathrm{m}^{-1}$ ($t_{k_+} = 20$s) and $\delta_c = 1/3$. The maximum value attained by $\beta(k)$ is $\beta_{max} \sim 10^{-990}$ located at $t_k \approx 10^{0.2}$s. The case $\delta_c = 0.7$ (not represented) gives $\beta_{max} \sim 10^{-4360}$.

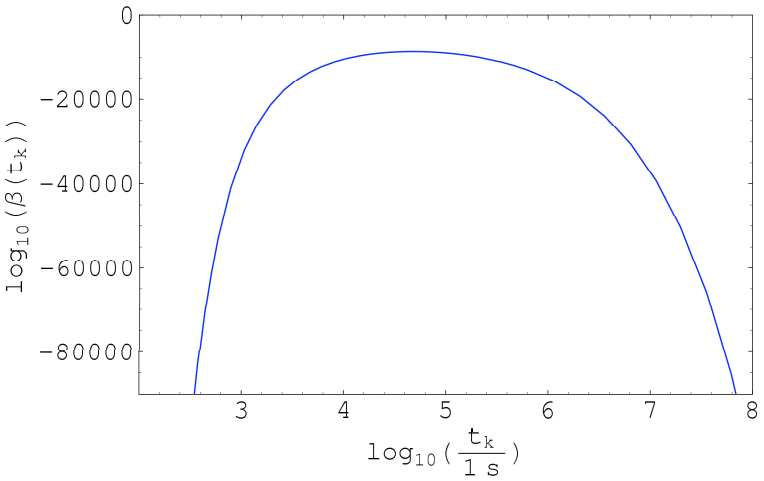

Figure 84: The function $\beta(k)$ for the running–tilt power spectrum when the maximum value of the spectral index is $n(k_+) = 1.4$ with $k_+ = 1.2 \times 10^{-21}\mathrm{m}^{-1}$ ($t_{k_+} = 2 \times 10^5\mathrm{s}$) and $\delta_c = 1/3$. The maximum value attained by $\beta(k)$ is $\beta_{max} \sim 10^{-8578}$ located at $t_k \approx 10^{4.7}\mathrm{s}$. The case $\delta_c = 0.7$ (not represented) gives $\beta_{max} \sim 10^{-37821}$.

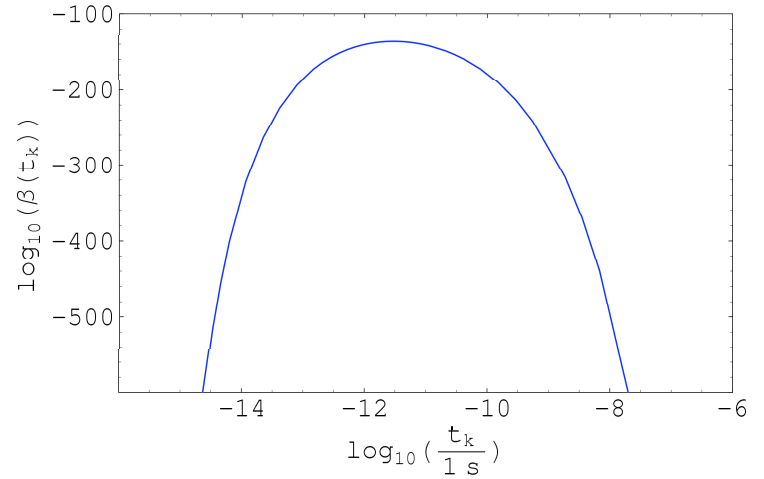

Figure 85: The function $\beta(k)$ for the running–tilt power spectrum when the maximum value of the spectral index is $n(k_+) = 1.3$ with $k_+ = 5.5 \times 10^{-14}\mathrm{m}^{-1}$ ($t_{k_+} = 10^{-10}\mathrm{s}$) and $\delta_c = 1/3$. The maximum value attained by $\beta(k)$ is $\beta_{max} \sim 10^{-136}$ located at $t_k \approx 10^{-11.5}\mathrm{s}$. The case $\delta_c = 0.7$ (not represented) gives $\beta_{max} \sim 10^{-596}$.

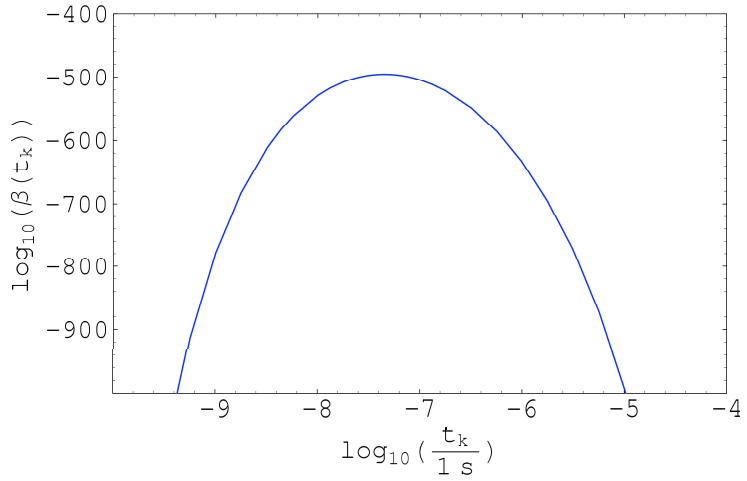

Figure 86: The function $\beta(k)$ for the running–tilt power spectrum when the maximum value of the spectral index is $n(k_+) = 1.3$ with $k_+ = 5.5 \times 10^{-16}\mathrm{m}^{-1}$ ($t_{k_+} = 10^{-6}$s) and $\delta_c = 1/3$. The maximum value attained by $\beta(k)$ is $\beta_{max} \sim 10^{-495}$ located at $t_k \approx 10^{-7.3}$s. The case $\delta_c = 0.7$ (not represented) gives $\beta_{max} \sim 10^{-2178}$.

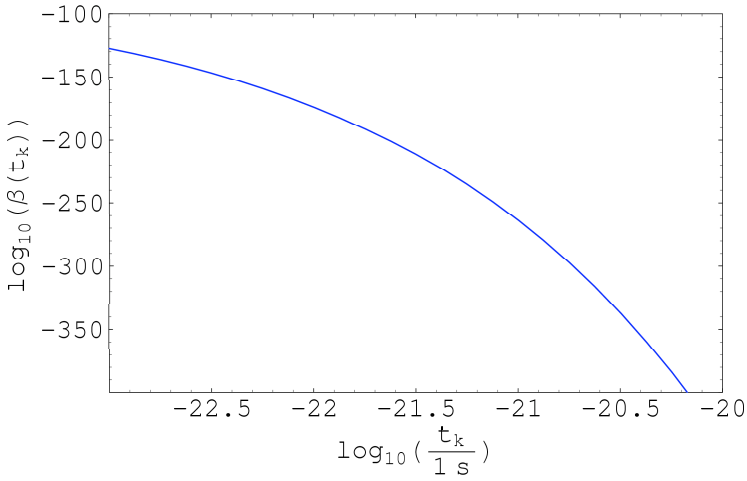

Figure 87: The function $\beta(k)$ for the running–tilt power spectrum when the maximum value of the spectral index is $n(k_+) = 1.2$ with $k_+ = 1.7 \times 10^{-7}\mathrm{m}^{-1}$ ($t_{k_+} = 10^{-23}$s) and $\delta_c = 1/3$. When $t_k = 10^{-23}$s we have $\beta(k) \sim 10^{-127}$. The case $\delta_c = 0.7$ (not represented) gives for $t_k = 10^{-23}$s the value $\beta(k) \sim 10^{-556}$.

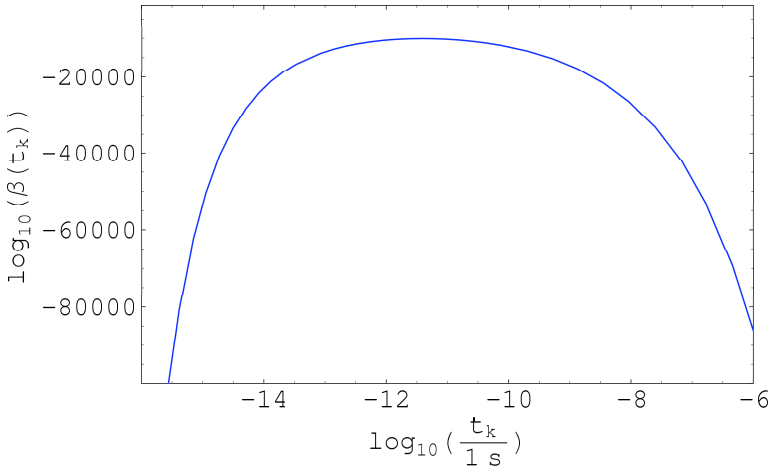

Figure 88: The function $\beta(k)$ for the running–tilt power spectrum when the maximum value of the spectral index is $n(k_+) = 1.2$ with $k_+ = 5.5 \times 10^{-14}\mathrm{m}^{-1}$ ($t_{k_+} = 10^{-10}$s) and $\delta_c = 1/3$. The maximum value attained by $\beta(k)$ is $\beta_{max} \sim 10^{-2295}$ located at $t_k \approx 10^{-11.3}$s. The case $\delta_c = 0.7$ (not represented) gives $\beta_{max} \sim 10^{-10102}$.

which means that in this case $n_2 \approx 0.010686$ and $n_3 \approx -0.00054967$. Second, when $k_\mp = 1.2 \times 10^{-21}\mathrm{m}^{-1}$ ($t_{k_\mp} = 2 \times 10^5$s) we have

$$n_3 \approx 0.00227979 - 0.271459 n_2 \tag{157}$$

which means that in this case $n_2 \approx 0.010283$ and $n_3 \approx -0.00051162$. In Figure 89 we have the curve of $n(k)$ for these two examples and in Figure 90 we have the corresponding curves for $\beta(k)$. Notice that $\beta(k)$ is of order 10^{-28} when $t_k = 10^{-23}$s and decreases very rapildly with time. When $t_k \sim 10^{-21}$s we already have for both cases $\beta(k) \sim 10^{-60}$.

With the data obtained from Figures 80 to 84 it is possible to find a relation between t_{k_+} (i.e. the point where $n(k)$ gets its maximum value) and the location of the maximum value allowed for $\beta(k)$. In Figure 91 it is represented the dependence between $t_{k_{max}}$ (the instant corresponding to β_{max}) and t_{k_+}. This relation can be written as

$$t_{k_{max}} \approx 0.0866 \times t_{k_+}^{1.064} \tag{158}$$

In Figure 92 we have the relation between β_{max} and t_{k_+} when $n(k_+) = 1.4$ and $\delta_c = 1/3$. In Figure 93 we have the same situation but now with $\delta_c = 0.7$. We have interpolated this relation with a quartic polynomial.

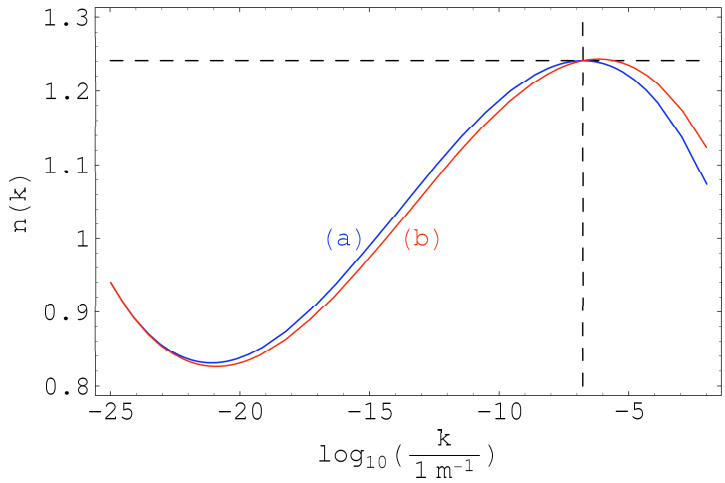

Figure 89: The function $n(k)$ in two cases such that $n(1.7\times10^{-7}\mathrm{m}^{-1}) \approx 1.2412$ (leading to $\beta(1.7\times10^{-7}\mathrm{m}^{-1}) \sim 10^{-28}$ when $\delta_c = 1/3$). The two cases are (a) $n_2 \approx 0.010686$, $n_3 \approx -0.00054967$ ($k_+ = 1.7\times10^{-7}\mathrm{m}^{-1}$) and (b) $n_2 \approx 0.010283$ and $n_3 \approx -0.00051162$ ($k_- = 1.2\times10^{-21}\mathrm{m}^{-1}$).

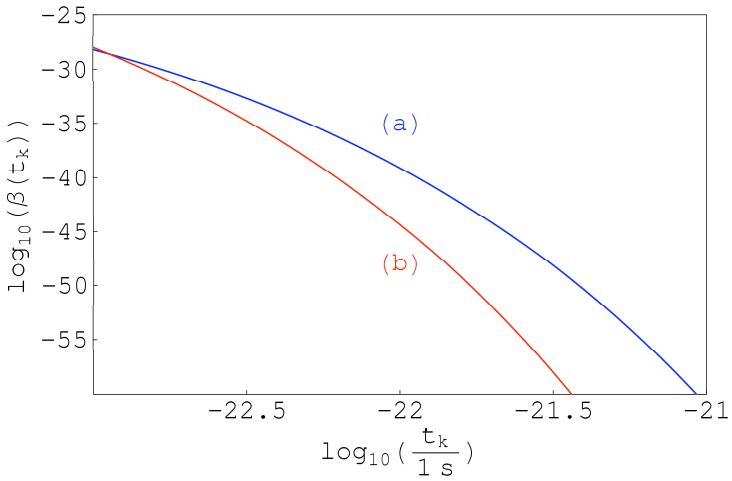

Figure 90: The function $\beta(k)$ for the running–tilt power spectrum when the maximum value of the spectral index is $n(k_+) = 1.2412$ with $\delta_c = 1/3$ and $\beta(10^{-23}\mathrm{s}) \sim 10^{-28}$. We have considered the cases (a) $k_+ = 1.7\times10^{-7}\mathrm{m}^{-1}$ and (b) $k_- = 1.2\times10^{-21}\mathrm{m}^{-1}$ (cf. Figure 89 for more details).

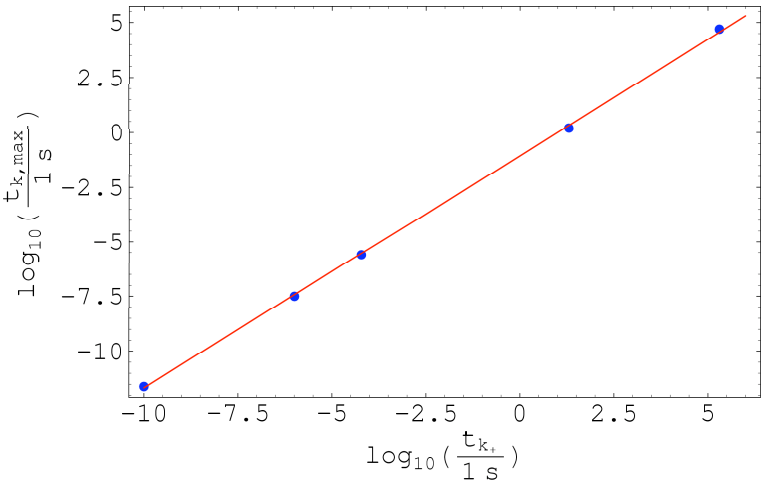

Figure 91: The relation between $t_{k_{max}}$ (corresponding to the instant for which $\beta(k)$ gets its maximum) and t_{k_+} (corresponding to the point where the spectral index $n(k)$ reaches its maximum value) for the running–tilt power spectrum.

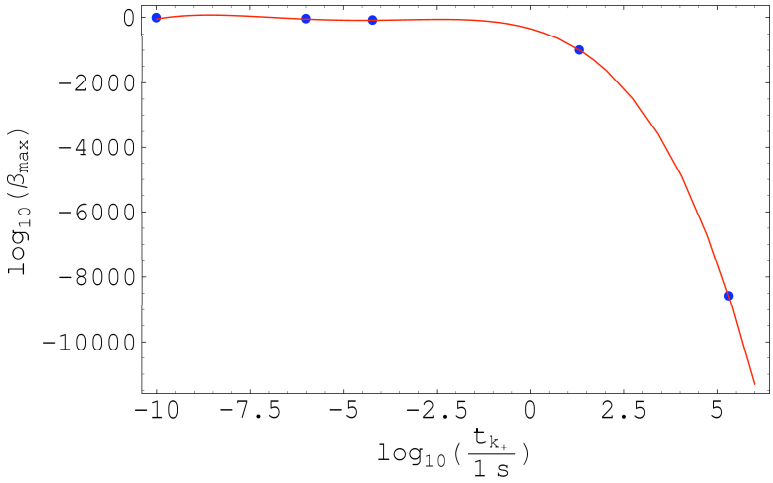

Figure 92: The relation between β_{max} and t_{k_+} when $n(k_+) = 1.4$ and $\delta_c = 1/3$ for the running–tilt power spectrum. The blue dots represent the obtained values (see Figures 80 to 84) and the red line represents the quartic interpolation $\beta_{max} = 10^{-343-312x-118x^2-17.4x^3-0.843x^4}$ with $x = \log_{10} t_{k_+}$.

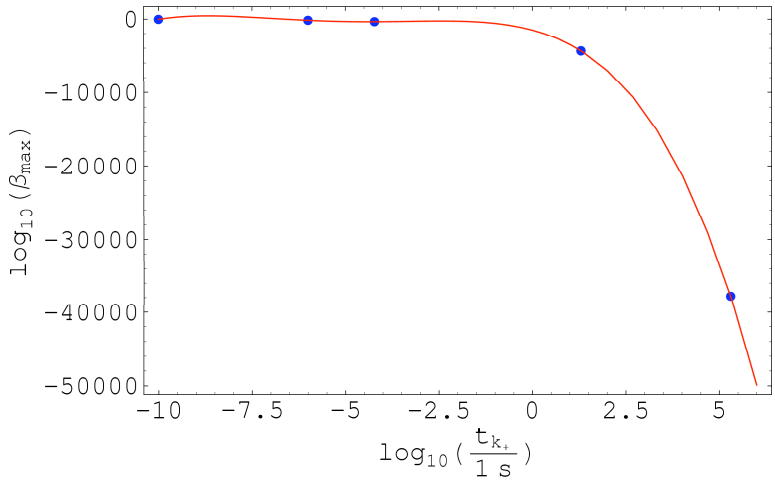

Figure 93: The relation between β_{max} and t_{k_+} when $n(k_+) = 1.4$ and $\delta_c = 0.7$ for the running–tilt power spectrum. The blue dots represent the obtained values (see Figures 80 to 84) and the red line represents the quartic interpolation $\beta_{max} = 10^{-1509-1377x-519.2x^2-76.86x^3-3.723x^4}$ with $x = \log_{10} t_{k_+}$.

6 Conclusions and Future work

6.1 Obtained results and conclusions

The Universe is a well developed structure on the scale of galaxies and smaller formations. This requires that at the beginning of the expansion of the Universe there should have existed fluctuations which leaded to the formation of such structures.

Now we have in cosmology a successful paradigm based on the existence of an inflationary stage which allow us to consider the quantum origin of the fluctuations. The quantum fluctuations produced during inflation are then stretched to scales much larger than the Hubble radius (at the time when they were produced) and, as the expansion of the universe goes on, each fluctuation will reenter inside the Hubble radius at some later epoch, depending on its wavelength. With this mechanism we can explain not just all the inhomogeneities we see today, even on the largest cosmological scales, but also the production of PBHs.

However, only the fluctuations with amplitude δ above some threshold δ_c can lead to the formation of PBHs (Section 2.2). If $\delta < \delta_c$ the fluctuation dissipates and there is no PBH formation at all (Section 2.4.3). Thus, it is very important to know the correct value of δ_c. Analytical considerations point to $\delta_c = 1/3$. Recent numerical simulations revealed different values for δ_c, all in the range $1/3$ – 0.7 (cf. Table 3).

It was believed for a long time that when a PBH forms its mass is of the order of the horizon mass M_H (equation 17). The aplication of critical phenomena to the mechanism of PBH formation has shown us that there exists an IMF for PBHs (Section 2.3, equation 32). It seems that PBHs could form with masses ranging from $10^{-4}M_H$ up to $1M_H$. The IMF introduces two additional parameteres besides δ_c: a normalization factor K and an exponent γ.

If one wants to determine the fraction of the universe going into PBHs at a given epoch, $\beta(k)$, then it is very important to know which values we should give to the parameters δ_c, K and γ. At the present these values are to be find numerically doing the simulation of the process of PBH formation (Section 2.4). These simulations are, in general, very complicated due to the fact that we are dealing with a dynamic process which leads to the formation of an horizon with a singularity in its interior. Here we have described, in some detail, the mechanism of PBH formation in a radiation dominated Universe (the formation of PBHs in other possible scenarios will be part of future work). In Table 3 we have summarized the values obtained for the parameters δ_c, K and γ by different authors.

In order to determine the probability of PBH formation at a given epoch or, equivalently, the fraction of the universe going into PBHs at that epoch, we must know the value of the mass variance $\sigma(k)$ at that epoch. In fact, this is one of the main problems in the calculation of $\beta(k)$. Recent studies have shown that a correct evaluation of the mass variance requires convolution with a filtering window function (equation 76) and with a transfer function (see equations 84

and 85). The expression for the mass variance can be splitted into two parts (see equations 86, 87 and 88). One of the parts includes the observational input which derives from the anisotrpy on the CMB. The other part includes a non–trivial relation $\alpha^2(k)$ between the observational input and the mass variance at some epoch in the past.

In order to determine the mass variance it is also crucial to know the shape of the primordial spectrum of the fluctuations. It is known for a long time that a scale–free power law spectrum (Section 4.1) explains quite well the formation of the LSS observed in the Universe. However, if we consider this kind of spectrum in the context of PBH formation then we will obtain negligible results to $\beta(k)$ for all epochs (Section 5.1).

If we want to go on studying the hypothesis of PBH formation then we must move to a more suitable primordial spectrum. It should be a spectrum equivalent to the scale–free power law spectrum during the era of LSS formation, matching the background normalisation, but also a spectrum which is more powerfull during the epochs relevant to PBH formation. Thus, we have considered three alternatives to the primordial spectrum of the fluctuations:

1. *Scale–free Power Spectrum with a Pure Step* – A scale–free power law spectrum with a step at some instant in the past giving more power to the fluctuations in the early stages of the Universe. Note that this is a pure phenomenological spectrum (Section 4.2).

2. *Broken Scale Invariance Spectrum* – A spectrum based in an inflationary model with a jump in the first derivative of the inflaton potential at some scale. This is a more natural alternative than the previous one (Section 4.3).

3. *Running–tilt Power Spectrum* – A power law spectrum with a variable index $n(k)$ highly supported by recent WMAP observations (Section 4.4).

Each one of these spectrums introduces a pair of additional parameters to the equations. In general, one of the parameters tells us the location of the peak in the spectrum and the other one tells us the amplitude of the spectrum at that peak. At the present the best we can do is to constrain these parameters in accordance with observational results. There are several observational constraints that we can impose to $\beta(k)$ (see Figure 29). Perhaps the strongest one is the constraint which arises from the γ–ray background radiation which tells us that when the universe was $\sim 10^{-23}$s old $\beta(k)$ should not exceed 10^{-28}. We have considered this value in our calculations in order to constrain the maximum amplitude of the peak.

PBHs form tipically with masses of $\sim M_H$ at the epoch of formation. This means that to give the location of the peak is equivalent to give the typical maximum mass allowed for the PBHs. The biggest SMBHs known candidates have masses of $\sim 10^{10} M_\odot$ which corresponds to the horizonn mass when the Universe was 2×10^5s ($k = 1.2\times10^{-21}\mathrm{m}^{-1}$). On the other hand PBHs, exploding today were formed with masses of $\sim 10^{15}$g when the Universe was 10^{-23}s ($k_s =$

$1.7 \times 10^{-7}\mathrm{m}^{-1}$). Thus, we have considered for the location of the peak some values in the range $1.7 \times 10^{-7}\mathrm{m}^{-1} \geq k_s \geq k = 1.2 \times 10^{-21}\mathrm{m}^{-1}$ or, equivalently, in the range $10^{-23}\mathrm{s} \leq t_s \leq 2 \times 10^{5}\mathrm{s}$ (cf. Table 2).

For a scale–free power law spectrum with a pure step and for a BSI spectrum the maximum amplitude of the peak is attained when the parameter p is minimum. This minimum value was calculated considering the constraint $\beta(10^{-23}\mathrm{s}) = 10^{-28}$. We have noticed that the minimum value allowed for p is model dependent, depends on the value of δ_c and also on the location of the peak k_s (cf. Table 4, Figure 30, Table 5 and Figure 50).

In the case of a running–tilt power spectrum the location and the amplitude of the peak are given by a pair of coefficients n_2 and n_3 (cf. equation 131). We have chosen for n_2 and n_3 values leading to peaks at the some locations as on the previous cases and also leading to blue spectrums but without overheading the value $n(k) = 1.4$ as well as the value $\beta(10^{-23}\mathrm{s}) = 10^{-28}$ (cf. Table 7).

We have done the integration of $\beta(k)$ for all the considered spectrums and for all the values of k_s presented in Table 2. We have considered for δ_c the "extreme" values $1/3$ and 0.7.

In the case of a scale–free power law spectrum with a pure step and in the case of a BSI spectrum we have considered first the minimum value allowed for p which leads to the maximum values allowed for $\beta(k)$. Secondly we have considered, for the same cases, higher values for p and that has shown us a drastic decrease on the values of $\beta(k)$ (Sections 5.2 and 5.3).

In the case of a running–tilt power spectrum we have considered in first place sets of values for n_2 and n_3 such that $n(k_{peak}) = 1.4$. Then we have considered lower values for $n(k_{peak})$ and that has shown us again a drastic decrease on the values of $\beta(k)$ (Section 5.4).

In Table 8 we present a list of the studied cases for which $\beta_{max} > 10^{-40}$. On the top of the list we have the results for the scale–free power law spectrum with a pure step. Considering that this is a pure phenomenological spectrum these results must be regarded with caution. For the BSI spectrum we have obtained interesting results with $\beta_{max} \sim 10^{-16}$ for all the considered epochs and for the running–tilt power spectrum it seems that the most interesting result occurs for $t_s = 10^{-10}\mathrm{s}$ with the formation of $10^{28}\mathrm{g}$ PBHs.

Table 8: The cases for which the fraction of the Universe going into PBHs, $\beta(k)$, is higher than 10^{-40}. Here p/n represents the parameter p in the case of a pure step or BSI spectrum (cf. Tables 4 and 5) and the spectral index $n(k)$ in the case of a running–tilt power spectrum. The value t_s (or t_{k_+}) represents the instant for which the primordial spectrum is maximum. PS represents the Pure Step power spectrum and RT the Running–tilt power spectrum.

t_s(s)	δ_c	p/n	$\log_{10}\beta_{max}$	$\log_{10}\frac{t_{k,max}}{1\text{s}}$	Fig.	Spec.
2×10^{5}	1/3	0.0014	-7	-5.1	39	PS
10^{-10}	1/3	1.4	-8	-11.6	80	RT
20	1/3	0.0014	-8	-1.1	38	PS
6×10^{-5}	1/3	0.0014	-11	-4.5	37	PS
10^{-6}	0.4	0.0012	-12	-6.3	44	PS
10^{-6}	0.7	0.00066	-12	-6.3	44	PS
10^{-6}	1/3	0.0014	-12	-6.3	36	PS
10^{-10}	1/3	0.0014	-14	-10.3	35	PS
10^{-10}	1/3	0.0040	-16	-10.2	58	BSI
10^{-6}	1/3	0.0040	-16	-6.2	59	BSI
10^{-6}	0.4	0.0033	-16	-6.2	67	BSI
6×10^{-5}	1/3	0.0040	-16	-4.4	60	BSI
20	1/3	0.0040	-16	1.1	61	BSI
2×10^{5}	1/3	0.0040	-16	5.1	62	BSI
10^{-6}	0.7	0.0019	-16	-6.2	67	BSI
2×10^{5}	0.7	0.0014	-26	-5.1	39	PS
10^{-23}	1/3	0.0050	-28	-23	57	BSI
10^{-23}	1/3	1.2412	-28	-23	90	RT
10^{-23}	1/3	0.0014	-30	-23	34	PS
10^{-10}	0.7	1.4	-32	-11.6	80	RT
20	0.7	0.0014	-32	1.1	38	PS
10^{-6}	1/3	1.4	-38	-7.5	81	RT

6.2 Future Work

In this section we present some objectives and ideas for future work. In the near future we want to improve the calculus of the fraction of the universe going into PBHs at a given epoch $\beta(k)$.

So far we have determined $\beta(k)$ within the assumption that PBHs form with masses of the order of the horizon mass at the epoch of formation. The horizon mass is the most probable mass for a PBH formed at a given epoch. However, the existence of an IMF for PBHs tells us that there is also some probabiltiy that a PBH could form with a smaller mass, in fact, according to recent results, the PBH mass could be as small as $10^{-4}M_H$. Thus as a first step we want to incorporate the IMF into the calculus of $\beta(k)$ for each primordial spectrum.

We have considered PBH during the radiation dominated era. However we know that during that era the universe experienced some phase transitions (e.g. end of inflation, quark–hadron phase transition, electroweak phase transition) during which it becomed for an instant matter (dust) dominated. Those transitions could have been very favorable for the production of PBHs. We want to review the mechanism of PBH formation during phase transitions and determine the coresponding possible values for $\beta(k)$.

The previous objectives will be part of immediate work. With the obtained reults we want to determine a first approach to the density distribution function of PBHs on the universe.

When a PHB forms at a given epoch it could swallow smaller mass PBHs existing in the neighboord. We want to study the importance of this process and evaluate how it affects the values of $\beta(k)$.

It is not clear if a PBH leaves a relic behind as a final result of the evaporation due to the the Hawking radiation mechanism. This is a very important subject because PBH relics would affect the values of the observational constraints. In the previous study we have considered that there are no PBH relics.

With the IMF we are taking into account the formation of horizon size and sub–horizon size PBHs ($10^{-4}M_H$–M_H). Recent studies point also to the possibility of formation of super–horizon sized PBHs. We want to explore this subject and study how it affects $\beta(k)$.

In the not so near future we want to study more deeply the PBH distribution in the Universe. There are two main ideas: (a) the distribution of PBHs is homegeneous throught the entire universe and (b) PBHs are clustered around galactic halos. We want to explore the two possibilities and, taking into account the obtained results, determine the distance to the nearest PBH.

References

Afshordi, N., McDonald, P. & Spergel, D. N. 2003, *Primordial black holes as dark matter: the power spectrum and evaporation of early structures* , ApJL, 594, 74 [arXiV: astro-ph/0302035]

Anchordoqui L. A., et al. 2002, *Black holes from cosmic rays: probes of extra dimensions and new limits on TeV-scale gravity*, het-ph/0112247.

Bardeen, J. M., et al. 1986, *The statistics of peaks of Gaussian random fields*, ApJ, 304, 15.

Baumgarte T. W., Shapiro S. L. and Teukolsky S. A., 1995, *Computing supernova collapse to neutron stars and BHs*, ApJ, 443, 717.

Bicknell G. V. and Henriksen R. N., 1979, *Formation of PBHs*, ApJ, 232, 670.

D. Blais, T. Bringmann, C. Kiefer, and D. Polarski, 2003, *Accurate results for primordial black holes from spectra with a distinguished scale*, Phys. Rev. D 67, 024024 [arXiv:astro-ph/0206262].

S.L. Bridle, A.M. Lewis, J. Weller and G. Efstahiou, 2003, *Reconstructing the primordial power spectrum*, MNRAS, 342, L72 [astro–ph/0302306].

Bringmann T., Kiefer C. & Polarski D., 2002, *PBHs from inflationary models and without broken scale invariance*,Phys. Rev. D 65, 024008 [astro–ph/0109404].

Carr B. J., 1975, *The PBH mass spectrum*, ApJ, 201, 1.

Carr B. J., 2003, *Primordial Black Holes as a Probe of Cosmology and High Energy Physics*, astro–ph/0310838

Carr B. J., 2005, *Primordial black holes: recent developments*, 22nd Texas Symposiun at Stanford, Dec. 2004 [astro–ph/0504034].

Carr B. J. & Hawking S. W., 1974, *BHs in the early Universe*, MNRAS, 168, 399.

Carr, B.J., Gilbert, J. H. & Lidsey, J. E. 1994, *Black hole relics and Inflation: limits on blue perturbation spectra*, PhRvD, 50, 4853 [astro-ph/9405027].

Cavaglia M., Das, S. & Maartens, R. 2003, *Will we observe black holes at the LHC?*, CQGra, 20, L205 [hep-ph/0305223].

Chisholm J. R., 2006, *Clustering of primordial black holes: basic results*, Phys. Rev. D, 73, 83504 [hep–ph/0503267].

Choptuik M. W., 1993, *Universality and scaling in gravitational collapse of a massless scalar field*, Phys. Rev. D, 70, 9.

Choptuik M. W., 1998, *The (unstable) threshold of BH formation*, Talk given at 15th International Conference on General Relativity and Gravitation (GR15), Pune, India, 16-21 Dec 1997 [gr–qc/9803075].

Combes F. et al., 2002, *Galaxies and cosmology*, Astronomy & Astrophysics Library, Springer–Verlag, London.

Düchting N., 2004, *Supermassive black holes from primordial black hole seeds*, Phys. Rev. D 70, 064015 [astro–ph/0406260].

Eardley, D. M. & Press, W. H. 1973, *Astrophysical processes near black holes*, ARA&A, 13, 381.

Easther R., 2005, *Folded Inflation, Primordial Tensors, and the Running of the Scalar Spectral Index*, hep–th/0407042.

Evans C. R. and Coleman J. S., 1994, *Observation of critical phenomena and self–similarity in the gravitational collapse of radiation fluid*, Phys. Rev. L37, 72, 1782 [gr–qc/9402041].

Green A. M. and Liddle A. R., 1997, *Constraints on the density perturbation spectrum from PBHs*, Phys. Rev. D 56, 6166, [astro–ph/9704251].

Green A. M. and Liddle A. R., 1999, *Constraints Critical collapse and the primordial black hole initial mass function*, Phys. Rev. D, 60, 63509, [astro-ph/9901268].

Green A. M., Liddle A. R., Malik K. A. and Sasaki M., 2004, *A new calculation of the mass fraction of PBHs*, Phys. Rev. D 70, 041502 [astro–ph/0403181].

Gundlach C., 1998, *Critical phenomena in gravitational collapse*, Adv. Theor. Math. Phys., 2, 1 [gr–qc/9712084].

Harrison, E. R. 1970, *Fluctuations at the threshold of Classical Cosmology*, PhRvD, 1, 2726.

Hawke I. and Stewart J. M., 2002, *The dynamics of PBH formation*, Class. Qauntum Grav., 19, 3687.

Hawking S., 1971, *Gravitationally collapsed objects of very low mass*, MNRAS, 152, 75.

Hawking S., 1974, *Black Hole Explosions?*, Nature, 248, 30.

Hernandez W. C. and Misner C. W., 1966, *Observer time as a coordinate in relativistic spherical hydrodynamics*, ApJ, 143, 452.

d'Inverno R., 1993, *Introducing Einstein's relativity*, Oxford, Claredon Press

Jones, M. H., & Lambourne, R. J. A., 2004, *An introduction to galaxies and cosmology*, by Mark H. Jones and Robert J.A. Lambourne. Co-published with The Open University, Milton Keynes. Cambridge, UK: Cambridge University Press.

Kiefer, C. 2003, *Quantum aspects of black holes*, In *The Galactic black hole*– Lectures on general relativity and astrophysics; Edited by Heino Falcke & Friedrich W. Hehl; Series in high energy physics, cosmology and gravitation; Bristol: IoP; Institute of Physics Publishing [astro–ph/0202032].

Koike T., Hara T., and Adachi S., 1995, *Critical behaviour in gravitational collapse of radiation fluid A renormalization group (linear perturbation) analysis*, PhRvL, 74, 5170 [gr-qc/9503007].

Koike T., Hara T., and Adachi S., 1999, *Critical behaviour in gravitational collapse of a perfect fluid*, PhRvD, 59, 104008.

Kormendy, J. 2004, *The Stellar–Dynamical Search for Supermassive Black Holes in Galactic Nuclei* in Coevolution of Black Holes and Galaxies, from the Carnegie Observatories Centennial Symposia., ed. L. Ho (Cambridge University Press), 1. [astro–ph/0306353]

Kribs G. D., Leibovich A. K. and Rothstein I. Z., 1999, *Bounds from PBHs with a near critical collapse IMF*, PhRvD, 60, 103510 [astro–ph/9904021].

Liddle A. R. & Lyth D. H., 1993, *The cold dark matter density perturbation*, Physics Reports, 231, 1 [astro–ph/9303019].

Longair M. S., 1998, *Galaxy formation*, Astronomy & Astrophysics Library, Springer–Verlag, Berlin.

MacGibbon, J. H. and Carr, B. J. 1991, *Cosmic rays from primordial black holes*, ApJ, 371, 447.

Maison D., 1996, *Non–universality of critical behaviour in spherically symmetric gravitational collapse*, PhLB, 366, 82 [gr–qc/9504008]

Miller, J., 2005, *Computations of primordial black hole formation*, in Proceedings of RAGtime 6/7: Workshops on black holes and neutron stars, Opava, 16-18/18-20 September, 2004/2005; S. Hledík and Z. Stuchlík, editors, Silesian University in Opava, Czech Republic.

Misner C. W. & Sharp D. H., 1964, *Relativistic Equations for Adiabatic, Spherically Symmetric Gravitational Collapse*, Phys. Let., 136B, 571.

Mukherjee P. & Wang Y. 2003, *Model-independent reconstruction of the primordial power spectrum from WMAP data*, ApJ, 599, 1 [arXiv: astro-ph/0303211].

Musco I., Miller J. C. and Rezzolla L., 2005, *Computations of PBH formation*, CQG, 22, 1405 [gr–qc/0412063].

Nadëzhin D. K., Novikov I. D. and Polnarev A. G., 1978, *The hydrodynamics of PBH formation*, SvA, 22, 129.

Narlikar J. V., 2002, *An Introduction to Cosmology*, Cambridge University Press, Cambridge.

Narlikar, J. V. & Padmanabhan, T., 1991, *Inflation for Astronomers*, ARA&A, 29, 325.

Niemeyer J. C., 1998, *Numerical investigation of the threshold for PBH formation*, astro–ph/9806043.

Niemeyer J. C. and Jedamzik K., 1998, *Near–critical gravitational collapse and the IMF of PBHs*, PhRvL, 80, 5481 [astro–ph/9709072].

Niemeyer J. C. and Jedamzik K., 1999a, *Dynamics of PBH formation*, Phys. Rev D, 59, 124013 [astro–ph/9901292].

Niemeyer J. C. and Jedamzik K., 1999b, *PBH formation during first–order phase transitions*, PhRvD, 59, 124014 [astro–ph/9901293].

Novikov I. D., Polnarev A. G., Starobinsky A. A. and Zeldovich Ya. B., 1979, *Primordial Black Holes*, A&A, 80, 104.

Padmanabhan T., 2001, *Theoretical astrophysics* (Vol. 3), Cambridge University Press, Cambridge

Page, D. N. & Hawking, S. W. 1976, *Gamma Rays from Primordial Black Holes*, ApJ, 206, 1

Polarski D., 2001, *Classicality of primordial fluctuations and primordial black holes*, International Journal of Modern Physics D, 10, 927 [astro-ph/0109388].

Polarski D., 2002, *Primordial black holes in an accelerating Universe*, PhLB, 528, 193 [astro–ph/0112328].

Polarski, D. and Starobinsky A. A. 1996, *Semiclassicality and decoherence of cosmological perturbations*, CQG, 13, 377

Sobrinho J. L. G., 2003, *Possibilidade de detecção directa de Buracos Negros por radiação electromagnética*, Tese submetida nas Provas de Aptidão Pedagógica e Capacidade Científica para habilitação à categoria de Assistente, Universidade da Madeira.

Spergel D. N., et al. 2003, *First-Year Wilkinson Microwave Anisotropy Probe (WMAP) Observations: Determination of Cosmological Parameters*, ApJS, 148, 175 [astro–ph/0302209].

Spergel D. N., et al. 2006, *Wilkinson microwave anisotropy probe (WMAP) three year results: implications for Cosmology* [astro–ph/0603449].

Starobinsky A. A., 1992, *Spectrum of adiabatic perturbations in the universe when there are singularities in the inflaton potential*, JETP Lett., 55, 489.

Tegmark M., et al. 2004, *Cosmological parameters from SDSS and WMAP*, Ph. Rv. D 69, 103501 [astro–ph/0310723].

Unsöld A. & Baschek B., 2002, *The new cosmos : an introduction to astronomy and astrophysics*, Springer, Berlin.

Verde L., et al. 2003, *First-Year Wilkinson Microwave Anisotropy Probe (WMAP) Observations: Parameter Estimation Methodology*, ApJS, 148, 195 [astro–ph/0302218].

Yokoyama J., 1998, *Cosmological constraints on PBHs produced in the near–critical gravitational collapse*, PhRvD, 58, 107502 [gr–qc/9804041].

Zeldovich, Y. B. 1970, *Gravitational instability: an approximate theory for large density perturbations*, A&A, 5, 84.

Zeldovich Ya. B. and Novikov I. D., 1967, *The hypothesis of cores retarded during expansion and the hot cosmological model*, SvA, 10, 602.